STUDY ON HYDROCARBON REFORMING CATALYST FOR BIOMASS GASIFICATION PROCESS DERIVED BY PREOXIDATION OF NICKEL CONTAINING ALLOYS

A DISSERTATION

Submitted to

Graduate School of Enginering
Nagoya University

In partial fulfillment of
the requirements for the
degree of

Doctor of Engineering

By

Sharon Rose Baraquia de la Rama

June 2014

Abstract

Study on Hydrocarbon Reforming Catalyst for Biomass Gasification Process Derived by Preoxidation of Nickel Containing Alloys

Sharon Rose Baraquia de la Rama

Advisor: Professor Tomohiko Tagawa

Supported nickel catalysts are the most preferred alternative for noble metal catalysts used in hydrocarbon reforming reactions due to the relative abundance and low cost of nickel. However, this type of catalyst is rapidly deactivated by carbon formation. In this study, surface oxidation of nickel-containing alloys was hypothesized to produce a catalyst that has optimally dispersed and reducible nickel that is strongly interacted with the alloy matrix. The formation of metal oxide scale was also proposed to promote the reaction and retard carbon formation rate. This dissertation consists of 5 chapters which tackled the screening and evaluation of commercially available Ni-containing alloys applied as hydrocarbon reforming catalyst. Chapter 1 includes the background and motivation of this study. Chapter 2 discussed the screening test where tetradecane partial oxidation, steam reforming, and dry reforming reactions were performed at 730ºC to evaluate the catalytic activity of the alloys. It was a summary of the author's 3 published/accepted papers, namely:

1. Partial Oxidation Catalysts Derived from Ni Containing Alloys for Biomass Gasification Process authored by Tagawa T, de la Rama SR, Kawai, S, and Yamada H published in Chemical Engineering Transactions;
2. Preliminary Assessment of Oxidation Pretreated Hastelloy as Hydrocarbon Steam Reforming Catalyst authored by de la Rama, SR, Kawai, S, Yamada H, and Tagawa T published in Journal of Catalysts; and
3. Evaluation of Pre-oxidized SUS304 as a Catalyst for Hydrocarbon Reforming authored by de la Rama, SR, Kawai, S, Yamada H, and Tagawa T published in ISRN Environmental Chemistry.

The collected data showed that among the tested alloys, preoxidized Hastelloy is the most active towards partial oxidation and steam reforming. In the case of dry reforming reaction, "Superinvar" showed promising catalytic activity. Chapters 3 and 4 of this thesis highlighted the feasibility studies done on SUS304, the 2nd most catalytically active alloy, and Kovar, another Fe-Ni-Co alloy, as dry reforming catalysts using tetradecane as hydrocarbon model compound. The data presented were

composed of unpublished data on preoxidized SUS304 and the author's paper: "Effects of Oxidation Pretreatment Temperature on Kovar Used as CO_2 Reforming Catalyst". In Chapter 3, oxidation pretreatment was performed on SUS304 under O_2 flow at 1000ºC for 120 min before being evaluated at different reaction temperatures (700, 800, and 900°C) and CO_2 flow rates (14, 42, and 70 μmol/s). The collected data showed that CO_2 flow rate did not display any notable effect on the reaction rate when dry reforming was conducted at high reaction temperatures (>700ºC) while applying higher CO_2 flow rates (42 and 70 μmol/s) improved the reaction rate and lessened the amount of carbon formed on the surface of the catalyst when the reaction was conducted using low reaction temperature (700ºC).

In Chapter 4, experiments on the effect of oxidation pretreatment temperature (500-1000°C) on the catalytic activity of Kovar. Catalytic evaluation using tetradecane at 800°C with 70μmol/s CO_2 revealed 700 and 1000°C as the best pre-oxidation temperature in producing CO and H_2, respectively. XRD and SEM-EDS analyses conducted on preoxidized SUS304 and Kovar showed that oxidation pretreatment led to the formation of a mixed metal oxide matrix that served as the substrate for the dispersed active components (nickel and cobalt) while promoting the dry reforming reaction to proceed and preventing the formation of carbon.

Chapter 5 summarized the contents of this thesis, especially, with the view point from modification of alloy surface by oxidation pretreatment toward the stable catalytic activity.

Table of Contents

List of Figures

List of Tables

CHAPTER 1

Introduction to Preoxidized Ni-containing Alloys as Hydrocarbon Reforming Catalyst

1.1 World's Energy Trend

For centuries, our society had been dependent on technology and transportation powered by fossil derived fuel in the form of coal, oil, and natural gas. Comparing the rate at which fossil fuel is discovered and produced with the world's energy consumption, it was predicted that fossil sources would soon be depleted [1,2], thus it was proposed that renewable and sustainable energy sources should be utilized [3]. Global warming is another driving force behind researches on sustainable and environment-friendly energy development. Specifically, greenhouse gases (GHG) released to the atmosphere during fossil fuel burning is deemed to raise the world's average temperature and drastically change the climate. To address this issue, developed nations signed the Kyoto Protocol and agreed to reduce their respective GHG emissions. However, the continuous growth in population and economy of developing countries such as China and India increased the global energy demand and also heightened their GHG emissions. Although developing countries are not bounded by the Kyoto Protocol, they also participate in reducing GHG emissions by improving energy efficiency, reducing deforestation and supporting renewable energy sources.

The application of biomass as an energy source presents advantages, such as renewability, versatility and the prospect of utilizing waste products to generate energy. Agricultural crops and by-products can be converted to bioalcohols, synthetic gas (syngas), and dimethyl ether (DME); while marine fauna are also considered for biogas and biodiesel production [4-6]. Many scientists believe that maximizing the potential of these renewable sources in terms of energy production could improve both production and economic feasibility, thus providing the world a stable and environment-friendly energy source.

1.2 Hydrogen from Biomass

When H_2 is used as a fuel it does not emit any pollutant, instead it produces water which could be processed to form more H_2 [7-9]. It can be used in combustion engines to generate heat and in fuel cells to power electric cars [7,9]. Nath and Das [9] reported that H_2 fuel cells are 3 times more efficient than gasoline-powered engines while Balat and Kirtay [7] published that H_2 has 2.75 times more energy than conventional hydrocarbon fuels.

Today, H_2 is industrially produced mostly via hydrocarbon steam reforming [7,9,10] and partial oxidation of coal or heavy hydrocarbons [8]. These processes always yield CO_2 as a by-product that is managed by sequestration. Sequestration is an energy intensive technology, costly and a potential threat to the

environment [8]. A more promising and environmentally friendly way to produce H_2 is via biomass gasification. The use of biomass-derived H_2 was predicted to reduce the net amount of CO_2 released in the atmosphere since the quantity of CO_2 released during biomass gasification would be equal to that previously adsorbed from atmosphere during photosynthesis [7,8]. Despite the many advantages of using biomass-derived H_2, improvements on production cost, reactor efficiency, catalytic optimization, H_2 storage, and H_2 delivery are still necessary to realize the full potential of H_2 energy.

1.2.1 Biomass gasification

Biomass gasification is a thermal process where biomass is broken down into gas, volatiles, char, and ash. It includes 2 endothermic processes namely, pyrolysis and gasification steps. During pyrolysis (<600°C), the volatile components of the biomass are vaporized. The second step involves char gasification using air, O_2, or steam as gasification medium. High temperature gasification (>1200°C) would dominantly convert biomass into syngas (CO and H_2). On the other hand, low temperature biomass gasification (<1000°C) produces syngas, CO_2, H_2O, CH_4, hydrocarbon mixture, and tars [11]. Tar is one of the major drawbacks of biomass gasification since it can damage both the catalyst and reactor. As a solution, hydrocarbon and tar by-products could be catalytically reformed to produce CO and H_2 (syngas). Then, water-gas shift or WGS (Reaction 1.1):

$$CO+H_2O \rightarrow CO_2+H_2 \qquad (1.1)$$

could be applied on the produced syngas to increase the amount of H_2 produced [7,10,12]. Finally, biomass gasification is currently the most economical and feasible route in producing H_2 from biomass.

1.2.2 Syngas

In addition to H_2 production via WGS, syngas can also be used to generate electricity, Fischer-Tropsch fuels, methanol, and DME [11,13,14]. To produce electricity from syngas, hot syngas is typically combusted in a gas turbine to generate electricity. The exhaust gas can then be converted to steam and be utilized by a steam generator to produce additional electricity [13,14].

Hydrocarbons can be produced from syngas via Fischer-Tropsch (FT) reaction (Reaction 1.2):

$$CO+2H_2 \rightarrow -(CH_2)- +H_2O \qquad (1.2)$$

In non-selective catalytic FT synthesis, majority of the product is composed of straight-chain hydrocarbons and minor amounts of branched hydrocarbons, unsaturated hydrocarbons, and primary alcohols [11]. These hydrocarbons can substitute conventional fossil fuels. In South Africa and Malaysia, FT is commercially used to produce liquid fuel [14]. The most common catalysts used in FT synthesis are Fe and Co based. Iron based catalysts were reported to be cost-efficient, sulfur-tolerant and suitable for olefins and alcohol production. Cobalt based catalysts showed higher conversion rates, longer life time, and greater reactivity towards hydrogenation [11]. Although undesirable side-reactions and catalyst poisoning resulted into high production cost of FT fuels, its positive impacts to the environment continues to encourage further researches on improving the efficiency of gas cleaning and FT fuel synthesis.

Methanol and DME are storable liquid fuels that can be produced from syngas through catalytic hydrogenation of CO (Reaction 1.3) and methanol dehydration (Reaction 1. 4), respectively:

$$CO+2H_2 \rightarrow CH_3OH \qquad (1.3)$$

$$2CH_3OH \rightarrow CH_3OCH_3+H_2O \qquad (1.4)$$

Industrial methanol production employs zinc-chromium oxide for high pressure processes and copper-zinc-chromium catalyst for low pressure processes. When compared to gasoline, methanol has higher thermal efficiency, minimal emission problems, higher octane number, and lower heating value [5]. Despite these, only a few percent of produced methanol is used as a liquid fuel. It was predicted that developments in fuel cell technology would prove the importance of methanol as a liquid fuel. While methanol may replace gasoline in the future, DME is most suitable to substitute diesel. Even though it requires lubricant addition and fuel injection systems to be altered, its low-combustion noise and low GHG emissions makes it an attractive alternative fuel [5].

1.3 Hydrocarbon Reforming

Hydrocarbon steam reforming, mostly for methane reforming, is the most traditional and dominant technology applied for big-scale syngas production. Steam reforming (Reaction 1.5) is a highly endothermic catalyzed reaction

$$C_nH_m+nH_2O \rightarrow nCO+(n+{}^1/_2m)H_2 \qquad (1.5)$$

that converts liquid hydrocarbon stream to CO_2, CO, CH_4, and H_2. Steam reforming crude product gas yields the highest H_2 content at 70-80% of its volume [15] making its H_2/CO too high for most downstream processing [16,17]. The endothermic nature of the reaction also requires a large amount of energy. Contrastingly, hydrocarbon partial oxidation (Reaction 1.6) is a mild exothermic reaction

$$C_nH_m + {}^{n}/_{2}O_2 \rightarrow nO_2 + {}^{m}/_{2}H_2 \qquad (1.6)$$

that could be performed with or without a catalyst making it an attractive alternative process in producing syngas [15,16,18,19]. Although only 40-50% of its product gas is H_2 [15], its H_2/CO is suitable for FT synthesis [17,18]. Hydrocarbon partial oxidation also eliminates the problem of environmentally harmful gases such as CO_2. This process, unfortunately, requires pure O_2 stream making it expensive and prone to explosion [16].

Recently, considerable attention was given to dry (CO_2) reforming (Reaction 1.7), an endothermic reaction

$$C_nH_m + nCO_2 \rightarrow 2nCO + {}^{m}/_{2}H_2 \qquad (1.7)$$

This technology offers the possibility of recycling CO_2 produced from steam reforming and sequestered from other industrial processes. Compared to steam reforming, dry reforming involves fewer side reactions since both reactants and products are in gas phase [20]. Dry reforming is also the advantageous route in producing syngas with H_2/CO ratio suitable for liquid fuel synthesis. Nevertheless, this process requires the development of an active catalyst that minimizes or retards carbon formation [16,17,20].

1.3.1 Mechanism and Thermodynamics of Dry Reforming

The first comprehensive paper on dry reforming was published by Fischer and Tropsch in 1928 [21]. Studies on the kinetics, thermodynamics and catalysis of the reaction were then conducted over the years. A study conducted by Rostrup-Nielsen and Bak Hansen in 1993 [21] using methane, the simplest and most studied hydrocarbon feedstock, showed that methane dry and steam reforming are almost the same [21]. The first step involves the breaking of C-H bond and adsorption of the CH_3* species on the catalyst active site [21,22]. Subsequent, step-wise dehydrogenation of the adsorbed CH_3* species will then

convert it to adsorbed C* (Reaction 1.8). The active C* species then reacts with the adsorbed oxygen originating from the dissociation of CO_2 [23] (Reaction 1.9).

$CH_4 \rightarrow CH_3^* \rightarrow CH_2^* \rightarrow CH^* \rightarrow C^*$ (1.8)

$C^* + CO_2 \leftrightarrow 2CO$ (1.9)

When longer hydrocarbons are used, hydrocarbon decomposition would yield a mixture of hydrocarbon fragments (C_nH_m). Depending on the relative amount of CO_2 in the feed, dehydrogenation or dry reforming may become the dominant reaction [23].

Dry reforming reaction is accompanied by several side reactions that could alter the relative compositions of the product gases or lead to carbon formation. Among which, reverse water-gas shift or RWGS (Reaction 1.10), methane decomposition (Reaction 1.11) and CO disproportionation or Boudouard reaction (Reaction 1.12)

$CO_2 + H_2 \rightarrow CO + H_2O$ (1.10)

$CH_4 \rightarrow C + 2H_2$ (1.11)

$2CO \rightarrow C + CO_2$ (1.12)

were cited as the most important [24]. Thermodynamics studies involving methane revealed that methane decomposition starts to take place at 557°C while the minimum reaction temperature for dry reforming is 640°C [20,25]. Increasing the temperature to 700°C and 820°C will respectively cease CO disproportionation and RWGS. Between 557-700°C methane decomposition and CO disproportionation can occur. Hence, it is considered to be a region of severe carbon formation [20].

In 1979, Topor et al. suggested that supplying excess CO_2 to the reactor would avoid carbon formation [25]. The data of Nakamura and Uchijima [26] showed that carbon formation is thermodynamically favored at 1:1 CO_2/CH_4 feed ratio and that increasing the amount of CO_2, would allow the dry reforming reaction to proceed with minimal carbon formation. Experimental data published by Takano et al. [27] using supported Ni catalysts showed that 1:2 feed ratio produced equimolar H_2 and CO while feed ratios greater than 1:1 produced lower H_2 because the excess CO_2 tend to react with H_2 via RWGS. A lower feed ratio was suggested to increase the H_2 selectivity although carbon is easily formed at this condition.

To prevent carbon formation, the reaction should be performed at temperatures higher than those indicated in Figure 1.1. However, an increase in temperature would require more energy input, thus adding to the production cost. Another concern is the loss of active sites resulting from the formation of nickel carbide that takes place at high temperature. In the case of fixed bed reactors, increasing the pressure would increase the minimum temperature for nickel carbide formation [25].

Takano et al.[7] have also pointed out from TG studies, that the corresponding active sites for coke formation and dry reforming reaction are located at different environments. Categorically, nickel particles having strong interaction with the support material were responsible for dry reforming reaction while large particles of nickel were accountable for coke formation [7].

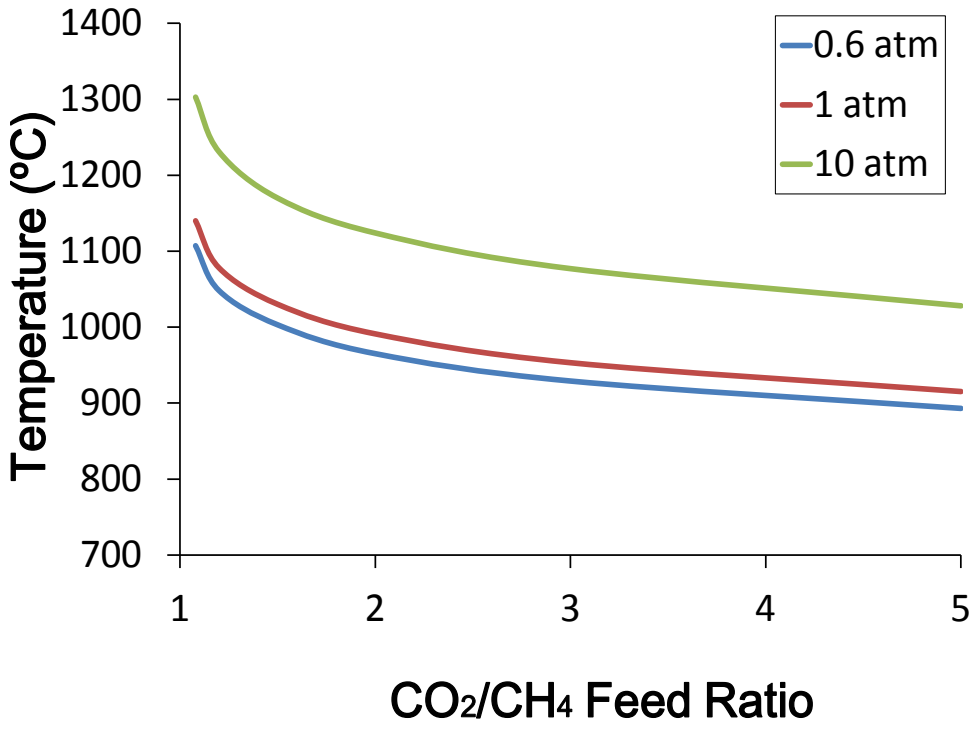

Figure 1.1. Effect of feed ratio on maximum reaction temperature where carbon formation is thermodynamically possible[25]

1.3.2 Dry Reforming Catalyst

Along with studies in reaction mechanism and thermodynamics involved in hydrocarbon dry reforming is the search for a highly active and robust catalyst. Particularly, supported Group VIII, IX and X were reported to be catalytically active towards dry reforming [28-30]. The noble metals ruthenium and rhodium were cited to show superior activity and resistant against carbon deposition [30-32]. On the other hand, nickel is most suitable for industrial application mainly because it is highly available and inexpensive [28,33]. Recently, cobalt was revealed as another possible substitute for noble metal catalysts [31]. In the case of Ni/Co bimetallic catalysts, the ratio of the 2 metals is vital in creating an active and stable catalyst. An excess in cobalt would result into metal oxidation while adding too much nickel will result to coking, both of these lead to catalyst deactivation [34].

To prevent coking and sintering, it is essential that the active metal component is pre-reduced or reducible [29,35,36]; well dispersed, and strongly interacted with the support material [18]. Aside from the active metal components, several factors have to be considered in developing an active and stable catalyst. Catalyst preparation technique, the type of support, and the kind of promoter, were cited to determine the stability and selectivity of the catalyst [30,31]. Pretreatment condition is also an important aspect since it determines the structural properties of the catalyst and consequently both its activity and stability [31,35]. Specifically, activation and calcination were found to enhance the activity of supported nickel [35] and cobalt [31] catalysts. Studies conducted on supported nickel catalysts indicated that a basic support improves the adsorption or dissociation of CO_2 [27,35], the addition of trivalent-metal oxides, Cr_2O_3 and La_2O_3, prevents coking by enhancing the mobility of the lattice O^{2-} [37], the addition of CoO to NiO-MgO catalyst improves its activity and eliminates the formation of filamentous carbon on its surface [38], and that the presence of iron in the support stabilizes nickel in the structure [33].

A screening test conducted by Takano et al. [39] on the effect of support material on the catalytic performance of nickel during methane dry reforming reaction showed that porous support materials reduce pressure drop caused by carbon accumulation by providing enough space and thus promoting optimum nickel dispersion.

1.4 Ni-containing Alloys: Alternative Dry Reforming Catalyst

Metals tend to undergo oxidation when exposed to air or oxygen and this tendency becomes higher at elevated temperatures. Depending on the environment, a thin and slow growing scale or a spalled layer may be formed. Initially, a thin oxide film will cover the whole surface of the metal. Metal ions from the substrate or oxygen ions from the atmosphere need to pass through the formed initial layer in order for the oxide layer to grow. The diffusion of these ions is usually dependent on the defects of the oxide layer structure. Thin layer oxidation is favored at low temperatures thus it is usually very slow that some metals obey the kinetics of noble metals. Most oxides formed at low temperatures are amorphous and metal oxide growth follows either a logarithmic or inverse logarithmic kinetics. That is, the initial oxidation rate rises rapidly and then slows down as the oxide layers becomes thicker [40]. Contrastingly, the initial layer is instantly formed at high temperature. Oxidation rate at high temperature follow a parabolic law. As the oxide scale becomes thicker, the oxidation rate decreases [40,41].

Transition metals (iron, cobalt, nickel, etc.) display moderate oxidation resistance and are often used as base elements for heat resistant alloys. Alloys generally display modified and complex oxidation behaviors when compared to their individual metal components [40,42]. Specifically, alloys may obey more than 1 oxidation rate laws depending on the oxidation condition (e.g. the oxidation temperature, oxygen pressure, preparation, etc.). For example, iron based alloys are usually mixed with nickel and chromium to impart better heat resistance. Adding chromium to iron results into the formation of a protective chromium oxide layer along with FeO (wustite). As the amount of chromium is increased more iron chromium spinels are formed, blocking the Fe^{2+} ions which results to thinner FeO and relatively thicker Fe_3O_4. Further increase in chromium content would result into the formation of a mixed spinel and a significant drop in the oxidation rate; leading to parabolic kinetics. The outer layer of the oxide scale would still be consists of iron since Fe ions are more mobile through this layer than Cr^{3+}. [40,42]. However, the protective function of chromium on iron is only evident when chromium content is more than 10% [41,42]. The required chromium amount becomes greater at higher temperature, 20% at 900°C and 25% at 1000°C. Nickel is another element that is usually alloyed with Fe-Cr alloys to improve its heat resistance [42] and mainly to generate an austenitic iron [40]. Austenitic iron has a face-centered cubic (fcc) structure and is stable at high temperatures.

Austenitic stainless steels are chromium-nickel and chromium-nickel-manganese stainless steels. SUS304 is an example of austenitic stainless steel that is 18-20 wt% chromium, 8-10 wt% nickel, with traces of carbon, silicon, manganese, phosphorus, and sulfur. A study conducted by Huntz et al., [43] stated that when SUS304 is oxidized at low oxygen partial pressure, parabolic kinetics is observed and is associated with Cr_2O_3 growth. However, at higher oxygen partial pressure and temperature greater than 850°C, parabolic oxidation pattern is not observed; instead, oxidation takes place in 2 stages. First, Cr_2O_3 is formed followed by the growth of iron oxide (Fe_2O_3) which consequently hastens the oxidation rate [40,43]. The loss of chromia layer may be due to Cr_2O_3 decomposing to CrO_3 which is volatile [40].

When cobalt is added to an iron-nickel alloy, its coefficient of thermal expansion becomes lower (invar effect) making it more tolerant towards thermal expansion and less susceptible to fractures [44]. It also promotes diffusion less transformation of ferrite from fcc to body centered cubic (bcc) structure called martensitic transformation [44]. Martensitic transformation proceeds rapidly and controlled by nucleation, instead of diffusion [45]. Depending on nickel-iron-cobalt alloy composition, varying ratios of austenite and martensite may be obtained which provides the possibility of controlling the thermal expansion. Kovar, is an iron-nickel-cobalt alloy (29 wt% nickel, 17 wt% cobalt, and traces of carbon, silicon and manganese) with a coefficient of thermal expansion similar to borosilicate glass making it widely used in glass-metal sealing in electronics. The type and thickness of the oxide scale is highly responsible for the strength between the molten glass and the metal [46] making studies on the oxidation of Kovar important in creating good quality seals. Lou and Shen [46] cited 3 types of iron oxides (FeO, Fe_2O_3, and Fe_3O_4) that form sequentially upon oxidation at high temperature. Their data on the oxidation behavior of Kovar also revealed that temperature and atmosphere controls the oxidation kinetics and consequently the types and amount of oxides that can be formed.

At present, majority of commercially produced catalysts contain noble metals on silica or silica-aluminum support. Coke formation remains to be the persistent cause of catalyst deactivation. Reforming catalyst development is continuously performed primarily aiming to promote marketability of biomass derived energy by providing a low-cost and robust catalyst.

Tagawa and Okada [47] proposed the application of oxidation pretreated alloys on H_2 related reactions while Chikamatsu et al. [48] published that oxidation of Mg_2Cu alloy resulted into the formation of mixed metal oxide composed of MgO and CuO;

oxidation pretreatment also rendered the alloy catalytically active towards hydrogenation of methyl linoleate to produce alcohol. Further studies conducted on the catalyst revealed that a special interaction existed between the active component, copper, and the support material, oxide(s) of magnesium [49].

1.5 Preliminary Data and Objectives of the Study

The National Institute for Environmental Studies (NIES) of Japan is particularly interested in producing H_2 from biomass via gasification of woodchips and waste paper at 650-850ºC followed by catalytic reforming of the hydrocarbon by-products and lastly, H_2 purification [50]. The simplified diagram of the research project is shown in Figure 1.2. The hydrocarbon by-products or "tar" were analyzed to contain long chain hydrocarbons, aromatic compounds and sulfur containing materials. In this NIES project, Tagawa et al. [51], selected tetradecane, toluene, naphthalene and thiophene as model compounds of tar. As a part of this project which is shown in red square part of Fig 1.2, the reactivity of these model compounds were tested under dry reforming conditions over SUS304 catalyst. It was reported that preoxidized SUS304 showed catalytic activity when employed as a catalyst for tetradecane dry reforming while untreated SUS304 only abruptly showed catalytic activity (Fig. 1.3a) indicating that the activity of metallic alloy surface was very small for the reaction. Improvements on catalytic activity and stability were noted when SUS304 was preoxidized using CO_2 (Fig. 1.3b) and O_2 (Fig. 1.3c) [51]. In addition, preliminary experiments conducted by the author also showed that among the preoxidation temperatures evaluated (600-1000ºC), SUS304 preoxidized in O_2 at 1000ºC showed superior catalytic activity towards tetradecane dry reforming [52]. Based on the noted improvements in catalytic activity upon oxidation, it was proposed to design a reforming catalyst via oxidation treatment of alloys especially those containing Ni since this metal was reported to be a good substitute for noble metal catalysts.

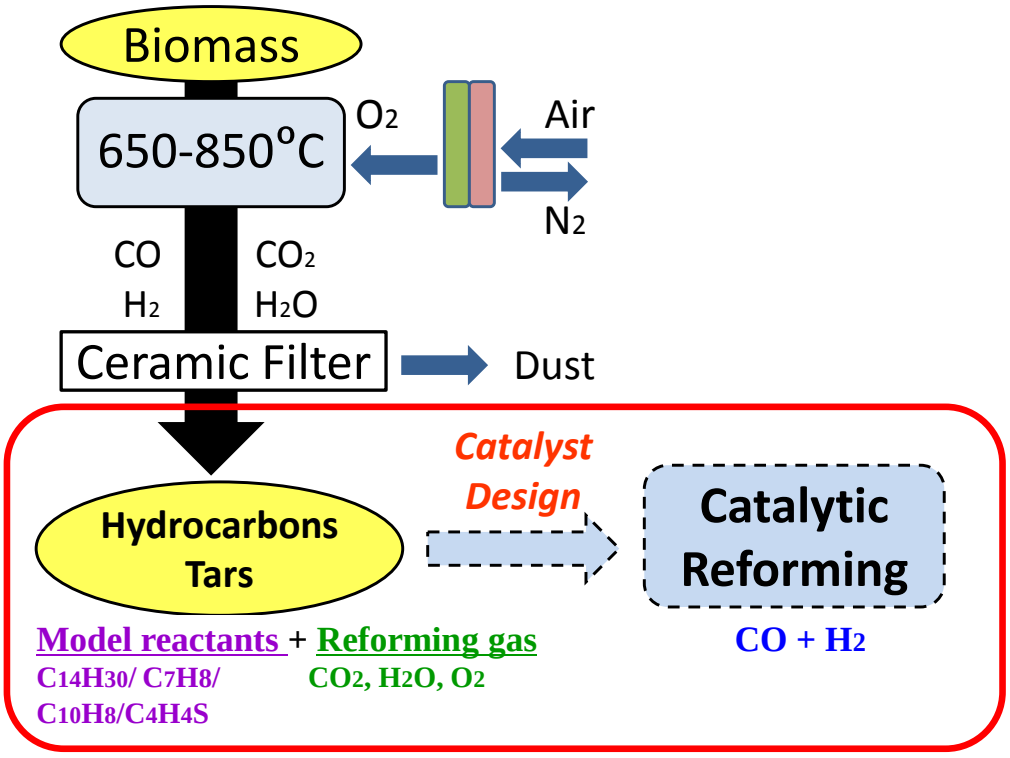

Figure 1.2. Simplified illustration of the biomass gasification research project conducted by NIES[50]

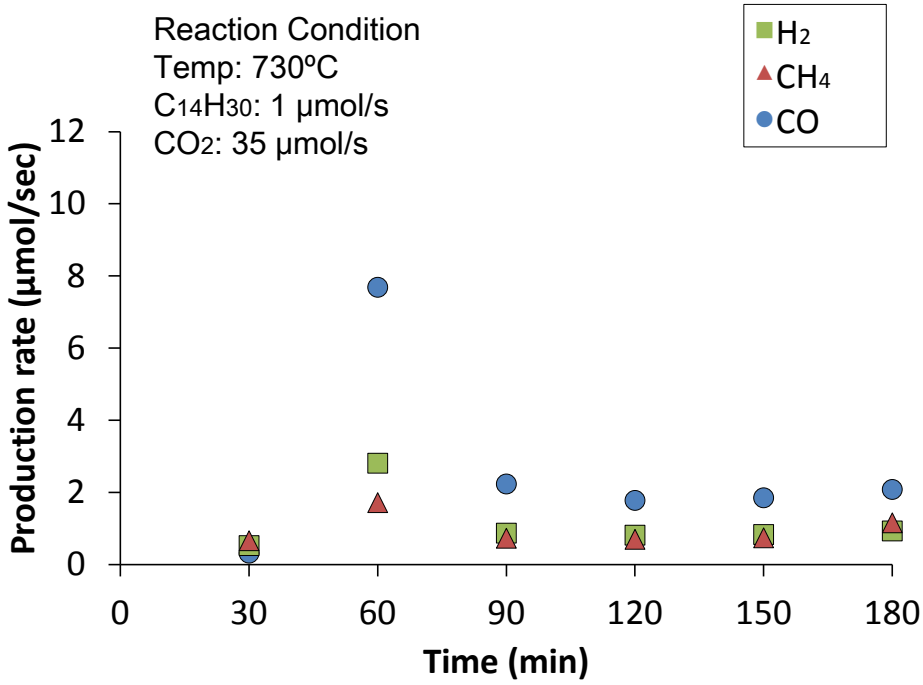

Figure 1.3a. Quantitative analysis of primary product gases during tetradecane dry reforming at 730°C conducted over untreated SUS304[51]

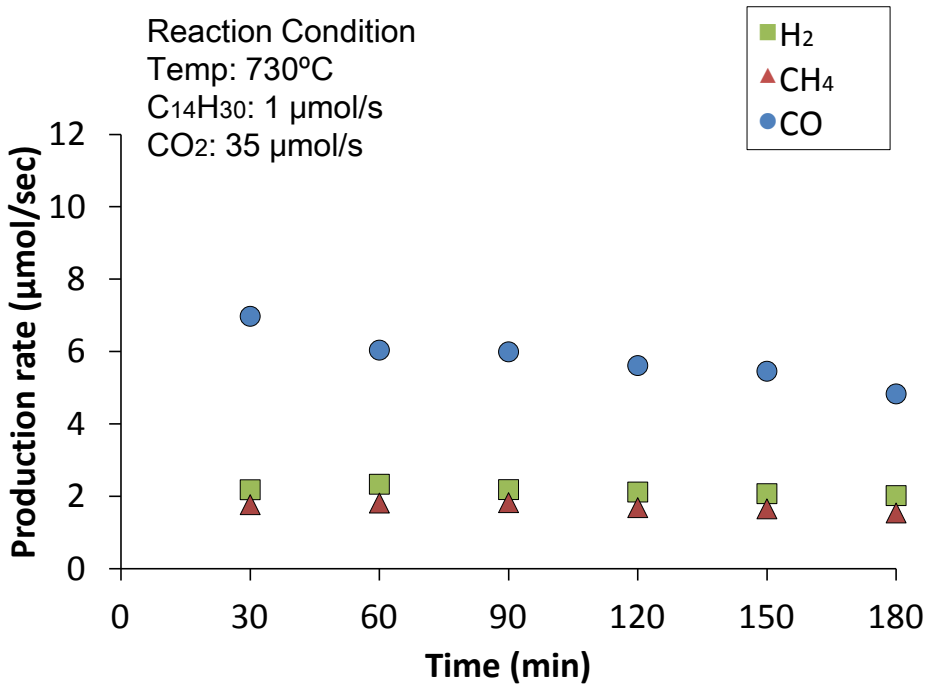

Figure 1.3b. Quantitative analysis of primary product gases during tetradecane dry reforming at 730ºC conducted over SUS304 preoxidized at 800ºC in CO_2 for 120 min[51]

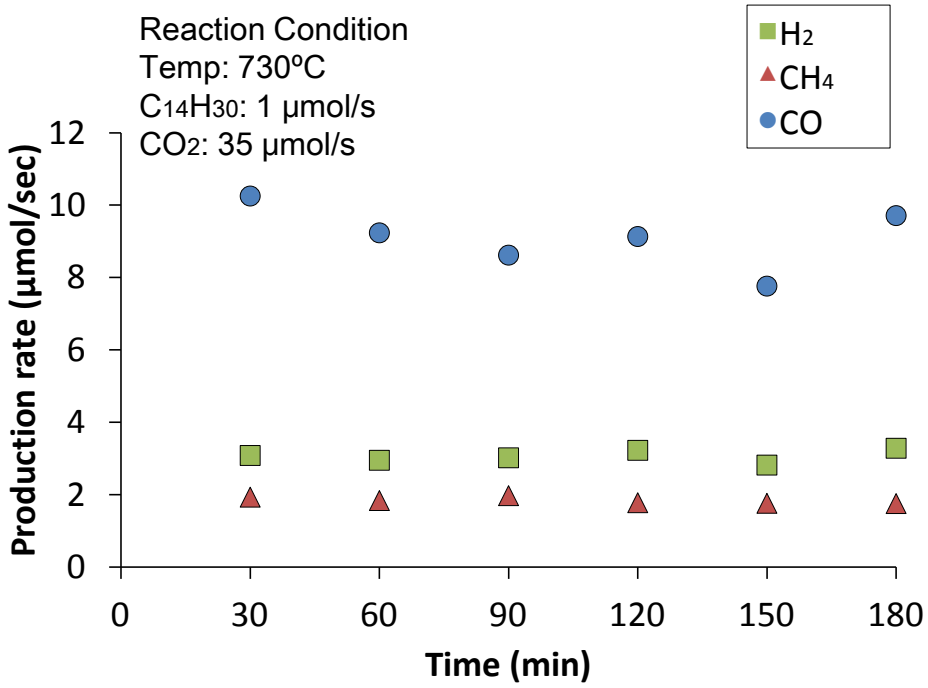

Figure 1.3c. Quantitative analysis of primary product gases during tetradecane dry reforming at 730ºC conducted over SUS304 preoxidized at 800ºC in O_2 for 120 min[51]

This thesis reports on the potential application of commercially available Ni-containing alloys as catalysts for reforming the hydrocarbons that are co-produced during biomass gasification. Specifically, the application of SUS304 and Kovar as tetradecane dry reforming catalyst was highlighted. The alloys were oxidized before being applied as catalysts to dry reforming reactions. Oxidation was conducted to facilitate the formation of mixed metal oxide scale on the surface of the alloy tubes as well as disperse the catalytically active component(s) on the metal oxide matrix. The alloy substrate was hypothesized to provide the necessary mechanical strength while maintaining a strong metal-metal oxide interaction. In addition, screening study suggested that tetradecane was chosen as a model compound for biomass-derived tar since its straight chained and simple structure would allow the fundamental reaction to be clearly observed without the complications of sulfur poisoning.

CHAPTER II

Screening Test: Hydrocarbon Reforming Reaction Catalyzed by Preoxidized Nickel-Containing Alloys

2.1 Introduction

In this study, 5 kinds of alloy materials were tested with four model compounds under reforming gas of steam, carbon dioxide and oxygen under various reaction conditions. Among this complex matrix of screening tests, representative results should be summarized in order to discuss for the better design of catalysts. Thus the screening results were summarized in this chapter classified by steam reforming, partial oxidation and dry reforming. As mentioned in the previous chapter, the model reactant was represented by tetradecane. Based on the data gathered from preliminary experiments [51,52] the alloy tubes were activated through oxidation pretreatment using O_2 at 1000ºC for 120 min. The catalytic performance of these preoxidized alloys were the evaluated by partial oxidation, steam reforming, and dry reforming of tetradecane. The data obtained are presented in this chapter as well as in the author's published works, as listed below:

1. Partial Oxidation Catalysts Derived from Ni Containing Alloys for Biomass Gasification Process;
2. Preliminary Assessment of Oxidation Pretreated Hastelloy as Hydrocarbon Steam Reforming Catalyst; and
3. Evaluation of Pre-oxidized SUS304 as a Catalyst for Hydrocarbon Reforming

2.2 Materials and Method

2.2.1 Experiment Set-Up

Commercially available nickel-containing alloy tubes evaluated in this study are listed in Table 2.1. Alloy tube preoxidation and tetradecane dry reforming reactions were performed using a bench top quartz tube reactor. The diagram of the set-up is shown in Figure 2.1. The apparatus was composed of a hydrocarbon syringe pump, a vaporizer, an electrically heated furnace, a fabricated quartz tube (inner diameter: 1 cm), a condenser, and a gas sampling valve. The alloy tube (outer diameter: 0.64 cm, length: 35cm) was inserted into the quartz tube, secured using a rubber plug and positioned at the center of the furnace. A teflon tube was used to seal and connect the upper (inlet) and lower (outlet) ends of the reactor to the vaporizer and condenser, respectively. The outer surface of the tube was used as a catalyst. The temperature of the vaporizer was maintained at 200°C while the condenser was cooled using a re-circulating coolant pump. Water vapor and unreacted hydrocarbon feedstock were condensed and collected inside the condenser located before the gas sampling valve. Gas samples were manually collected by a syringe every 30 min.

Table 2.1. Names and composition of nickel-containing alloys evaluated

Alloy	Metal Composition (wt. %)											
	C	Al	Co	Si	Mn	P	S	Ni	Cr	Mo	V	Fe
SUS 304	<0.08			<1.0	<2.0	<0.05	<0.03	10.0~14.0	18.0~20.0			Bal
Inconel 600	<0.15				<1.0			<72.0	14.0~17.0			6.0~10.0
Inconel 601		1.0~1.7						58.0~63.0	21.0~25.0	<1.00		Bal
Superinvar	0.07		4.0~6.0		0.3~0.4			31.0				Bal
Hastelloy	0.02		2.50	0.08				57.0	14.5~16.5	15.0~17.0		4.0~7.0
Kovar*	0.06		17.0	0.20	0.50			29.0			0.1	Bal

*Kovar was not included during the screening experiment. The effect of preoxidation temperature on the potential of Kovar as a dry reforming catalyst is discussed in Chapter 4.

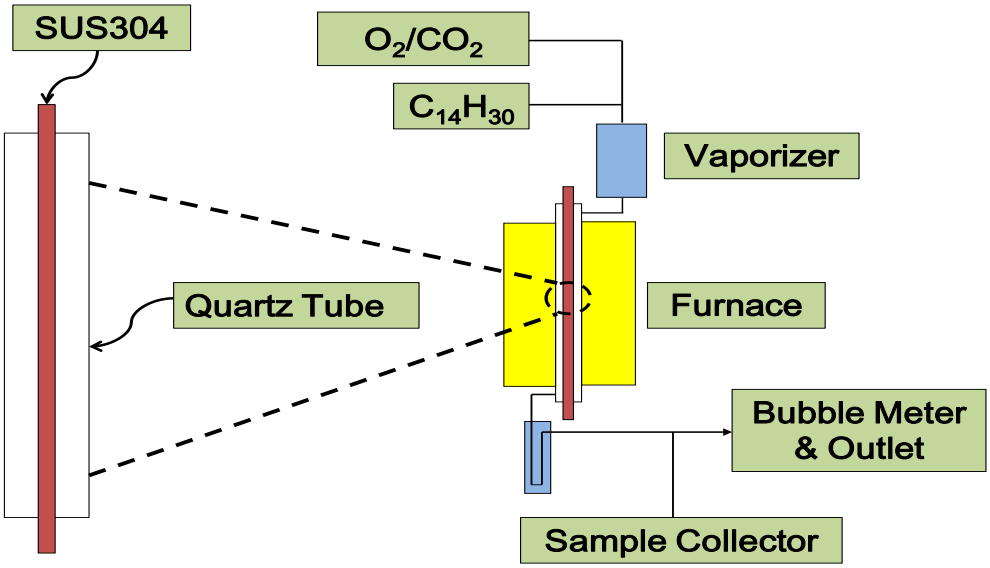

Figure 2.1. Diagram of the reactor used for SUS304 oxidation pretreatment and hydrocarbon dry reforming reactions

Mass flow controllers were employed to control and monitor the flow of reactant gases while a syringe pump regulated the flow rate and delivery of tetradecane into the vaporizer. To monitor the flow rate of the effluent gases, soap bubble meter was installed after the sampling valve.

2.2.2 Catalyst Screening and Gas Chromatography

Alloy tubes were preoxidized at 1000ºC in O_2 (1ml/s) for 120 min prior to their catalytic evaluation for hydrocarbon reforming reactions. The temperature of the reactor was set to reach and stabilize at 1000ºC within 30 min. After the 120 min preoxidation step, the reactor's temperature gradually adjusts to the desired reforming reaction temperature for approximately 30 min while O_2 is continuously supplied into the system. After the desired temperature is reached, reactant gases and hydrocarbon feedstock are then introduced into the reactor.

Tetradecane (1 μmol/s) was used as model compound during steam reforming, dry reforming and partial oxidation experiments. Catalytic evaluation was conducted at 730ºC. Corresponding reactant gases were supplied into the reactor; O_2 (7.5 μmol/s) for partial oxidation, H_2O (150 μmol/s) and N_2 (36.3 μmol/s) for steam reforming, and CO_2 (35 μmol/s) for dry reforming reaction. Gas hourly surface velocities (GHSV) for this study were calculated at standard ambient temperature and pressure (SATP). Effluent gas from each catalytic reaction was analyzed for CO_2, CO, CH_4, H_2, N_2 and O_2 in a dry basis using a

Thermal Conductivity Detector coupled Gas Chromatograph with a WG-100 column (GL-Sciences). The production rates (P_A) of each product gas was calculated using Equation 2.1 where molar ratio of the specific product gas (X_A) was divided by the effluent gas flow rate (Y_{EF}) measured at the reactor's outlet. Condensed water vapor was also not quantified because not enough volume was accumulated within the 30 min sampling interval.

$$P_A = \frac{X_A}{Y_{EF}} \qquad \text{(Eq. 2.1)}$$

In comparing the catalytic activity of the evaluated alloy tubes, CO production rate was used as a basis since H_2 can also be produced via hydrocarbon decomposition, a side reaction that could lead to carbon formation [23].

2.3 Results: Catalyst Screening

The main reaction involved during catalytic tetradecane partial oxidization (Reaction 2.1), steam reforming (Reaction 2.1) and dry reforming (Reaction 2.3):

$C_{14}H_{30}+7O_2 \rightarrow 14CO+15H_2$ (2.1)

$C_{14}H_{30}+14H_2O \rightarrow 14CO+29H_2$ (2.2)

$C_{14}H_{30}+14CO_2 \rightarrow 28CO+15H_2$ (2.3)

2.3.1 Catalytic Partial Oxidation Reaction

The production rates of CO, H_2, and CH_4 taken at the 120th min of the reaction conducted over the tested alloys are shown in Table 2.2. Arranging the preoxidized alloys in decreasing catalytic activity based on their respective CO production rates:

Hastelloy→ Superinvar→ SUS304→ Inconel 600→ Inconel 601

In addition, the experimental H_2/CO ratios of the reaction conducted over preoxidized alloy tubes, with the exception of Inconel 600 and 601, were higher than the calculated theoretical value (1.07). This was probably due to the complete oxidation of CO to CO_2 which resulted to lower CO in the effluent gas or the decomposition of the tetradecane and other hydrocarbon fragments which produced more H_2 and carbonaceous deposit. Also, no distinct pattern can be established from CH_4 production rate with respect to CO and H_2 production rates

thus it was concluded that methane production did not depend on the type of catalyst used; instead, it could have primarily been generated through hydrocarbon decomposition.

Based on the screening test results, a long term reaction experiment was done using preoxidized Hastelloy (Fig. 2.2). The observed CO production rate became stable on the 2nd day (>1000 min) with a H_2/CO ratio that was almost

Table 2.2. Activity of preoxidized alloys during tetradecane partial oxidation

Alloy	Production Rate (μmol/s)*			H_2/CO
	CO	H_2	CH_4	
SUS304	6.74	10.1	0.93	1.50
Inconel 600	1.7	0.89	1.13	0.52
Inconel 601	1.76	0.89	1.02	0.51
Superinvar	6.51	13.7	0.24	2.10
Hastelloy	7.18	10.3	1.68	1.43

*data presented were from gas samples collected at the 120 min of the reaction

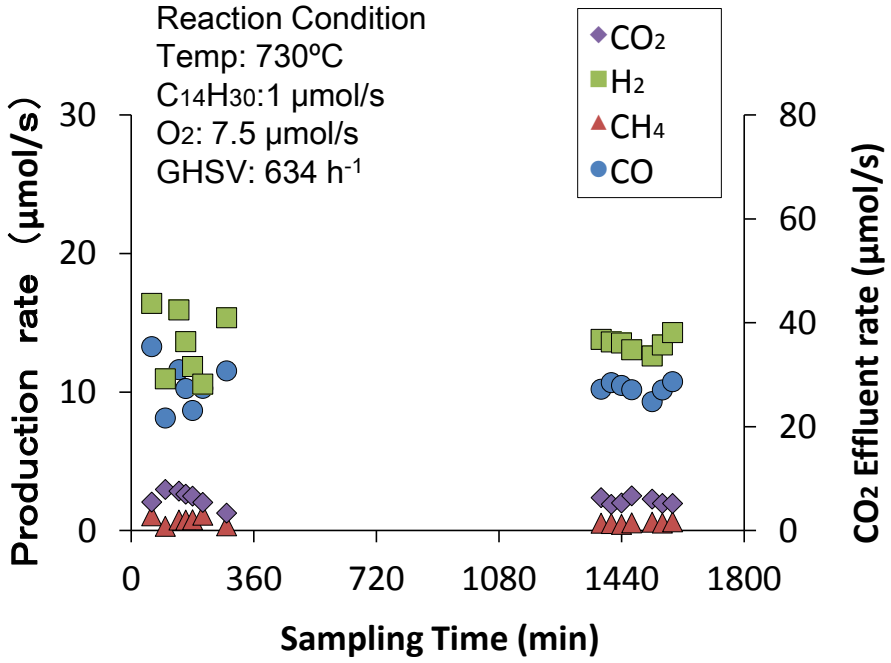

Figure 2.2. Quantitative analysis of effluent gas during tetradecane partial oxidation performed over Hastelloy preoxidized at 1000ºC for 120 min

equal to the theoretical value; it was deduced that time affects the reaction rate of the catalyst. The reaction was terminated on the 3rd day due to massive carbon build up which plugged the reactor. It was suspected that during the long term reaction, the formerly dispersed catalytically active cites gradually formed larger particles via sintering which then decreased the catalyst's surface area while consequently acting as nucleating cites for carbon formation.

2.3.2 Catalytic Steam Reforming

When the preoxidized alloys were applied to tetradecane steam reforming (Table 2.3), their catalytic activity can be arranged as:

Hastelloy→ Superinvar→ Inconel 600→ Inconel 601, SUS304

with Hastelloy being the most active. Noticeably, when the reaction was conducted over Inconel 601 and SUS304, only H_2 and CH_4 were generated. It was inferred that hydrocarbon thermal decomposition produced H_2, CH_4, and possibly carbonaceous deposits. The absence of CO in the effluent gases during Inconel 601 and SUS304 catalyzed reactions indicated that steam reforming reaction did not take place. The collected data coincides with the published data of other researchers saying that during hydrocarbon steam reforming the total volume of product gas is usually 70-80% H_2 [15,16]. This made the experimental H_2/CO ratios for all catalytically active alloys (Inconel 600, Superinvar, and Hastelloy) higher than the reaction's theoretical value (2.07). Based on these observations, it was inferred that the CO produced through steam reforming reaction are being simultaneously consumed by the WGS reaction (Reaction 1.1) to produce more H_2 and CO_2.

Table 2.3. Activity of preoxidized alloys during tetradecane steam reforming

Alloy	Production Rate (μmol/s)*			**H_2/CO**
	CO	**H_2**	**CH_4**	
SUS304	0	0.73	0.74	--
Inconel 600	2.75	24.4	1.13	8.87
Inconel 601	0	2.23	1.63	--
Superinvar	2.76	9.44	1.44	3.42
Hastelloy	7.45	21.5	0.99	2.89

*data presented were from gas samples collected at the 120 min of the reaction

A long term reaction was then performed over Hastelloy, the most active alloy. The collected data (Fig. 2.3) showed that it was able to maintain a stable activity for 2 days (≤ 2880 min) followed by gradual deactivation. The decline in CO, H_2 and CO_2 were interpreted to be a manifestation of catalyst deactivation most likely brought about by the accumulation and conversion of hydrocarbon fragments to carbonaceous deposits.

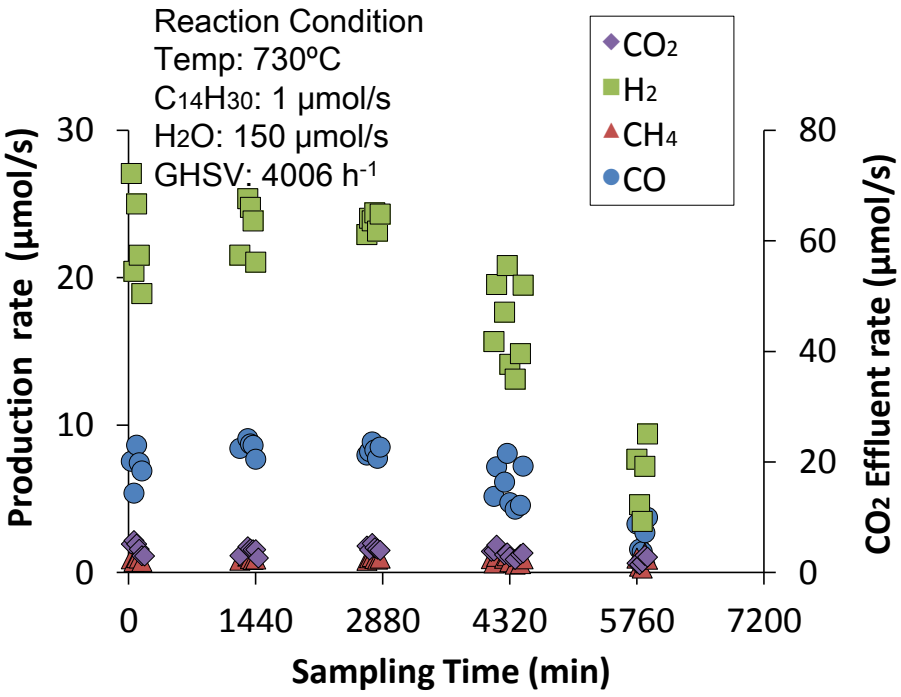

Figure 2.3. Quantitative analysis of effluent gas during tetradecane steam reforming performed over Hastelloy preoxidized at 1000ºC for 120 min

2.3.3 Catalytic Dry Reforming

As suggested by Takano et al. [27] to prevent the rapid deactivation of the tested alloys, approximately 2 times the stoichiometric equivalence CO_2 was supplied to the reactor during tetradecane dry reforming reaction (Table 2.4). Using CO as an indicator of the alloy's activity, listing the alloys in decreasing activity

Superinvar→ SUS304→ Hastelloy→ Inconel 600, Inconel 601

Table 2.4. Activity of preoxidized alloys during tetradecane dry reforming

Alloy	Production Rate (μmol/s)*			H_2/CO
	CO	H_2	CH_4	
SUS304	7.62	2.61	1.88	0.34
Inconel 600	0	0.98	1.16	--
Inconel 601	0	1.02	1.28	--
Superinvar	22.6	6.55	0.79	0.29
Hastelloy	3.01	2.73	1.42	0.91

*data presented were from gas samples collected at the 120 min of the reaction

The distinctively high CO production rate observed when the reaction was conducted over Superinvar was attributed to the synergistic effects of cobalt and nickel [34] on the catalytic activity of preoxidized Superinvar. Hastelloy, another Co-containing alloy (Table 2.1), was expected to follow Superinvar in terms of CO production rate. However, this was not observed thus, it was concluded that the relative abundance of the alloying metals significantly affects the catalytic activity of an alloy.

Contrary to the high experimental H_2/CO observed during partial oxidation and steam reforming reactions, experimental H_2/CO ratio during tetradecane dry reforming was lower than its theoretical value (0.52). This implied that H_2 was consumed possibly by RWGS reaction (Reaction 1.10) and/or CO hydrogenation (Reaction 2.4).

$$H_2+CO \rightarrow H_2O+C \qquad (2.4)$$

2.4 Conclusion

Catalyst screening showed that oxidation pretreatment at 730ºC rendered the alloys catalytically active towards tetradecane partial oxidation, steam reforming, and dry reforming. For partial oxidation, preoxidized Hastelloy exhibited the highest catalytic activity but was deactivated due to sintering consequently leading to carbon build up in the reactor. Preoxidized Hastelloy also showed the highest activity during tetradecane steam reforming. However, it should be noted that WGS reaction significantly affects the H_2/CO of its product gas. Catalyst deactivation, due to carbon deposit, was also observed after 3 days (≤2880 min). Based on the alloying composition of the tested alloys (Table 2.1), it was deduced that the relatively high amount of molybdenum, 15-17 %wt, present in Hastelloy could have contributed to its activity towards tetradecane partial oxidation and steam reforming. However, further studies are needed to confirm this assumption. In the case of dry reforming reaction, it was inferred from the collected data that cobalt and nickel synergistically functioned as a catalyst making Superinvar the most active alloy among those discussed in this chapter.

At this point of the study, the author decided to focus on dry reforming reaction with the prospect of CO_2 utilization. Also, instead of Superinvar another Co-containing alloy (Kovar) was evaluated for dry reforming reaction (Chapter 4). In addition to Kovar, SUS304 was also subjected to further study since it is relatively low-priced and does not contain other potential active components such as cobalt and molybdenum; thus, data collected from SUS304 catalyzed reactions can be used as arbitrary baseline.

CHAPTER III

Influence of Reaction Parameters on the Performance of Preoxidized SUS304 as Dry Reforming Catalyst

3.1 Introduction

From 2012, The National Institute for Environmental Studies (NIES) of Japan has started a new biomass gasification project using partial oxidation reaction. The possibility of electrochemical separation of air to oxygen has been widely studied. In this system catalytic dry reforming of the tar materials should be quite important in addition to steam reforming reaction. As mentioned in the previous chapter, the author decided to concentrate on the use of preoxidized alloy catalyst in the dry reforming reaction system. This chapter investigates the influence of reaction parameters on the catalytic activity of preoxidized SUS304 applied in tetradecane dry reforming (unpublished data). Based on the data collected from the preliminary experiment conducted on alloy preoxidation temperature, SUS304 was preoxidized at 1000°C for 120 min in O_2 [52]. Oxidation studies conducted on SUS304 revealed that at 1000°C the protective Cr_2O_3 layer is decomposed [40] thus exposing the other alloy components, making the catalytically active component (nickel) accessible to the reactants and consequently rendered SUS304 catalytically active. Different reaction temperatures and CO_2 flow rates were used during tetradecane reforming reactions performed over preoxidized SUS304. The effects of these parameters on the activity and stability of the reaction were compared and correlated in terms of CO and H_2 production rates.

3.2 Materials and Method

3.2.1 Tetradecane Dry Reforming and Gas Chromatography

Oxidation pretreatment and catalyst evaluation were done using the bench-top reactor described in Chapter 2 (Fig. 2.1). SUS304 preoxidized at 1000°C in oxygen (1ml/s) for 120 min was used as a catalyst during tetradecane (1 µmol/s) dry reforming conducted at 700, 800 and 900°C using 14, 42 and 70 µmol/s of CO_2. The corresponding GHSV at SATP were respectively calculated as 1150 h^{-1}, 3408 h^{-1}, and 5666 h^{-1} when 14, 42, and 70 µmol/s of CO_2 was fed into the reactor. Temperature-CO_2 flow rate combinations used are listed in Table 3.1. Effluent gas was analyzed for CO_2, CO, CH_4, and H_2 in a dry basis as described in Chapter 2. Hydrocarbons above C_2 resulting from tetradecane decomposition as well as unreacted tetradecane were not quantified since the column used did not allow this. In addition, carbon atomic mass balance was used to indicate the formation of carbonaceous deposits and qualitatively evaluate the conversion of tetradecane to gas products. Carbon mass balance (CMB) was calculated by dividing the sum of the molar flow rates of CO (F_{CO}), CH_4 (F_{CH4}), and CO_2 (F_{CO2}) in the effluent gas to the sum of the molar flow rates of the reactants, $C_{14}H_{30}$ and CO_2, introduced into the reactor as shown by

Table 3.1. Reaction temperature-CO_2 flow rate combinations used

CO_2 Flow Rate (µmol/s)	**Reaction Temperature (°C)**		
	700	**800**	**900**
14	700-14	800-14	900-14
42	700-42	800-42	900-42
70	700-70	800-42	900-70

Equation 3.1. This was adapted from the method used by the Environmental Protection Agency (EPA) to measure fuel consumption [53]. CMB was based on the fundamental principle that mass can neither be created nor destroyed; thus, when CMB<1 it was assumed that the unaccounted carbon in the effluent gas were retained on the surface of the catalyst as carbon [54]. Finally, condensed water vapor was not quantified because not enough volume was accumulated inside the condenser within the 30 min sampling interval.

$$\mathrm{CMB} = \frac{F_{CO}+F_{CH_4}+F_{CO_2}}{14F_{(C_{14}H_{30})}+F_{(CO_2)}} \qquad \text{(Eq. 3.1)}$$

3.2.2 Catalyst Characterization

The types of metal oxide formed after SUS304 preoxidation were determined using an X-ray Diffractometer (Rigaku RINT-25000TTR) with CuKα as the source (50 kV, 100 mA, λ=1.54); scanning was done from 30° to 60°. In addition, morphological and elemental analyses were performed with a Scanning Electron Microscope (JSM-6330F) with Energy Dispersive Spectrometer (SEM-EDS). The above mentioned analyses were performed on an approximately 1 cm portion of the sample alloy tube that was manually cut and pressed.

3.3 Results:Catalytic Dry Reforming Reaction

Considering the reaction temperatures applied in this study and the mechanism proposed by Solymosi et al. [23] with propane as a model compound, it was assumed that aside from the main reaction (Reaction 3.1) hydrocarbon fragments resulting from tetradecane decomposition also react with CO_2 (Reaction 3.2) to give CO and H_2 or decompose to carbon and H_2 (Reaction 3.3) at high temperatures (>700°C). On the other hand, carbon was formed via CO hydrogenation (Reaction 2.4) when conducting the reaction at low temperatures (≤700°C) [20]. RWGS reaction (Reaction 1.10) was also considered to take place with dry reforming.

$$C_{14}H_{30}+14CO_2 \leftrightarrow 28CO+15H_2 \quad (3.1)$$

$$C_mH_n+CO_2 \leftrightarrow CO+H_2 \quad (3.2)$$

$$C_mH_n \leftrightarrow mC+2H_2 \quad (3.3)$$

3.3.1 CO_2 Flow Rate: 14 µmol/s

Applying the stoichiometric amount of CO_2 (14µmol/s) at 700°C showed a gradual decrease in CO production and CO_2 consumption rates, while H_2 and CH_4 production rates were stable (Fig. 3.1a). The decline in CO production rate may be caused by CO hydrogenation (Reaction 2.4), which produced carbon from the reaction of CO and H_2. Although this reaction also consumes H_2, it must be noted that additional H_2 was being simultaneously produced via tetradecane decomposition; therefore its effect on H_2 is relatively unnoticeable. Despite the gradual drop in dry reforming reaction, the rate of tetradecane decomposition was assumed to be stable based on the production rates of H_2 and CH_4. Further, the obtained H_2/CO (Fig. 3.1b) indicated high H_2 production rate, a probable result of low RWGS reaction rate because of the limited amount of CO_2 in the system. Lastly, the obtained carbon balance of the reaction suggested that the formation of carbon was at a constant rate. The details of carbon formation will be discussed in section 3.3.5.

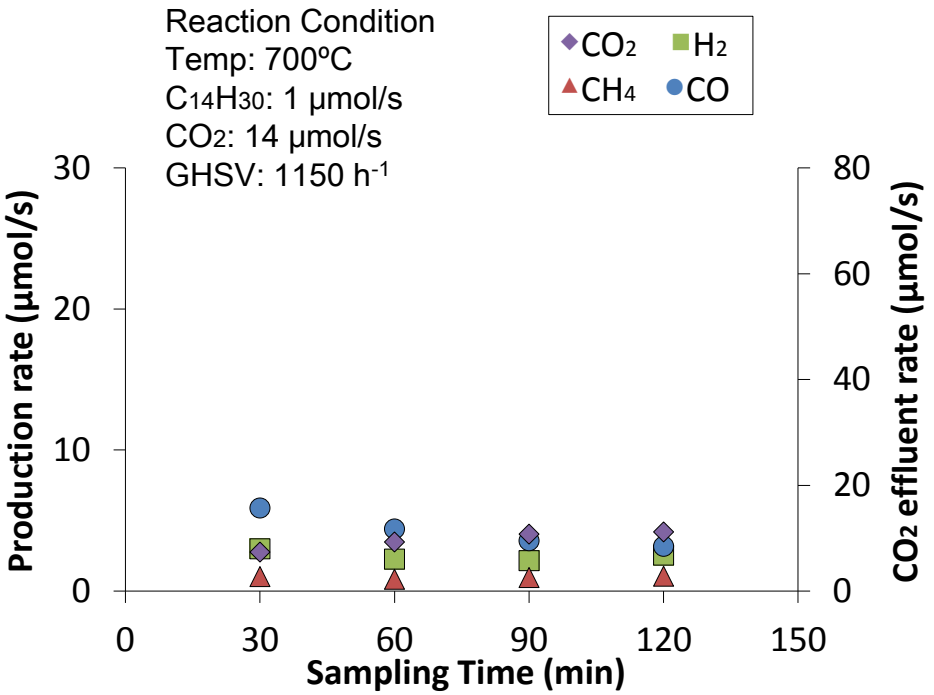

Figure 3.1a. Quantitative analysis of effluent gas during tetradecane reforming at 700°C with 14µmol/s CO_2 performed over SUS304 preoxidized at 1000ºC for 120 min

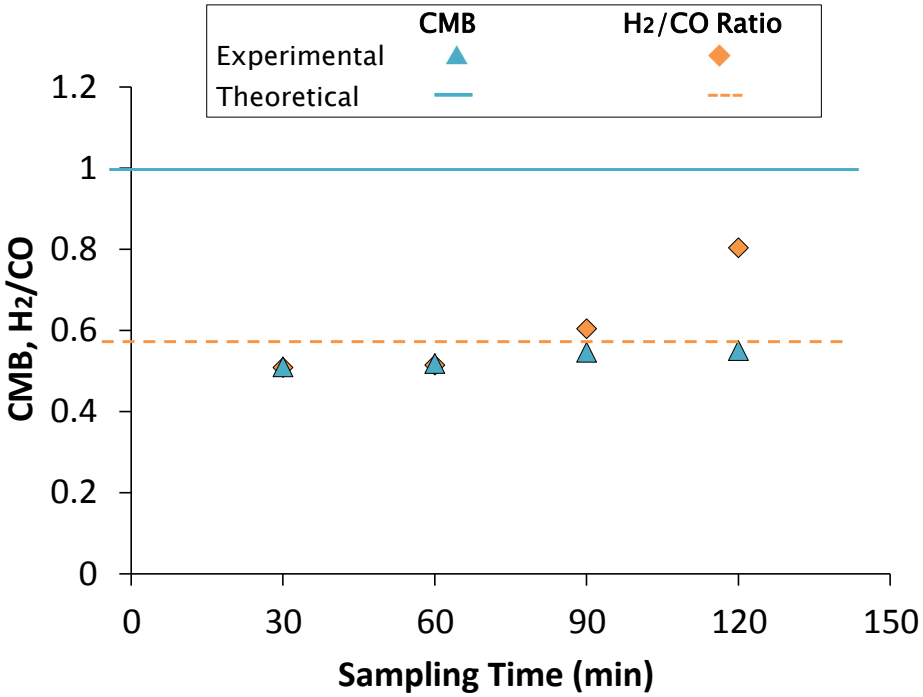

Figure 3.1b. Carbon mass balance and H_2/CO ratio of effluent gas during tetradecane reforming at 700°C with 14µmol/s CO_2 performed over SUS304 preoxidized at 1000ºC for 120 min

When the reaction temperature was increased to 800°C the very low CO_2 consumption rate observed 30 min after the reaction was started indicated slow rate of dry reforming reaction (Fig. 3.2a). Based on its corresponding CO and H_2 production rates, it was deduced that hydrocarbon decomposition produced hydrocarbon fragments (C_mH_n) and H_2. Since H_2 was mainly generated via hydrocarbon decomposition, high H_2/CO during this particular sampling time (Fig. 3.2b) was noted. On the other hand, the C_mH_n were assumed to be eventually reformed to produce CO and H_2. During the first 30 min of the reaction, the catalysts was inferred to experience morphological and/or compositional changes which consequently improved its catalytic activity as shown by the subsequent increase in CO_2 consumption and CO production rates (Fig. 3.2a). At this point, H_2 production was assumed to be primarily generated through dry reforming reaction. The catalyst was able to keep its activity at a generally stable rate up to the end of the 120 min experiment (Fig. 3.2a) with minamal amount of carbon formed as suggested by its high CMB (Fig. 3.2b). The observed H_2/CO ratio (Fig. 3.2b) also implied that the effect of RWGS reaction remained insignificant at 800°C probably because of the limited amount of CO_2 available in the system.

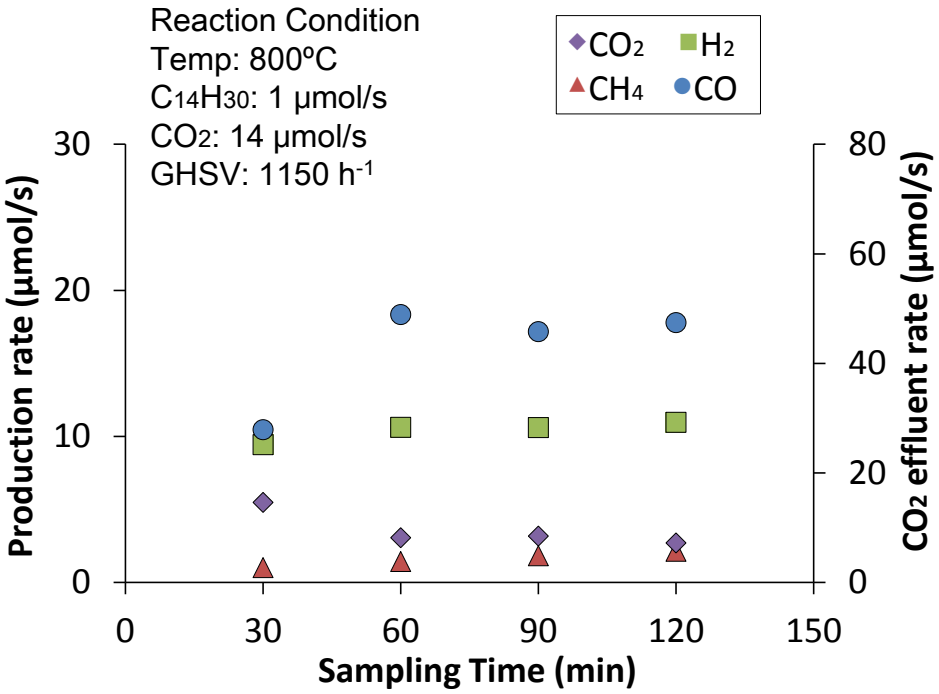

Figure 3.2a. Quantitative analysis of effluent gas during tetradecane reforming at 800°C with 14µmol/s CO_2 performed over SUS304 preoxidized at 1000ºC for 120 min

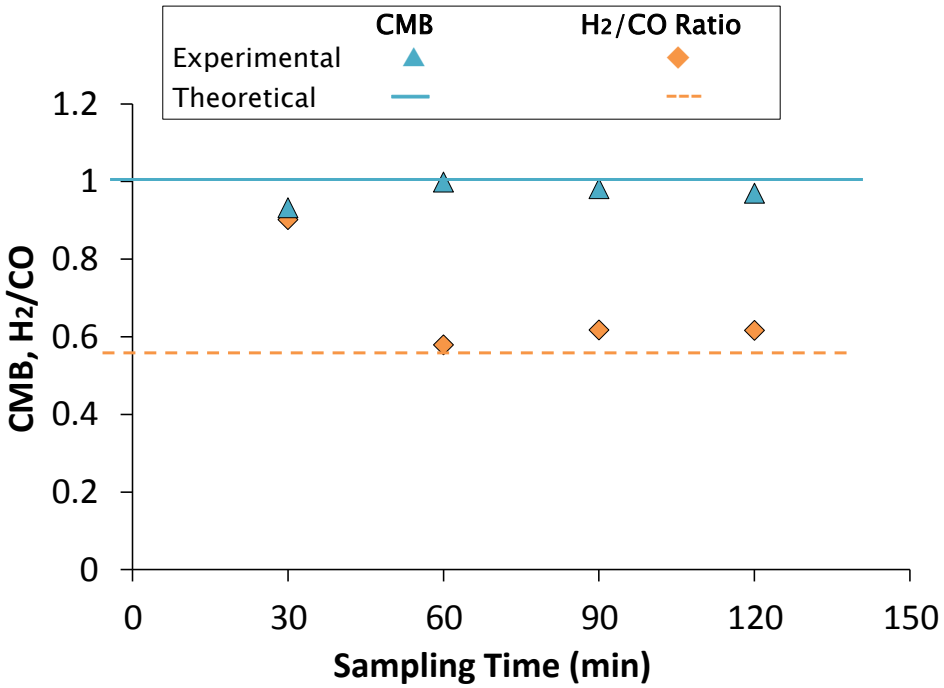

Figure 3.2b. Carbon mass balance and H_2/CO ratio of effluent gas during tetradecane reforming at 800°C with 14µmol/s CO_2 performed over SUS304 preoxidized at 1000ºC for 120 min

When the reaction was conducted at 900°C, CO and H_2 production rates were higher (Fig. 3.3a) when compared to reactions conducted at 700 and 800°C. An initial increase in CO production rate was observed before being stable, a pattern that was also observed when the reaction was conducted at 800°C. It was also assumed that morphological and composition changes on the catalyst simultaneosuly occurred with the reaction. In addition, high experimental H_2/CO (Fig. 3.3b) may have resulted from the additional H_2 produced via tetradecane decomposition which simultaneaously took place with dry reforming reaction. Although tetradecane decomposition also produces hydrocarbon fragments that may eventually turn into carbon deposit on the surface of the catalyst, the catalyst continued to exhibit good catalytic activity with minimal carbon formed as suggested by its carbon balance (Fig. 3.3b). Lastly, high H_2/CO suggested that the effect of RWGS reaction remained to be insignificant due to the limited amount of CO_2.

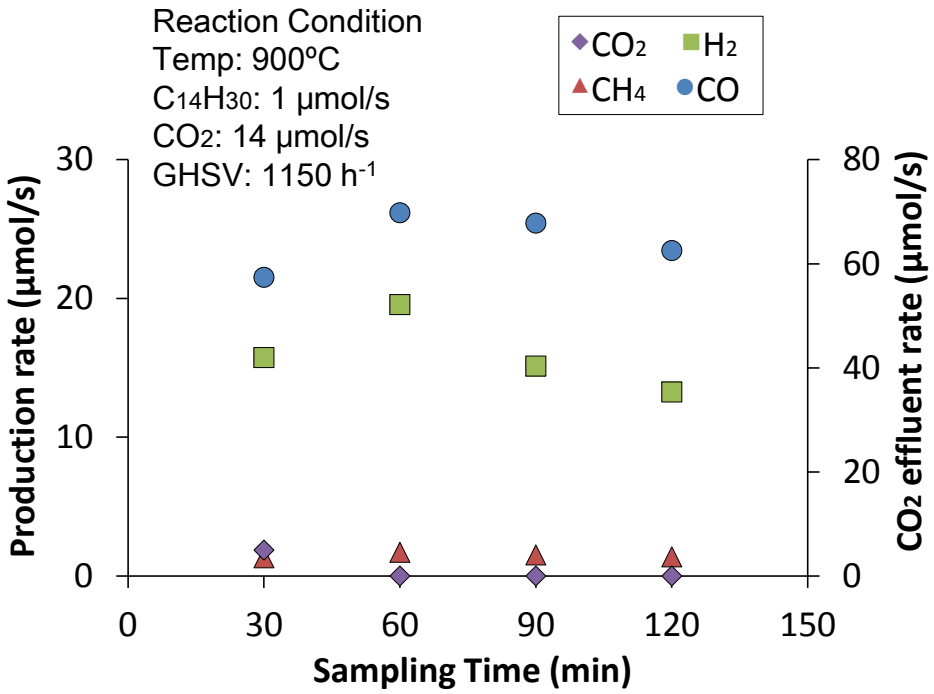

Figure 3.3a. Quantitative analysis of effluent gas during tetradecane reforming at 900°C with 14µmol/s CO_2 performed over SUS304 preoxidized at 1000ºC for 120 min

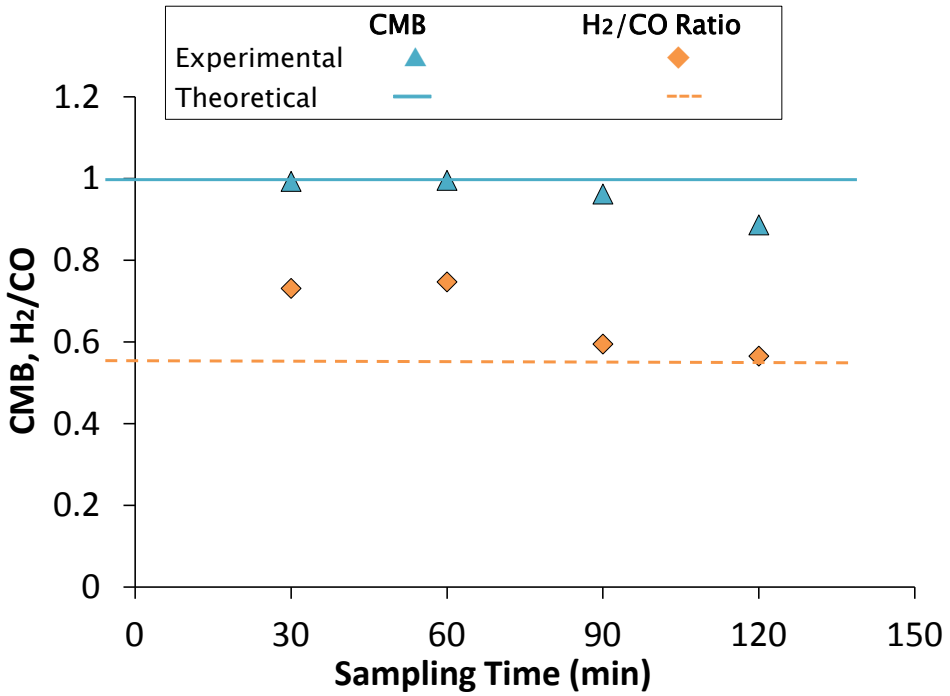

Figure 3.3b. Carbon mass balance and H_2/CO ratio of effluent gas during tetradecane reforming at 900°C with 14µmol/s CO_2 performed over SUS304 preoxidized at 1000ºC for 120 min

3.3.1.1 Section Summary

The collected data from this section showed that although preoxidized SUS304 displayed relatively good and stable catalytic activity towards tetradecane dry reforming, its application at low reaction temperature (700°C) resulted into poor activity and low carbon balance. Supplying excess amount of CO_2 was reported to retard carbon formation thus the effect of supplying higher CO_2 flow rates into the reactor was investigated in the next sections.

3.3.2 CO_2 Flow Rate: 42 µmol/s

When the reaction was performed at 700°C, stable CO and H_2 production rates were observed up to the 90th min of the reaction (Fig. 3.4a). After which, both CO and H_2 production rates abruptly dropped, probably because the catalyst was deactivated by carbon that has accumulated on its surface as suggested by its low carbon balance (Fig. 3.4b). Also, correlating CO and H_2 production rates with the sudden increase in H_2/CO at 120 min indicated that the decrease in CO production rate was more pronounced than that of H_2. From this, it was inferred that H_2 was generated by hydrocarbon decomposition that continuously occurred even after the catalyst was deactivated. Aside from hydrocarbon decomposition,

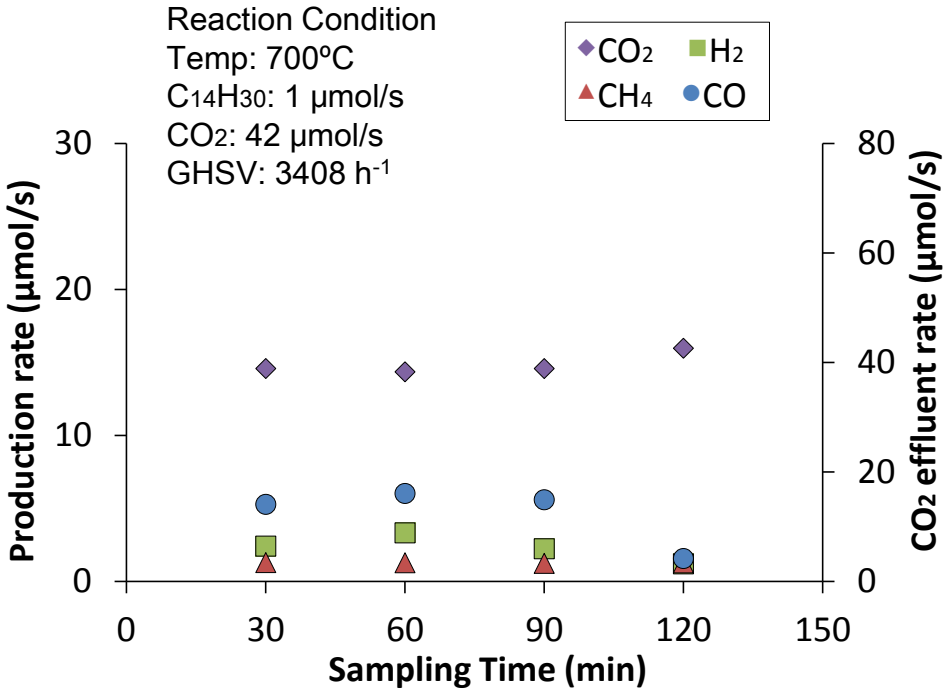

Figure 3.4a. Quantitative analysis of effluent gas during tetradecane reforming at 700°C with 42µmol/s CO_2 performed over SUS304 preoxidized at 1000ºC for 120 min

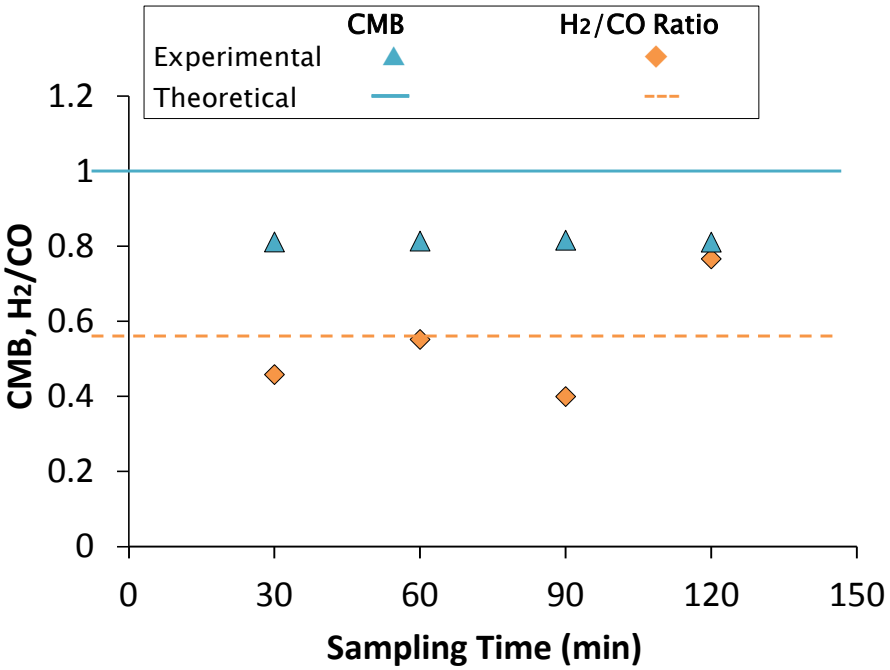

Figure 3.4b. Carbon mass balance and H_2/CO ratio of effluent gas during tetradecane reforming at 700°C with 42µmol/s CO_2 performed over SUS304 preoxidized at 1000ºC for 120 min

carbon could have formed through CO hydrogenation (Reaction 2.4). CO hydrogenation consumed CO and H_2 thus negatively affecting both the reaction products and the catalyst. The excess CO_2 supplied could have also reacted with H_2 through RWGS reaction which lowered the amount of H_2 in the effluent gas and in effect gave the reaction a lower H_2/CO ratio (Fig. 3.4b). The unstable H_2/CO despite stable CO and H_2 production rates suggested that catalyst site responsible for RWGS reaction was more sensitive towards the negative effects of carbon deposited on the surface of the catalyst while active sites responsible for dry reforming reaction remained active, stable and accessible up to 90 min.

When the reaction was conducted at 800°C, CO and H_2 production rates gradually increased with time (Fig. 3.5a). Hydrocarbon decomposition rate was assumed to be stable since CH_4 production rate was practically constant. The effect of RWGS reaction was clearly manifested by the low H_2/CO of the reaction (Fig. 3.5b). The slow increase in H_2/CO indicated that RWGS reaction rate decreased with time. The excess CO_2, a soft oxidant, could have reacted with H_2 through RWGS while concurrently reacting with the catalyst and caused morphological and/or compositional changes as the reaction progressed. These changes could have improved the catalyst's activity towards dry reforming reaction. Further,

carbon formation was also minimal as suggested by carbon balance of the reaction (Fig.3.5b).

At 900°C, fluctuating CO production rate was observed during the first 60 min which then became stable; while both H_2 production and CO_2 consumption were relatively stable (Fig. 3.6a). Hydrocarbon decomposition was assumed to be at a constant rate based on the observed CH_4 production rate. Again, the initial change in activity could have been caused by the changes in the morphology and composition of the catalyst. Experimental H_2/CO ratio also indicated the occurrence of RWGS while carbon balance suggested minimal carbon formation (Fig. 3.6b).

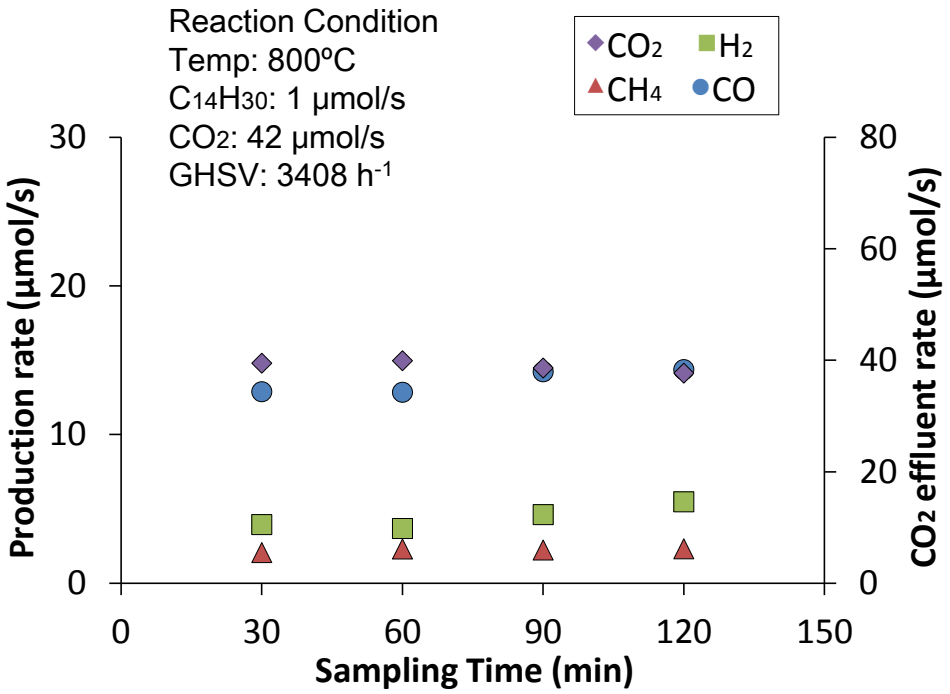

Figure 3.5a. Quantitative analysis of effluent gas during tetradecane reforming at 800°C with 42µmol/s CO_2 performed over SUS304 preoxidized at 1000ºC for 120 min

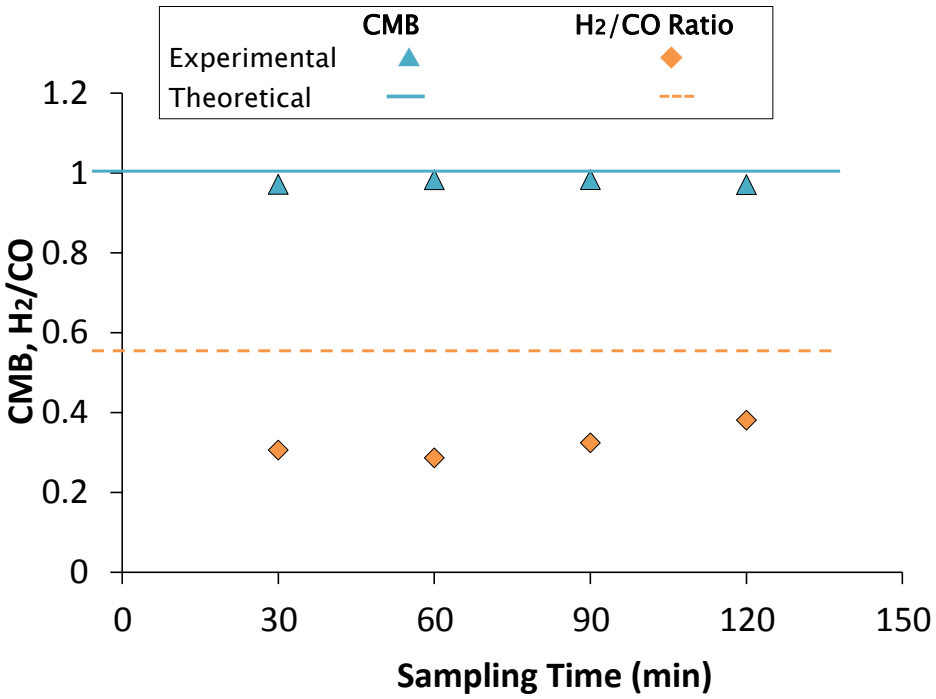

Figure 3.5b. Carbon mass balance and H_2/CO ratio of effluent gas during tetradecane reforming at 800°C with 42μmol/s CO_2 performed over SUS304 preoxidized at 1000ºC for 120 min

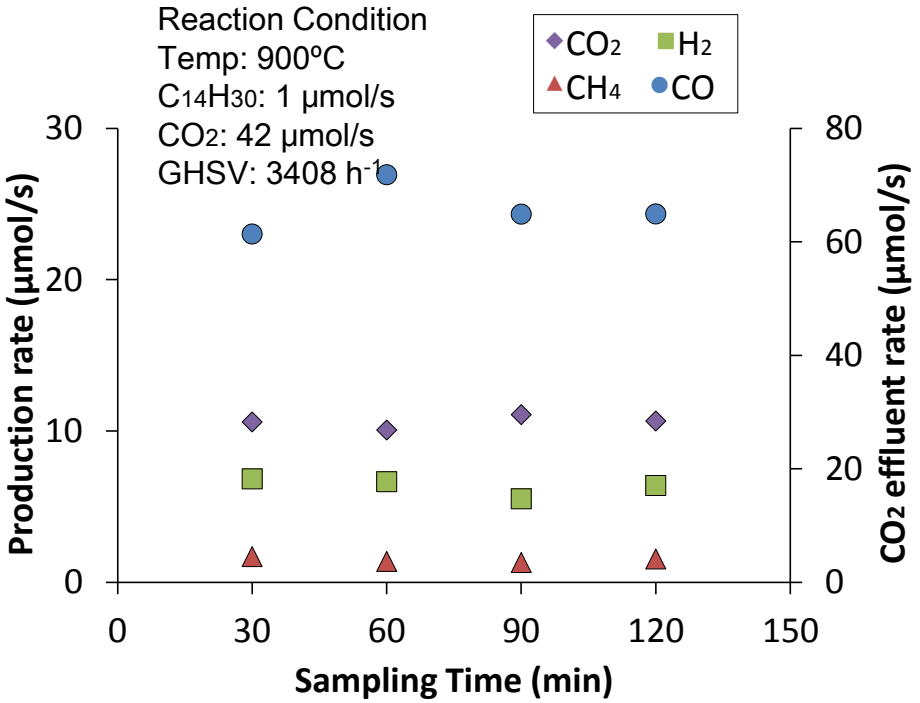

Figure 3.6a. Quantitative analysis of effluent gas during tetradecane reforming at 900°C with 42μmol/s CO_2 performed over SUS304 preoxidized at 1000ºC for 120 min

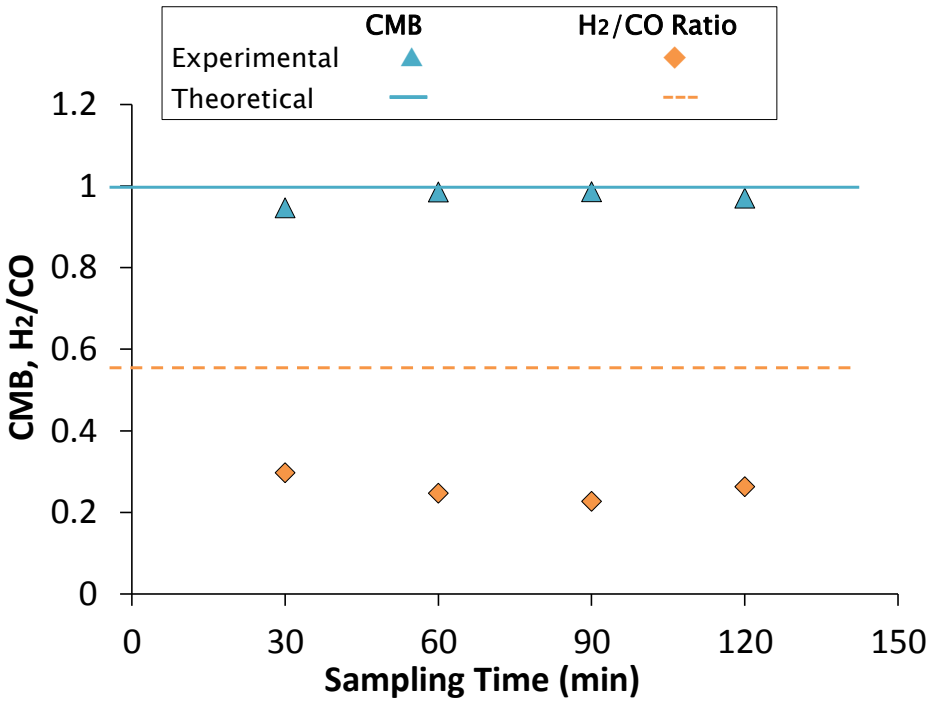

Figure 3.6b. Carbon mass balance and H_2/CO ratio of effluent gas during tetradecane reforming at 900°C with 42µmol/s CO_2 performed over SUS304 preoxidized at 1000ºC for 120 min

3.3.2.1 Section Summary

The presence of excess CO_2 in the reactor favored the occurrence of RWGS reaction which gave H_2/CO ratios that were lower than the theoretical value (~0.50). Also, the data collected implied that the structure and/or composition of the catalyst were changed after sometime in the reaction. CO_2, being a soft oxidant, could have oxidized other alloying components of the catalyst while the reaction was taking place. Further, increasing the CO_2 flow rate from 14 to 42µmol/s reduced the amount of CO and H_2 produced at all reaction temperatures; a possible consequence of shorter catalyst-reactant contact time. Notably, the change in CO is very minimal when compared to H_2 production rate. It was suspected that the excess CO_2 reacted with H_2 via RWGS reaction as indicated by the low H_2/CO ratios obtained from the reactions. As for the amount of carbon formed, higher carbon balance was achieved at all reaction temperatures. Although the most apparent improvement in carbon balance was at 700°C, its CO and H_2 production rates were almost the same when 14 and 42µmol/s of CO_2 was supplied into the reactor.

3.3.3 CO_2 Flow Rate: 70 µmol/s

When the reaction was conducted at 700°C, CO and H_2 production rates were stable (Fig. 3.7a) with high carbon balance (Fig. 3.7b). These implied that the catalyst was able to maintain a stable activity while preventing carbon to form on its surface. In addition, RWGS reaction simultaneously occurred as suggested by the low H_2/CO (Fig. 3.7b).

Raising the reaction temperature to 800°C did not significantly increase the production rate of CO (Fig. 3.8a); however, it reduced the rate of RWGS reaction up to the 90th min of the reaction (Fig. 3.8b). The suppression of RWGS reaction translated into more H_2 in the effluent gas (Fig. 3.8a). Surprisingly, when compared with the reaction conducted at 700°C, lower carbon balance was noted for this reaction temperature (Fig. 3.8b). It was deduced that by increasing the reaction temperature, the amount of C_mH_n being produced via tetradecane decomposition was significantly greater than the amount of C_mH_n being consumed by dry reforming reaction. Unreacted hydrocarbon fragments could have condensed on the surface of the catalyst, resulting into a low carbon balance. In addition, CO_2 consumption also increased with reaction temperature but CO and H_2 production rates did not significantly changed. It was assumed that aside

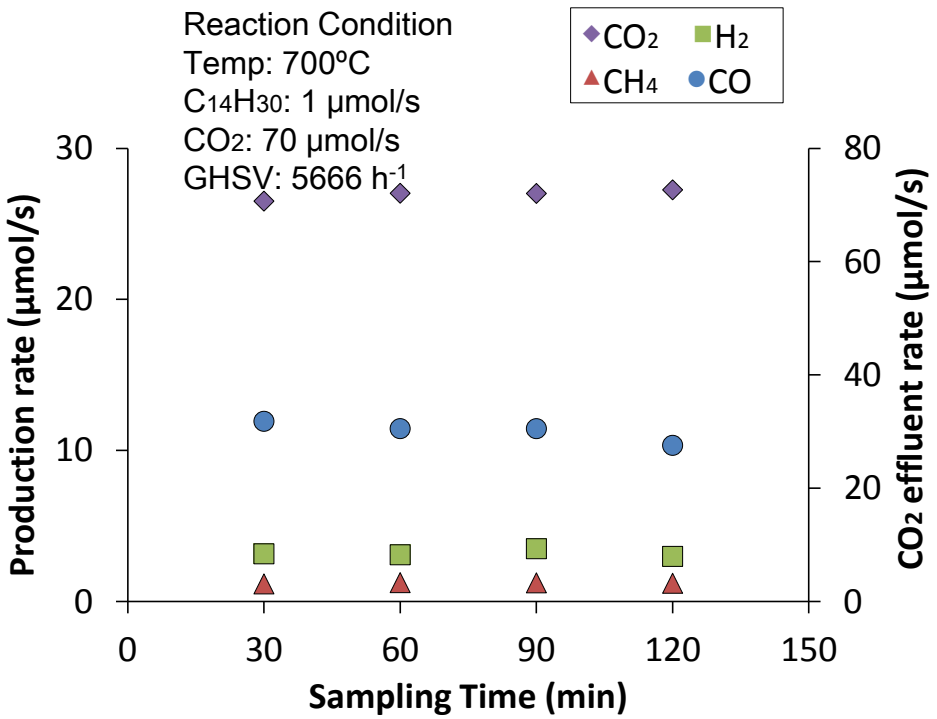

Figure 3.7a. Quantitative analysis of effluent gas during tetradecane reforming at 700°C with 70µmol/s CO_2 performed over SUS304 preoxidized at 1000ºC for 120 min

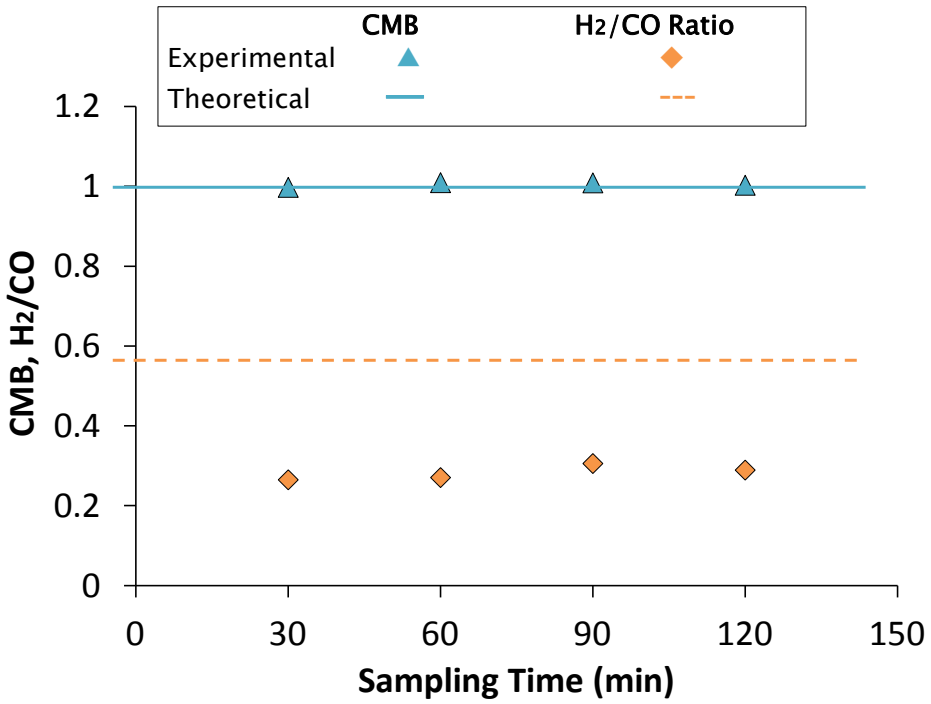

Figure 3.7b. Carbon mass balance and H_2/CO ratio of effluent gas during tetradecane reforming at 700°C with 70µmol/s CO_2 performed over SUS304 preoxidized at 1000ºC for 120 min

from being consumed in the RWGS reaction, CO_2 could have continued on reacting with the catalyst components which eventually resulted into the abrupt change in activity noted at the end of the experiment. Specifically, RWGS was favored over dry reforming reaction therefore the detected CO in the effluent gas at this point (120 min) was possibly generated via RWGS reaction. The observed drop in CO_2 consumption also coincided with this interpretation.

When the reaction temperature was further raised to 900°C, H_2 production rate (Fig. 3.9a) as well as carbon balance (Fig. 3.9b) remained stable throughout the reaction although CO production rate decreased in small increments. CO_2 consumption rate was also noticeably high probably due to the concerted usage of dry reforming and RWGS reactions. In addition, the slight increase in RWGS reaction rate (Fig. 3.9b) was consistent with the decrease in CO production rate (Fig. 3.9a) which implied that the rate of RWGS reaction very slightly decreased with time.

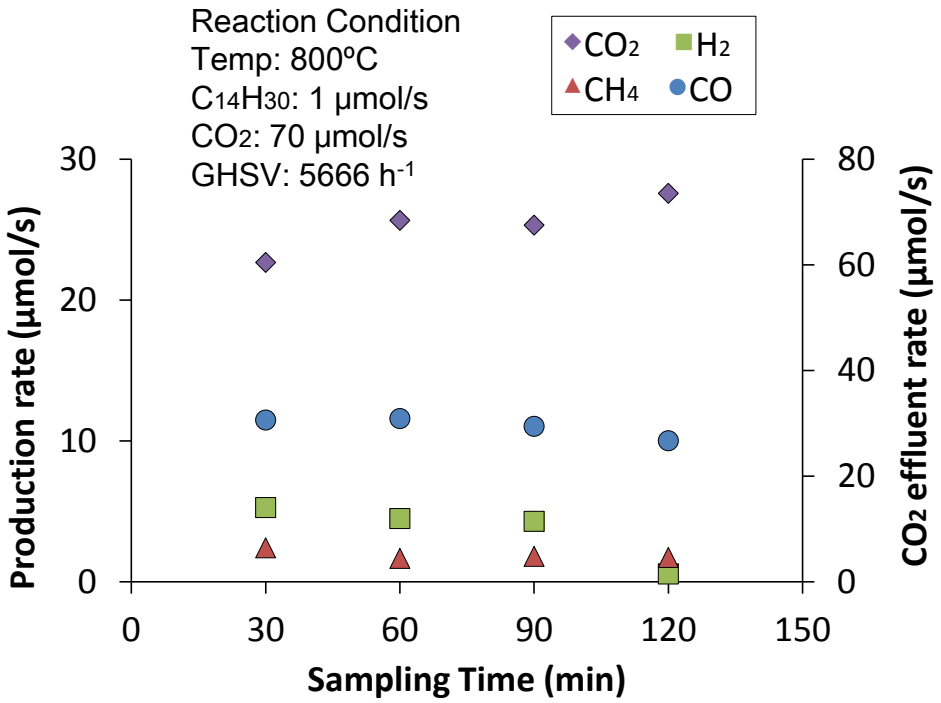

Figure 3.8a. Quantitative analysis of effluent gas during tetradecane reforming at 800°C with 70µmol/s CO_2 performed over SUS304 preoxidized at 1000ºC for 120 min

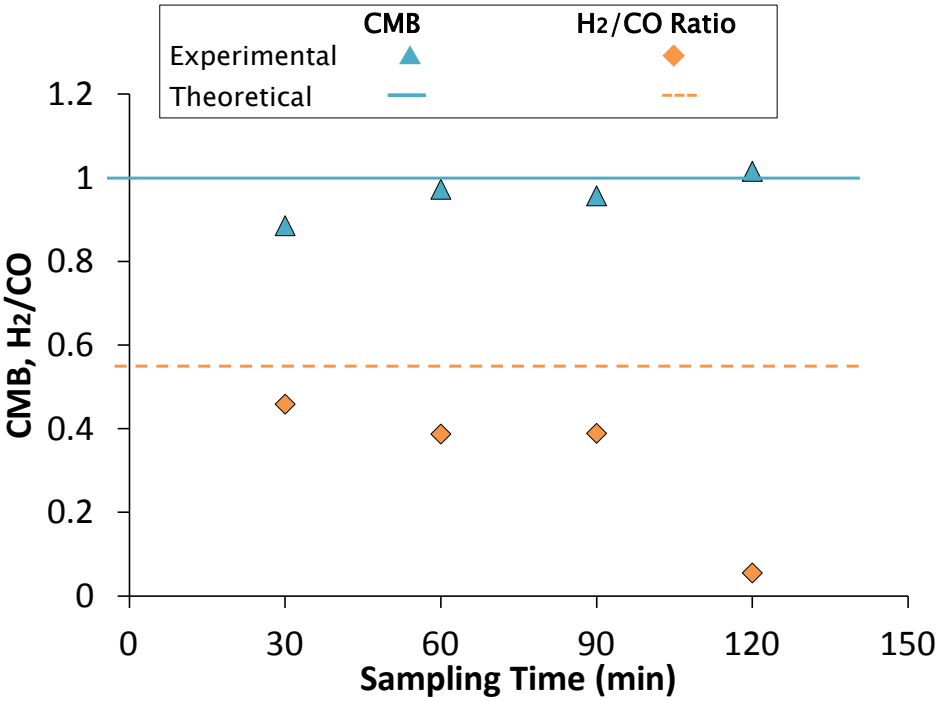

Figure 3.8b. Carbon mass balance and H_2/CO ratio of effluent gas during tetradecane reforming at 800°C with 70µmol/s CO_2 performed over SUS304 preoxidized at 1000ºC for 120 min

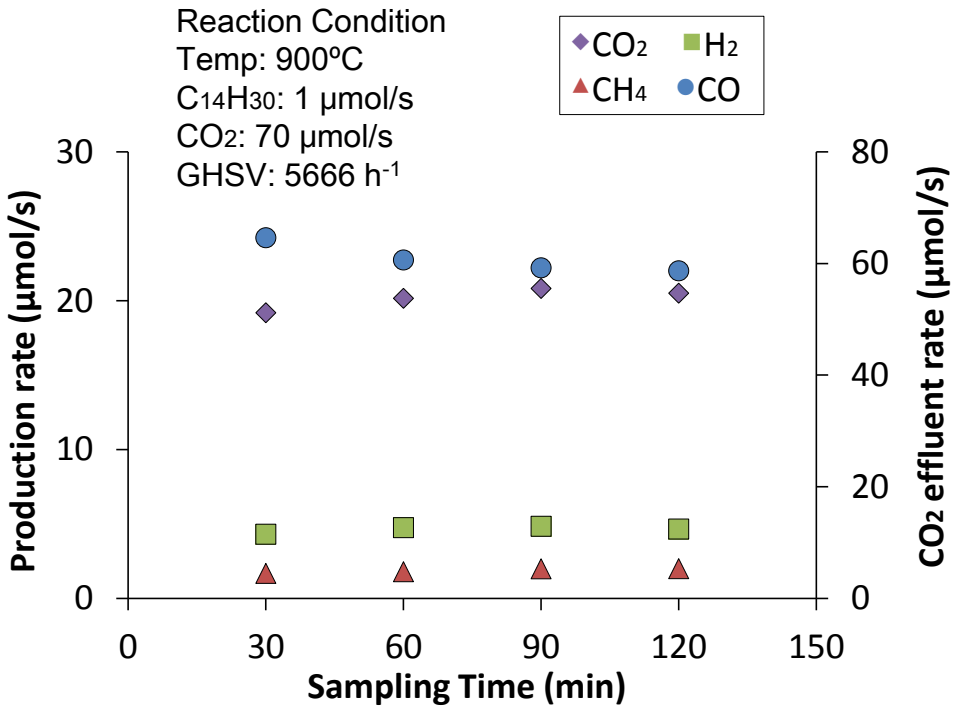

Figure 3.9a. Quantitative analysis of effluent gas during tetradecane reforming at 900°C with 70µmol/s CO_2 performed over SUS304 preoxidized at 1000ºC for 120 min

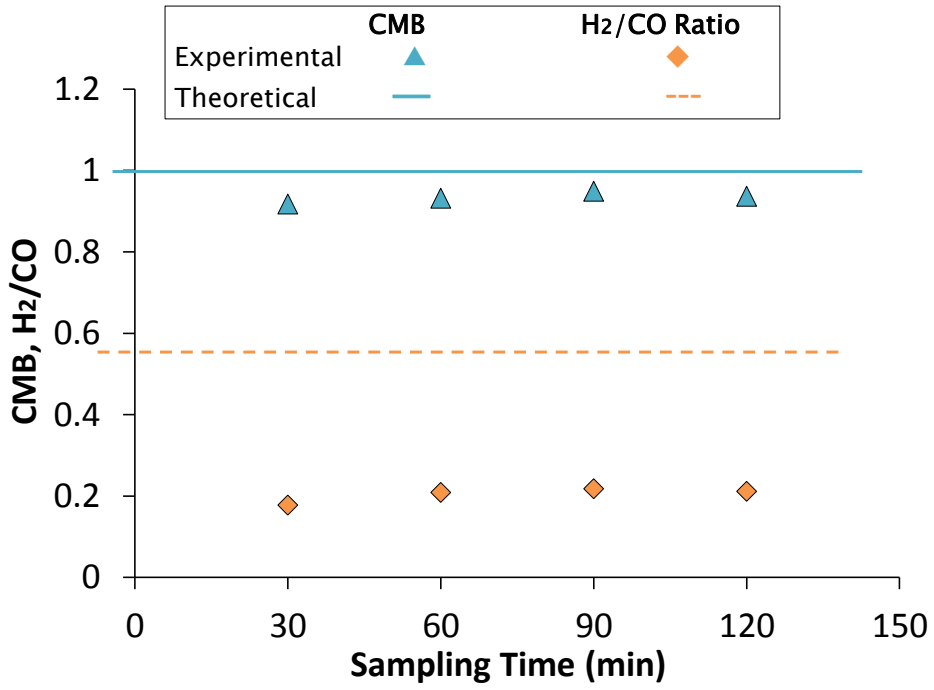

Figure 3.9b. Carbon mass balance and H_2/CO ratio of effluent gas during tetradecane reforming at 900°C with 70µmol/s CO_2 performed over SUS304 preoxidized at 1000ºC for 120 min

3.3.3.1 Section Summary

Based on the previous data discussed, further increase in CO_2 flow rate was predicted to have a negative impact on CO and H_2 production rates while also lowering the amount of carbon formed. Experimental data suggested that RWGS reaction is enhanced when CO_2 flow rate was at 70 µmol/s. In addition, conducting the reaction at high CO_2 flow rate indeed prevents the formation of carbon even at low reaction temperature (700°C).

3.3.4. H_2 and CO production

Figure 3.10 depicts the production rate of H_2 at different CO_2 flow rates and reaction temperatures. When the reaction was performed at 700°C, H_2 prodcution rate did not exhibit any noticeable change with respect to the different CO_2 flow rates. In addition, H_2 production rates at 42 and 70µmol/s CO_2 remained equal for all reaction temperatures tested in this study. When CO_2 flow rate was equimolar with that of tetradecane (14 µmol/s), RWGS reaction was hindered by the limited supply of CO_2. At higher CO_2 flow rates (>equimolar) tetradecane, the source of H_2, became the limiting reactant. Since CO_2 was in

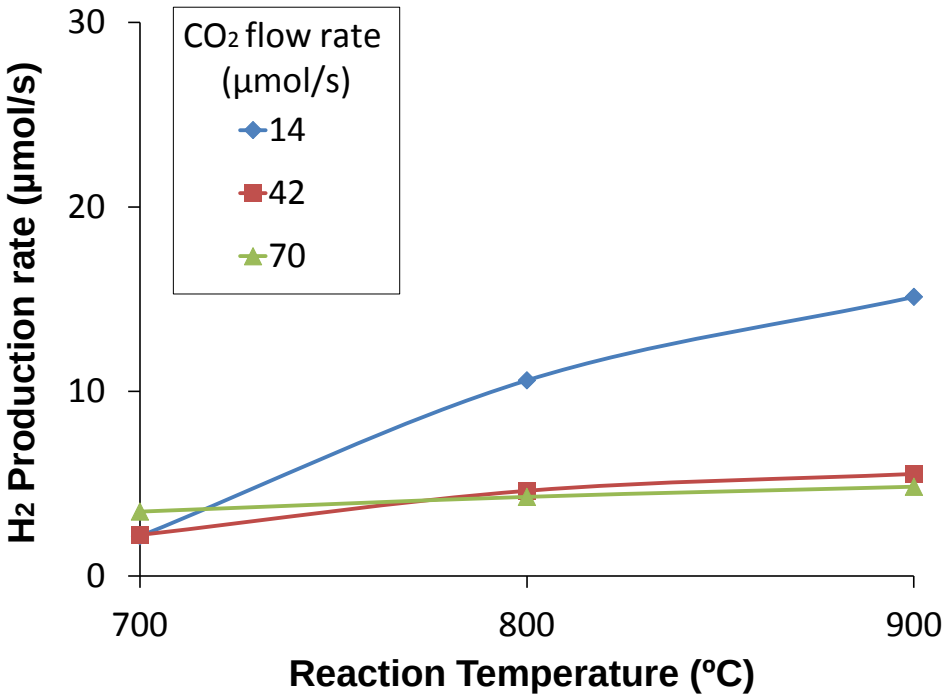

Figure 3.10. Production rate of H_2 during preoxidized SUS304 catalyzed tetradecane dry reforming at different CO_2 flow rates and reaction temperatures

excess, H_2 produced via tetradecane dry reforming and decomposition reactions were presumed to be consumed via RWGS; thus, H_2 production rate decreased with increasing CO_2 flow rates.

The endothermic nature of CO producing reactions (Reactions 2.4, 3.1, and 3.2) favored CO production at higher temperature at any CO_2 flow rate (Fig. 3.11) with 2 separate patterns displayed for low and high- temperature reactions. When the reaction was conducted at 700°C, which many authors categorized to be a low-temperature reaction, CO production rate increased as CO_2 flow rate became higher. Based on its corresponding H_2/CO ratio, RWGS reaction significantly contributed to the production rate of CO. An opposite trend was noted when higher temperatures (800 and 900°C) were applied to the reaction. At higher CO_2 flow rate, the residence time of the reactant gases were also shortened which were inferred to negatively affect the amount of reactive species (C_mH_n). In addition, when residence time is reduced the active species have lesser time to be able to interact with each other and allow the desired reaction to proceed completely.

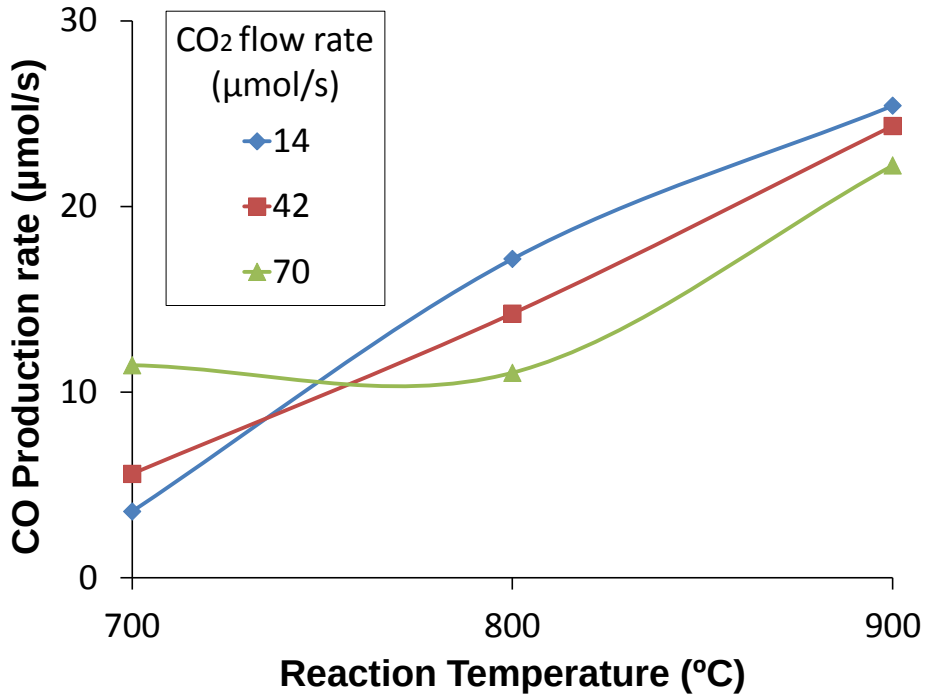

Figure 3.11. Production rate of CO during preoxidized SUS304 catalyzed tetradecane dry reforming at different CO_2 flow rates and reaction temperatures

3.3.5 Carbon Formation

In this section carbon mass balance (CMB) was used to represent carbonaceous deposits as it was difficult to measure the amount of carbon directly during the reaction. Ido et al. [54], reported that methane pulsed on Ni/Al_2O_3 was adsorbed and converted into inactive carbonaceous deposit while small amount was desorbed from the catalyst. In the case of continuous flow system, CMB could exclude the desorbed amount and could represent the carbon deposition unless they were converted into higher hydrocarbons. In this study, a cold trap set at the reactor outlet could accumulate liquid higher hydrocarbons. Since, condensed hydrocarbons were hardly detected in the trap CMB could be used as an indicator of carbon deposition on the catalyst surface.

Figure 3.12 shows the carbon formation trend as represented by CMB. The trend can be divided into 2 with respect to reaction temperature: low (700°C) and high (>700) reaction temperature. When reaction was done at 700°C, carbon formation decreases with increasing CO_2 flow rate. It is important to note that hydrocarbon decomposition facilitates both reforming reaction and carbon formation. If the amount of CO_2 supplied is not sufficient, hydrocarbon fragments adsorbed on the catalyst may eventually be converted to carbon. Conversely, higher CO_2 flow rate translates to sufficient CO_2 that could react with the hydrocarbon fragments to produce carbon dioxide and hydrogen. For dry reforming reactions conducted at temperatures greater than 700°C, methane decomposition (Reaction 1.11) is the main route of carbon formation thus CO_2 flow rate showed no significant effect on the carbon mass balance of reactions conducted at 800 and 900°C.

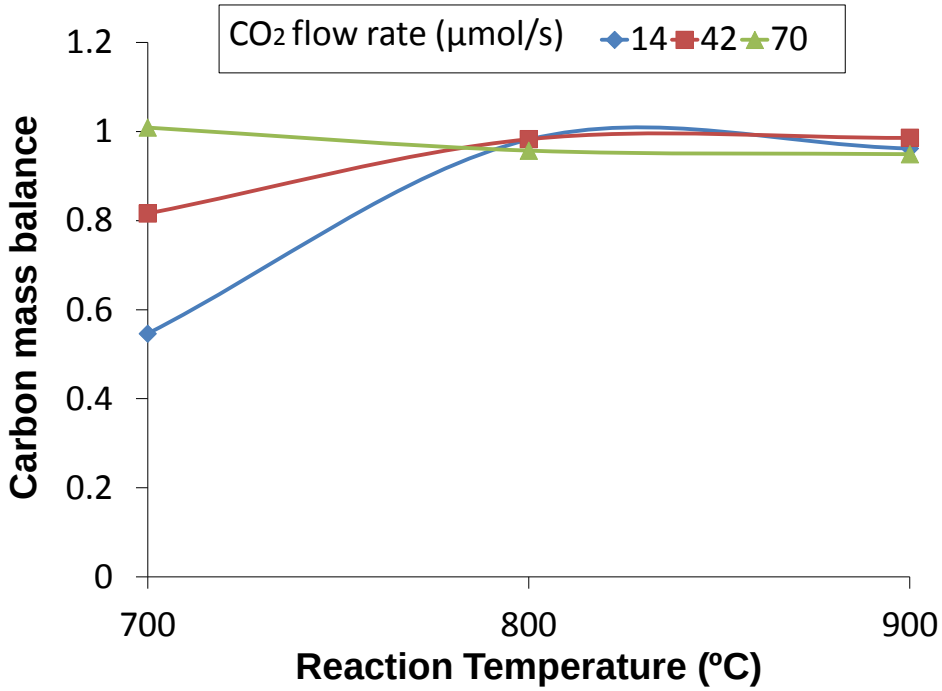

Figure 3.12. Carbon mass balance during preoxidized SUS304 catalyzed tetradecane dry reforming at different CO_2 flow rates and reaction temperatures

3.4 Results:Catalyst Characterization

As shown in Figure 3.13, preoxidation resulted into the formation mixed metal oxide on the surface of SUS304. Specifically, chromium oxide (Cr_2O_3) and iron oxide (Fe_2O_3) were identified on the surface of SUS304 upon preoxidation at 1000°C for 120 min. Based on previous metallurgical studies, chromium oxide is a passive oxide layer that prevents other alloy components from being oxidized. At 1000°C, the alloy must contain atleast 25% chromium for it to be resistant against heat and oxidation. Since SUS304 contains only 18-20% chromium, it was easily oxidized at 1000°C. In addition, chromium oxide may have also started to disintegrate to CrO_3 followed by the formation of iron oxide and possibly the migration of nickel from the alloy substrate to the metal oxide matrix. Metal

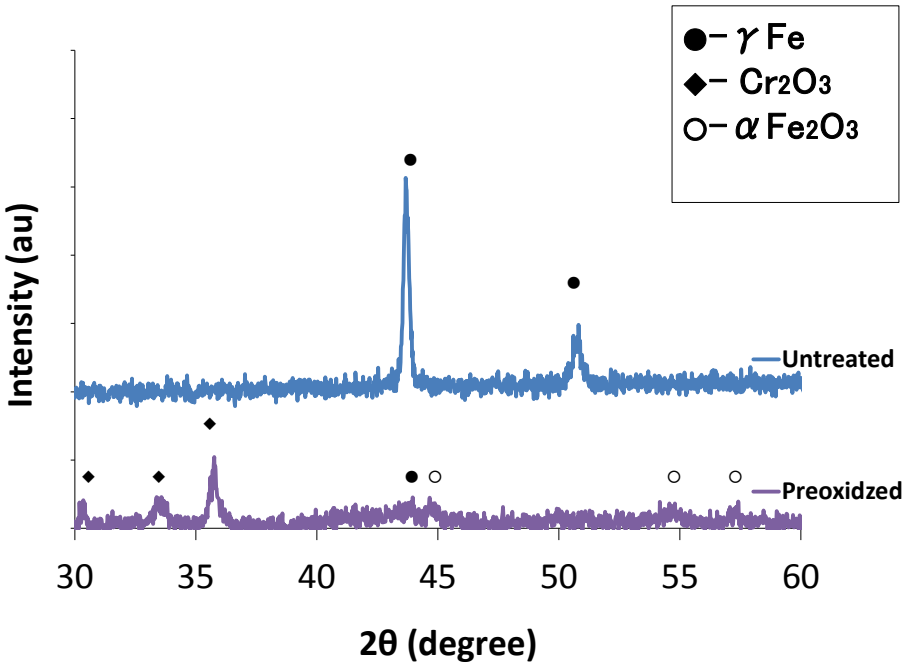

Figure 3.13. X-ray diffraction spectra SUS304 before and after preoxidation at 1000°C for 120 min

oxides are basic and studies conducted on supported nickel catalysts showed that support materials with basic nature promotes dry reforming reaction by improving the adsorption and dissociation of CO_2 [27,35] an essential step during dry reforming reaction. Trivalent-metal oxides, such as chromium oxide, were also reported to prevent coking by enhancing the mobility O^{2-} in the metal oxide matrix [37] which sped up its reaction with the hydrocarbon fragments; therefore, preventing carbon to form on the surface of the catalyst. As for the possibility of iron and chromium oxides functioning as dry reforming catalyst, no previous reports had been published. Based on this, it was suspected that the catalytic activity observed was rendered by amorphous nickel that was dispersed on the metal oxide matrix. Elemental analysis conducted on the sample confirmed this assumption (Fig. 3.14). Specifically, the collected micrograph showed a ragged surface made-up of clustered particles having round edges and random sizes. Some particles were separated by tiny gaps while some were relatively tightly packed. Mapping done by EDS showed that nickel, iron and chromium were dispersed on the surface of SUS304 while oxygen was mostly concentrated on parts were the particles were tightly clustered. It was assumed that oxide-rich areas were the top most layer of the metal oxide scale formed upon oxidation pretreatment; however, manually pressing the sample disrupted the arrangement of

the metal oxide scale. Nonetheless, the collected data proved that indeed the catalytically active nickel, probably NiO, was present on the metal oxide matrix.

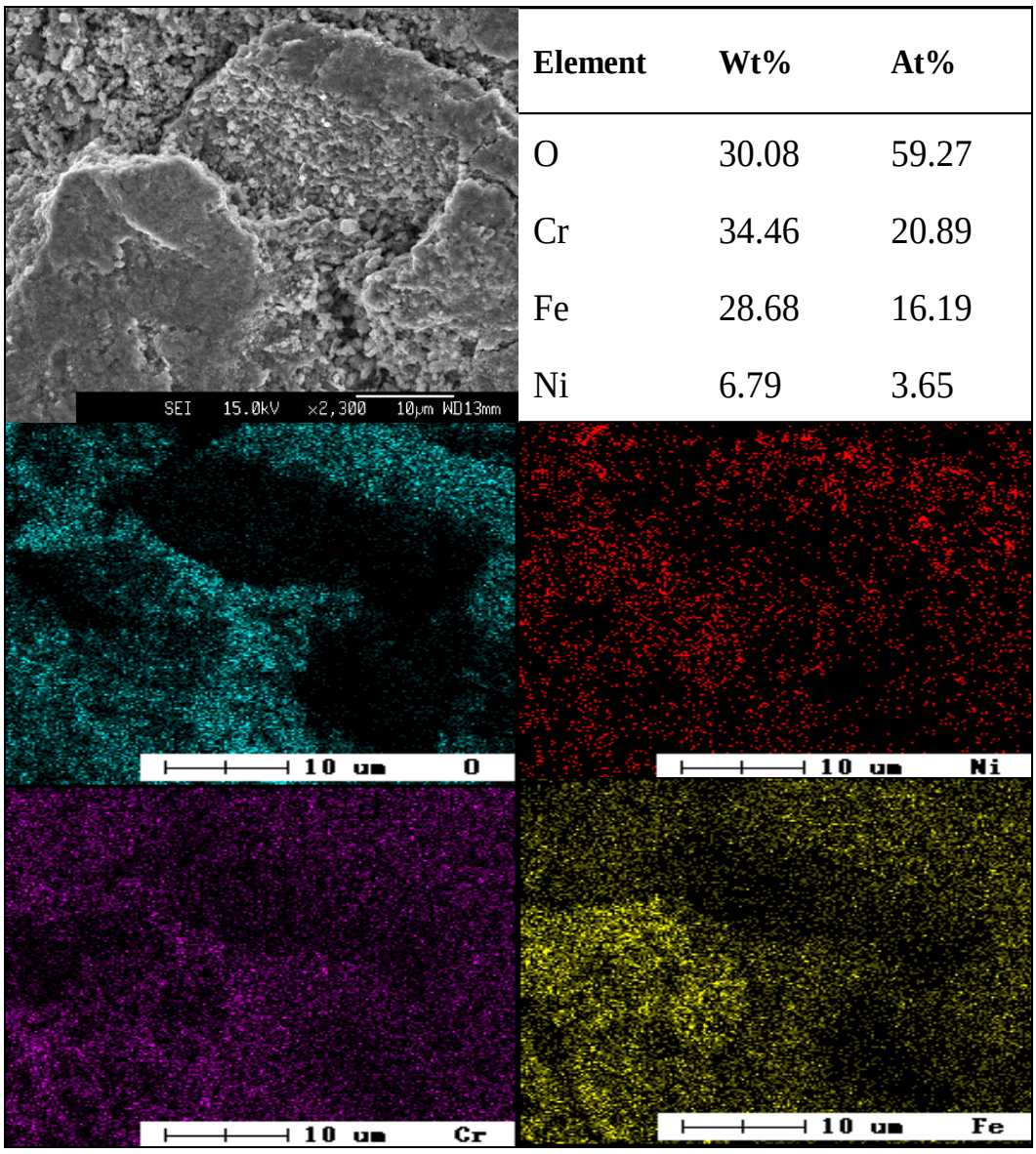

Element	Wt%	At%
O	30.08	59.27
Cr	34.46	20.89
Fe	28.68	16.19
Ni	6.79	3.65

Figure 3.14. Morphological and elemental profile of preoxidized SUS304 using SEM-EDS

3.5 Conclusion

Surface characterizations revealed that oxidation pretreatment at 1000°C for 120 min resulted into the formation of a metal oxide scale composed of Fe_2O_3, Cr_2O_3, and NiO. Aside from providing a substrate for the dispersed nickel, the metal oxide matrix also acted as a promoter and prevented carbon from being formed on the surface of the catalyst. Using preoxidized SUS304 as catalyst, tetradecane dry reforming proceeds faster at higher reaction temperatures. For all temperatures evaluated in this study, RWGS reaction rate became faster while carbon formation was reduced at higher CO_2 flow rates. Depending on the desired H_2/CO ratio of the product gas, the suitable reaction temperature and CO_2 flow rate combination should be applied. When the reaction was conducted at 700°C, higher reaction rate and lesser carbon formed were observe at higher CO_2 flow rates. Conducting the reaction at 800 and 900°C, CO_2 flow rate did not display any significant effect on carbon formation. Instead, increasing the flow rate of CO_2 reduced the production rates of H_2 and CO.

CHAPTER IV

Effect of Preoxidation Temperature on the Activity of Kovar Applied as a Dry Reforming Catalyst

4.1 Introduction

This chapter discusses the effect of preoxidation temperature on the composition, morphology and catalytic activity of Kovar towards tetradecane dry reforming. Specifically, 3 types of iron oxides were reported to form when Kovar is subjected under high temperature oxidation [46]; the implications of which on the catalytic function of preoxidized Kovar are reported in this chapter. In our case, oxidation pretreatment was hypothesized to facilitate the formation of a mixed metal oxide scale and disperse the catalytically active components (nickel and cobalt) on the metal oxide matrix. The potential of preoxidized Kovar as a dry reforming catalyst was evaluated based on CO and H_2 production rates.

4.2 Materials and Method

4.2.1 Kovar Preoxidation and Characterization

Kovar preoxidation and tetradecane dry reforming reactions were performed using a bench top quartz tube reactor (Fig. 2.1). Preoxidation was done in oxygen stream (1ml/s) for 120 min within the 500 to 1000°C temperature range. Changes in surface composition and morphologies brought about by the oxidation pretreatment were determined using an X-ray Diffractometer (RINT-2500TTR) and Scanning Electron Microscope (JSM-6330F) with Energy Dispersive Spectrometer (SEM-EDX). XRD analysis was performed using CuKα (50kV, 100mA, λ=1.54) in 2θ range from 30° to 60°, the same conditions used in Chapter 3 (3.2.2). For both analyses, approximately 1 cm portion was used for the analyses.

4.2.2 Tetradecane Dry Reforming and Gas Chromatography

Dry reforming reactions were performed over preoxidized Kovar tubes at 800°C for 120 min using 1μmol/s tetradecane and 70μmol/s CO_2 (GHSV= 5658 h^{-1}). Effluent gases (CO CO_2, CH_4, H_2) and carbon mass balance were determined using the method described in Chapters 2 (Eq. 2.1) and 3 (Eq. 3.1), respectively. The atomic mass balance of carbon was used to indicate the formation of carbon and qualitatively estimate the conversion of tetradecane to gas products. Unreacted hydrocarbon, hydrocarbon fragments from and above C_2, and H_2O formed via RWGS reaction were not quantified due to sample volume and equipment limitations.

4.3 Results: Surface Characterization of Preoxidized Kovar Tube

Oxidation pretreatment using different temperatures caused varied observable changes on the surface of Kovar tube (Table 4.1). Specifically, the surfaces of samples oxidized at 500 and 600°C turned dark gray while a separate layer was formed on the surfaces of those oxidized from 700 to 1000°C. In addition, the layer formed upon oxidation at 700°C appeared smooth and was light gray in color. Increasing the temperature to 800°C resulted into a rough and wrinkled layer with its thickness and texture being more defined at higher oxidation temperature. At 800°C, the formed layer was very thin, flaky and poorly attached to the Kovar tube. Contact between the formed layer and Kovar tube improved as the oxidation temperature increased. The same observations were published by Lou and Shen [46] which they termed as pegging and deduced to improve the bond between the oxides and the Kovar tube. For convenience and clarity, the collected XRD patterns were discussed in groups as indicated in Table 4.1 while only representative SEM micrographs for each group were shown to avoid redundancy.

4.3.1 Preoxidation Temperature: 500 to 600ºC

Oxidation at 500 and 600°C resulted into the formation of a rough scale with uneven coloration (Fig. 4.1a). When viewed at higher magnification (2300x), the appearance of the light (α) and dark (β) colored areas slightly differed. Referring to Figure 4.1b, the surface of the preoxidized sample was generally rough and pitted with the β area displaying more distinct particles which were presumed to be dominantly composed of Fe_3O_4 [46]. Conversely, the α area displayed relatively smoother edges while becoming rougher towards its center; these rough parts were possibly mixture of FeNi and Fe_3O_4. In addition, the

Table 4.1. Appearance of Kovar tube surface upon preoxidation at different temperatures for 120 min

Temperature (°C)	Description	
500	dark gray surface	
600		
700	Formation of separate layer	smooth, light gray layer
800		flaky, shiny, wrinkled layer
900		shiny, wrinkled layer
1000		shiny, wrinkled layer

interlaced needle-like structures on the upper right side of α area were presumed to be bimetallic Ni-Co based on the description provided by Osojnik et. al [55] in their published work on Kovar oxidation. The XRD profile collected (Fig. 4.2) shows the characteristic FeNi peaks for the untreated Kovar while oxidation at 500°C resulted into the formation of Fe_3O_4 on its surface. Moreover, Fe_3O_4 peaks were intensified as oxidation temperature increase resulting from the formation of more Fe_3O_4. Kovar preoxidized at 500°C also showed higher peak intensities for nickel and cobalt, possibly caused by the needle-like structure observed in the α area of Figure 4.1b. Increasing the oxidation temperature to 600°C resulted into the formation of a thicker iron oxide (Fe_3O_4) layer which partially covered nickel and cobalt; thus, lowering the peak intensities for both metals.

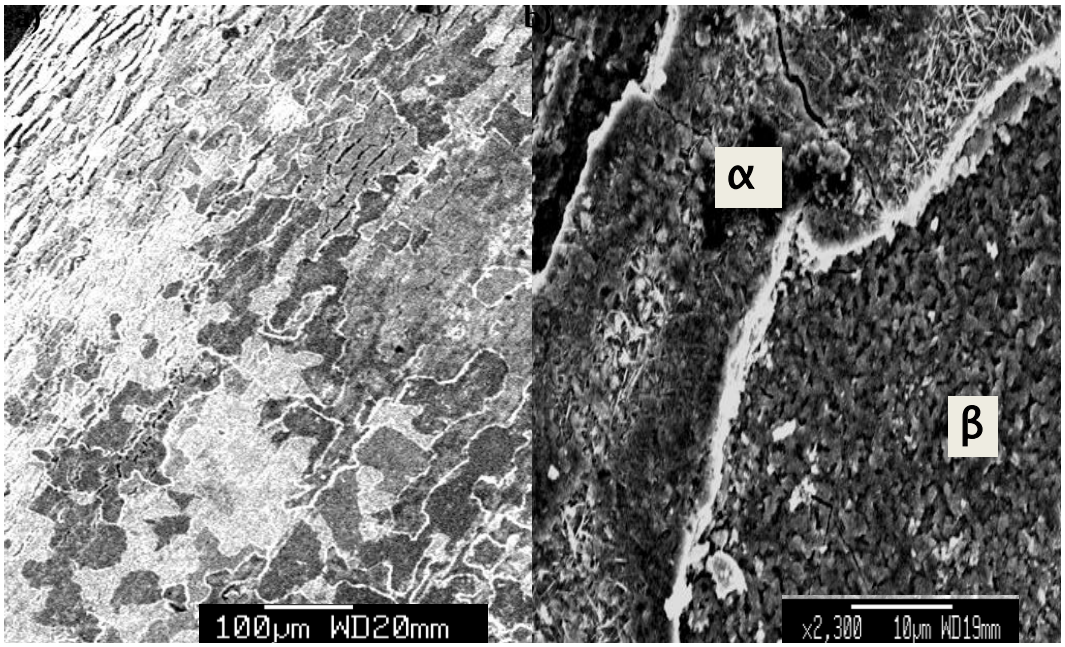

Figure 4.1. SEM micrograph of Kovar tube preoxidized at 600°C for 120 min magnified at a) 100x and b) 2300x

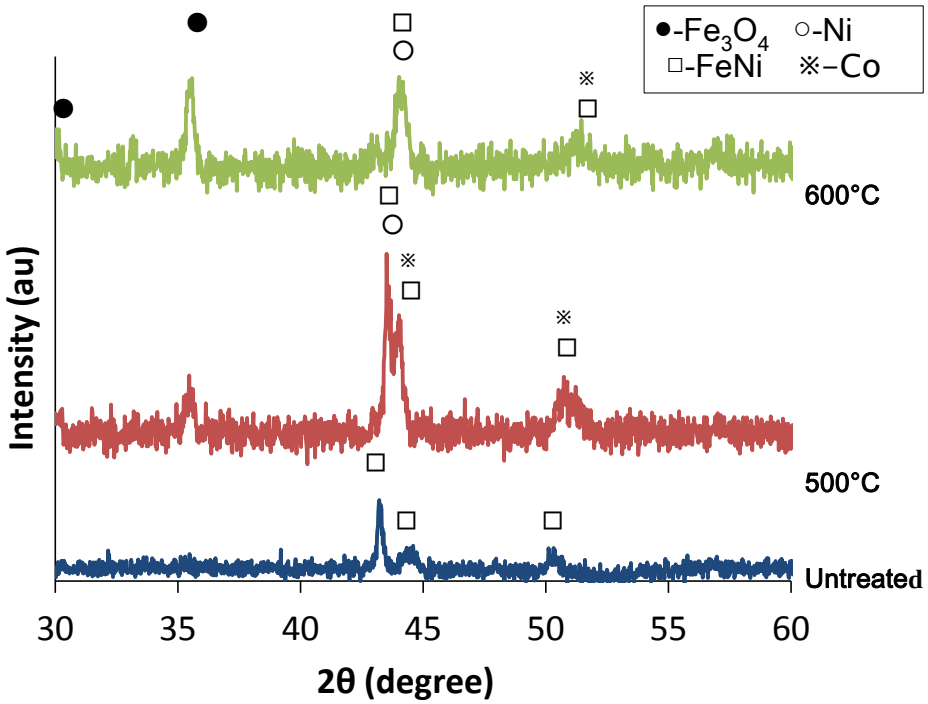

Figure 4.2. X-ray diffraction spectra of Kovar before and after preoxidation at 500 and 600°C for 120 min

4.3.2. Preoxidation Tempearture: 700ºC

When Kovar was preoxidized at 700°C, layer separation was noted. The surface of the separated layer was smooth and light gray in color. Low magnification SEM micrograph showed a ragged surface (Fig. 4.3a) that was composed of randomly stringed or clustered rounded particles separated by tiny gaps (Fig. 4.3b). Comparing the micrographs of samples preoxidized at 600ºC (Fig. 4.1) and 700ºC (Fig. 4.3), it was noted that the particles were relatively distinct when preoxidation was done at a higher temperature. When subjected to XRD analysis (Fig. 4.4), the characteristic FeNi peaks of Kovar were significantly reduced while the types of detected iron oxide (Fe_3O_4 and Fe_2O_3) increased. The formation of more metal oxides was expected since metallurgical principles indicate that an increase in temperature would facilitate the diffusion of metal ions [49] and oxygen ions which translates to metal oxidation. The less distinct particles of the oxide layer in Figure 4.3b were probably the loosely structured Fe_2O_3 co-existing with the more compact Fe_3O_4 [46]. As for nickel and cobalt bimetallic structure, it was suspected that both nickel and cobalt were dispersed on the iron oxide layer but were not detected because both were in their amorphous form or their crystalline structures were too small.

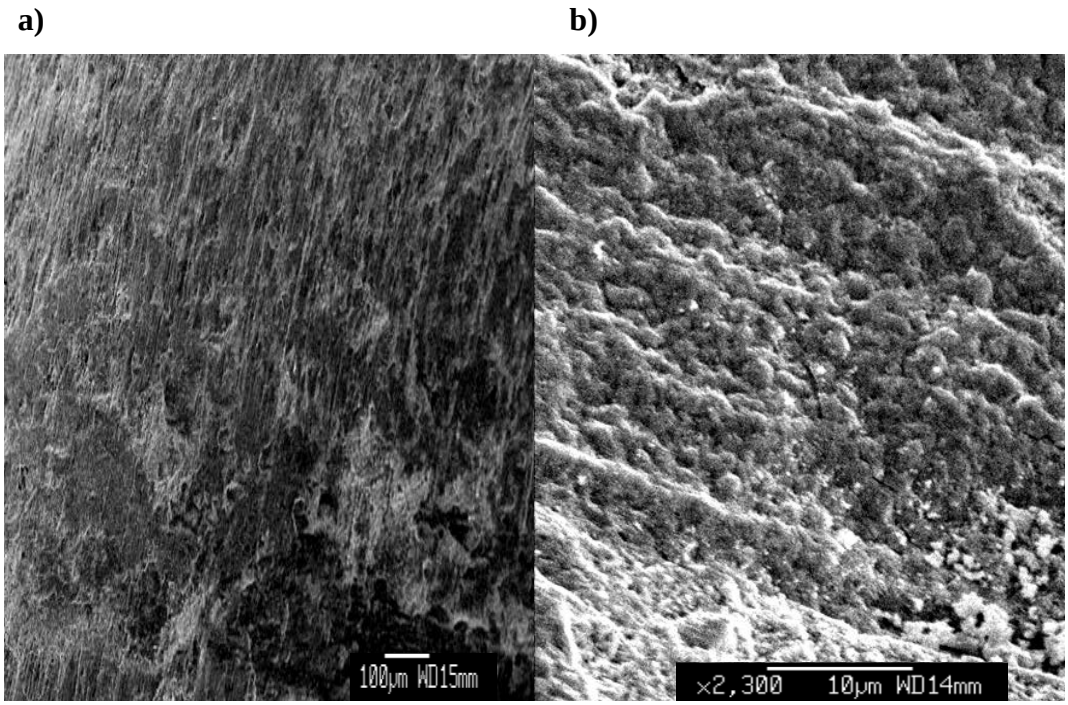

Figure 4.3. SEM micrograph of Kovar tube preoxidized at 700°C for 120 min magnified a) 100x and b) 2300x

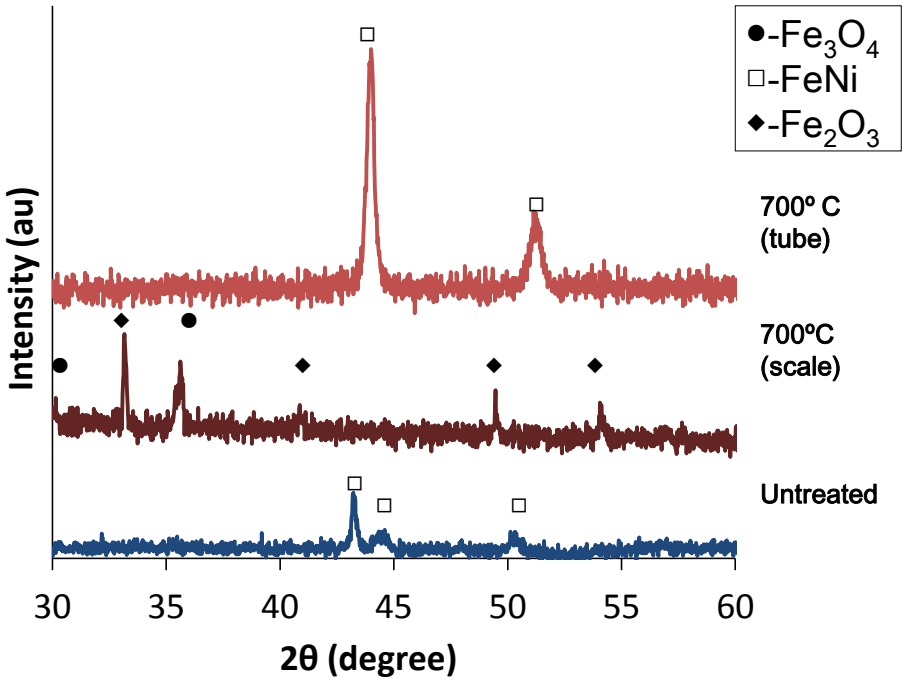

Figure 4.4. X-ray diffraction spectra of Kovar before and after preoxidation at 700°C for 120 min

In addition, the alloy substrate, referred as “tube” in Figure 4.4, was not oxidized and was able to retain the characteristic FeNi peak of the unoxidized Kovar alloy.

4.3.3. Preoxidation Temperature: 800 to 1000ºC

The layer became wrinkled when oxidation pretreatment was done at 800°C; it was also flaky and poorly attached to the alloy substrate. The oxide layer became more rigid, textured, and thick as preoxidation temperature increased. As shown by the SEM micrograph of the representative sample (Fig. 4.5), the wrinkled structure was composed of randomly spread craters. Inspecting this “crater structure” under higher magnification revealed that it is composed of 2 morphologies. Specifically, areas around the crater (Fig. 4.6a) are smooth and flat while the craters (Fig. 4.6b) are ragged and made up of randomly sized sharp-edged particles. The different morphologies were suspected to be a manifestation of sintering, predominantly of iron oxides, brought about by the high preoxidation temperature applied. The XRD patterns (Fig. 4.7) of samples preoxidized at 800 and 900°C revealed that the metal oxide layer was a mixture of Fe_3O_4 and Fe_2O_3 while that of Kovar preoxidized at 1000°C only contained Fe_3O_4. The increase in Fe_3O_4 peak intensities with higher preoxidation temperatures indicated that Fe_2O_3 is further oxidized and converted to Fe_3O_4. Since Fe_3O_4 posses a relatively compact structure, the metal oxide layer formed became more packed, textured and rigid as preoxidation temperature increased. In addition, the metal oxide layer formed at 900 and 1000°C were partially attached or pegged to the alloy tube. The same observations were published by Lou and Shen [46] at high temperature Kovar oxidation. This was confirmed by the presence of the FeNi, the characteristic peak of the Kovar alloy, on the XRD pattern of the metal oxide layer. Further, the presence of FeNi on the metal oxide layer suggested that some parts of the metal oxide scale were indeed attached to the Kovar alloy substrate. However, composition and thickness could have also contributed to the bond between the metal oxide scale and the Kovar alloy substrate, making the flaky metal oxide scale formed at 800°C to be easily detached from the alloy substrate. Moreover, XRD patterns of the preoxidized Kovar alloy substrates (Fig. 4.8) implied that preoxidation done beyond 800°C facilitated the oxidation of the alloy substrate by possibly supplying enough energy for oxygen ions to penetrate the exterior iron oxide layer which initially covered the alloy substrate. Nonetheless, the peak intensities displayed in Figure 4.7 do not clearly illustrate the relative amount of the components since pegging may not be uniformly distributed throughout the alloy tube.

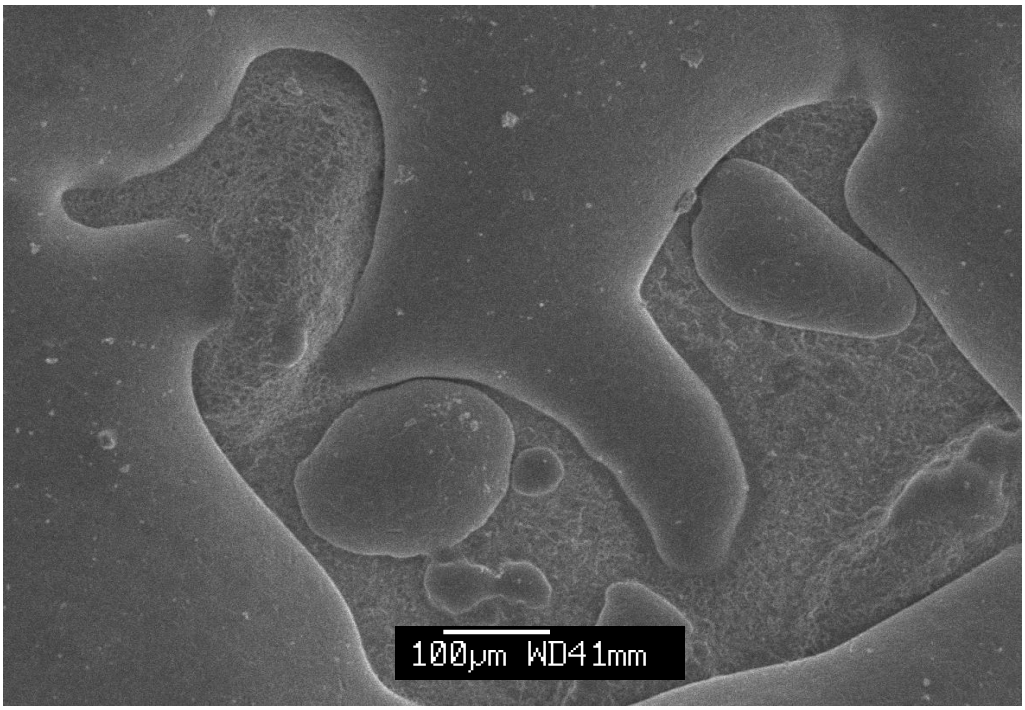

Figure 4.5. SEM micrograph of Kovar surface magnified 100x showing the wrinkled surface and the crater structure formed after preoxidation at 1000ºC for 120 min

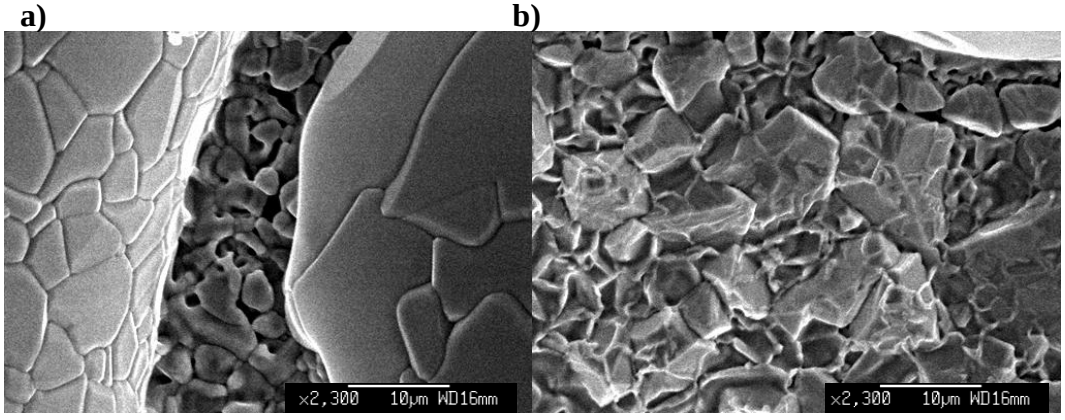

Figure 4.6. SEM micrograph of Kovar surface magnified 2,300x showing the a) relatively smooth area around the crater structure and the b) ragged surface of the crater formed after preoxidation at 1000ºC for 120 min

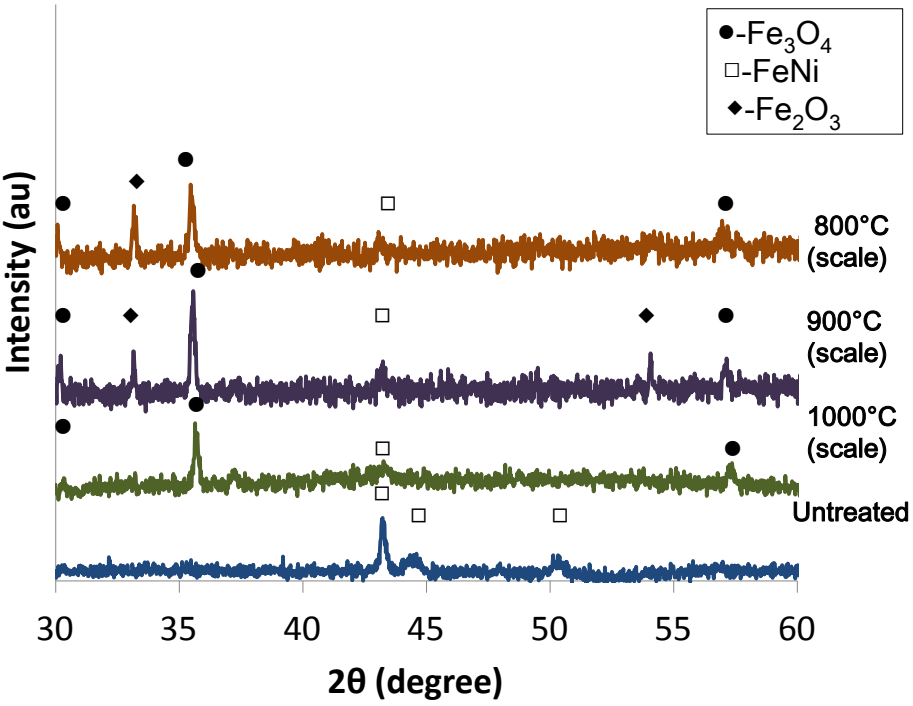

Figure 4.7. X-ray diffraction spectra of the separate layer formed on the surface of Kovar after preoxidation at 800 to 1000°C for 120 min

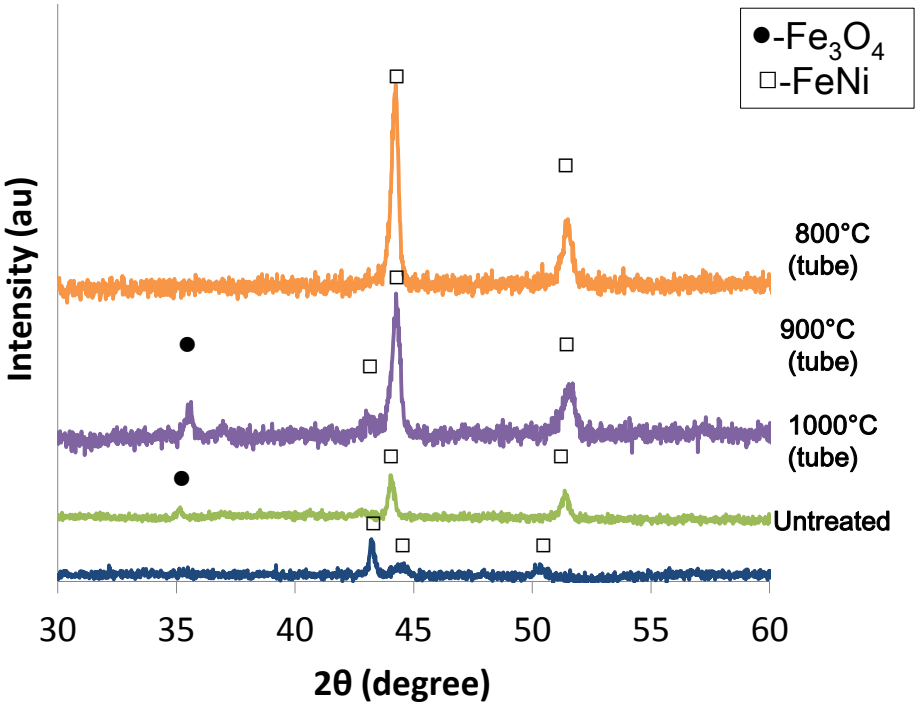

Figure 4.8. X-ray diffraction spectra of the Kovar alloy substrate after preoxidation at 800 to 1000°C for 120 min

4.3.4. Section Summary

The data collected from this section conformed to previously reported data on Kovar oxidation [46] stating that the type and amount of metal oxides formed upon Kovar oxidation depends on the oxidation conditions used. Specifically, a more compact, textured, and rigid metal oxide layer was formed at higher oxidation temperature. Also, pegging was observed when oxidation was conducted at temperatures ≥900ºC.

4.4 Results: Tetradecane Dry Reforming Over Preoxidized Kovar

Based on the proposed reaction mechanism of Solymosi et al. [23], the dominant reactions involved were assumed to include tetradecane CO_2 reforming (Reaction 3.1), CO_2 reforming of hydrocarbon fragments produced via tetradecane decomposition (Reaction 3.2), reverse water-gas shift reaction or RWGS (Reaction 1.10), and methane decomposition (Reaction 1.11). It is generally considered that RWGS reaction occurs simultaneously with CO_2 reforming reaction while the most viable route for carbon formation at 800°C is methane decomposition.

4.4.1 Kovar Preoxidation Temperature: 500 and 600ºC

Based on the data shown in Figure 4.9a, Kovar is catalytically active towards CO_2 reforming of tetradecane upon oxidation at 500°C. In addition to CO and H_2, CH_4 was also produced in relatively small amounts possibly from tetradecane decomposition. Further, the low H_2/CO indicated RWGS reaction also took place (Fig. 4.9b). Minimal carbon was also formed during the reaction as suggested by its CMB (Fig. 4.9b). However, decreasing CO and H_2 production rate indicated that the catalyst was deactivated after 60 min. Although the contribution of carbon deposition cannot be completely eliminated as the cause of catalyst deactivation, it was suspected that the morphology and metal dispersion mainly determined the activity and stability of the catalyst.

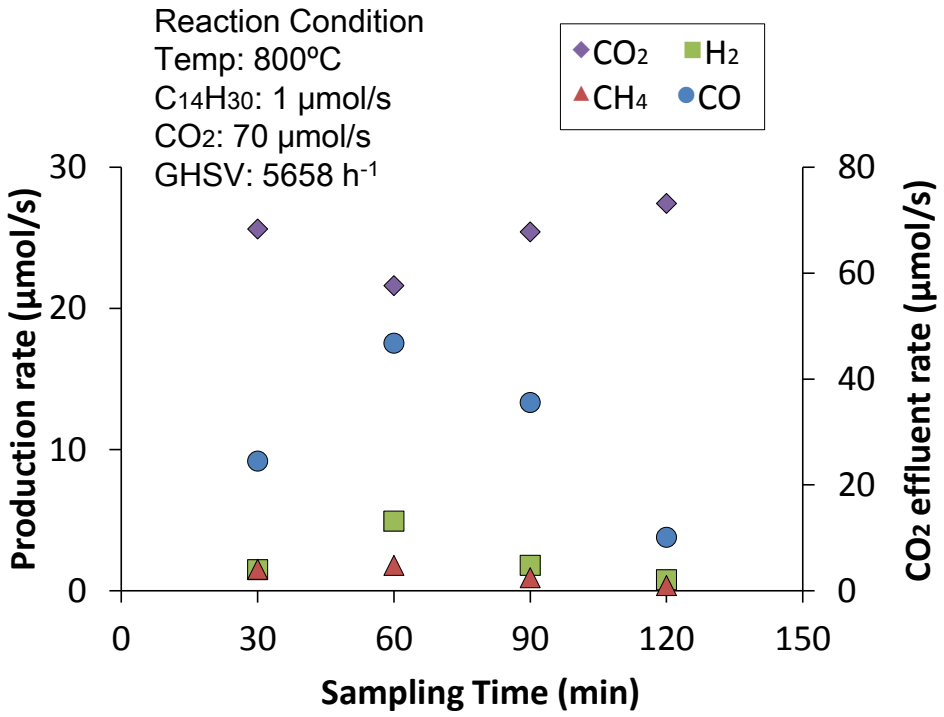

Figure 4.9a. Quantitative analysis of effluent gas during tetradecane reforming at 800ºC with 70µmol/s CO_2 performed over Kovar preoxidized at 500ºC for 120 min

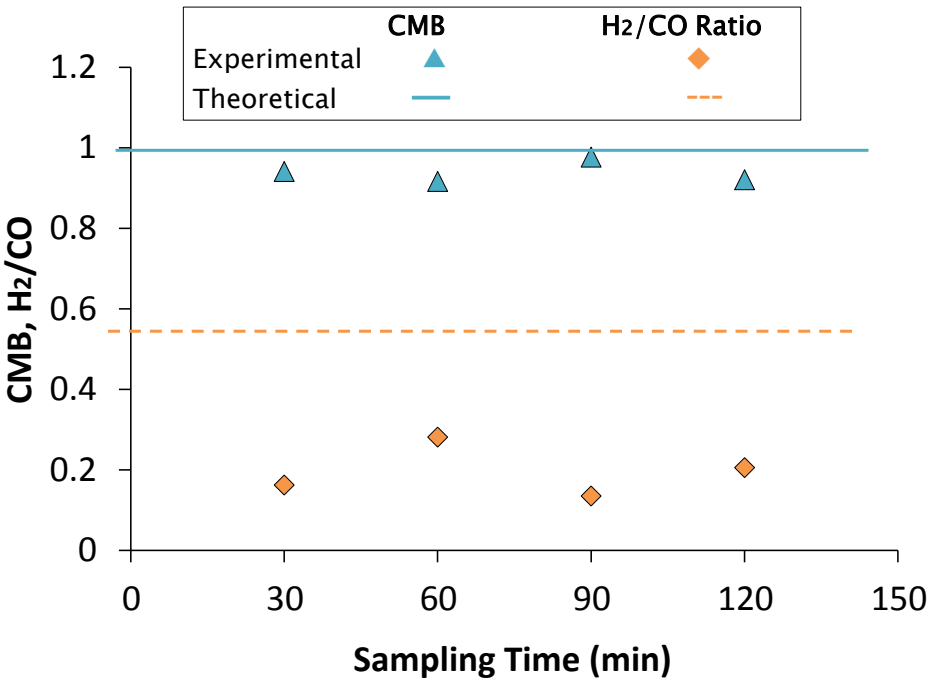

Figure 4.9b. Carbon mass balance and H_2/CO ratio of effluent gas during tetradecane reforming at 800ºC with 70µmol/s CO_2 performed over Kovar preoxidized at 500ºC for 120 min

Further, when the reaction was conducted over Kovar preoxidized at 600°C the catalytic activity generally improved as shown by its CO and H_2 production rates (Fig. 4.10a). Specifically, CO and H_2 production rates increased until the 90th minute of the reaction (Fig. 4.10a). Together with the corresponding increase in CO_2 consumption, it was inferred that CO_2 reforming reaction rate (Reactions 3.1 and 3.2) continuously increased. Additional CO may have been produced through RWGS reaction as suggested by the H_2/CO in Figure 4.10b. At the end of the reaction (120 min), the effect of RWGS reaction became more pronounced by the abrupt drop in H_2 production rate (Fig. 4.10a) and H_2/CO (Fig. 4.10b). In this case, catalytic deactivation was dominantly caused by the shift in catalytic selectivity rather than carbon deposition as shown by the high carbon balance of the reaction (Fig. 4.10b). Changes in catalyst morphology and composition could have occurred with the reaction, leading to the observed shift in selectivity towards RWGS reaction.

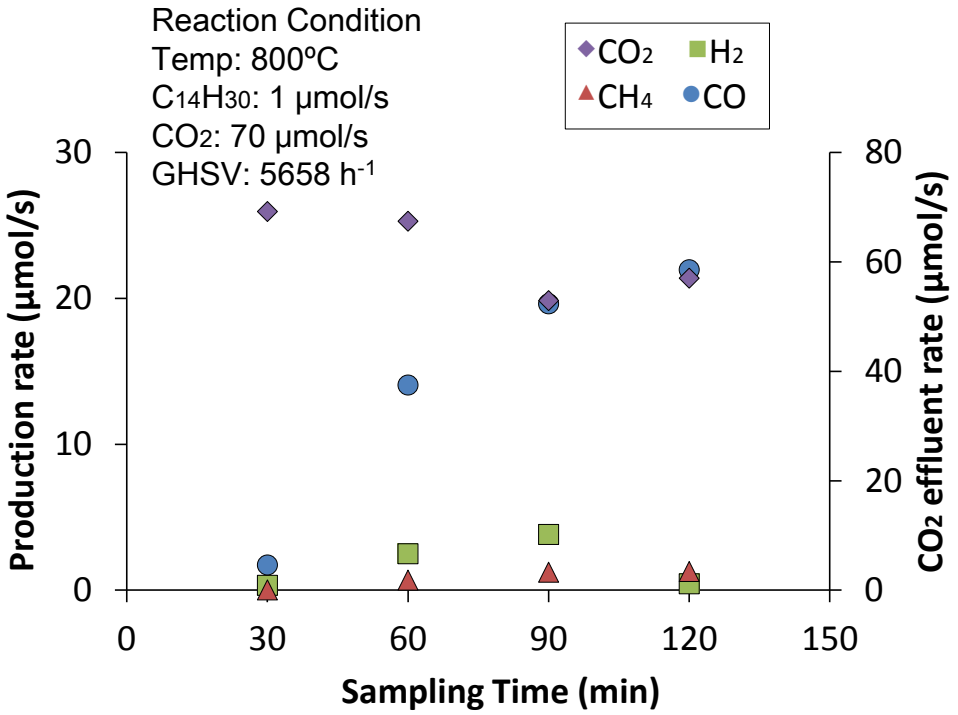

Figure 4.10a. Quantitative analysis of effluent gas during tetradecane reforming at 800ºC with 70µmol/s CO_2 performed over Kovar preoxidized at 600ºC for 120 min

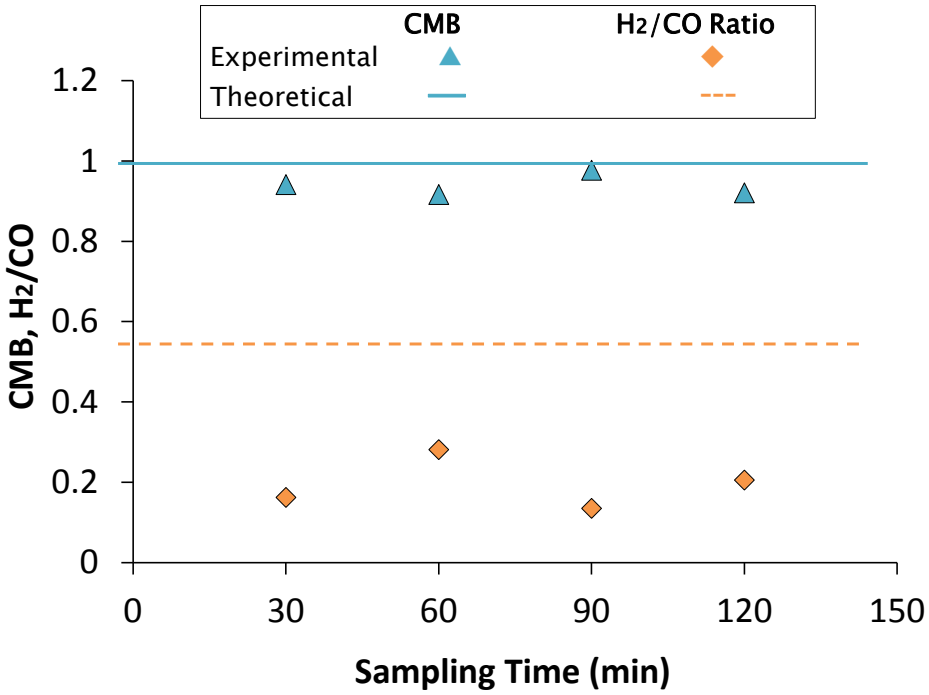

Figure 4.10b. Carbon mass balance and H_2/CO ratio of effluent gas during tetradecane reforming at 800ºC with 70µmol/s CO_2 performed over Kovar preoxidized at 600ºC for 120 min

4.4.2 Kovar Preoxidation Temperature: 700ºC

Increasing the preoxidation temperature of Kovar caused both catalytic activity and stability to improve as shown in Figure 4.11. It is also important to note that reaction rate increased after 30 min (Fig. 4.11a) possibly due to changes in catalyst morphology and component during the first 30 min of the reaction. After 30 min, the reaction became stable followed by a slight decrease in activity towards the end of the operation. Despite the observed decrease in both CO and H_2 production rate, their respective ratio did not change which resulted into constant H_2/CO throughout the experiment (Fig 4.11b). In addition, despite the noted decrease in carbon balance (Fig. 4.11b), CH_4 production rate remained stable (Fig. 4.11a). Based on this observation, it was inferred that hydrocarbon fragments (C_mH_n) produced via hydrocarbon decomposition were accumulated on the surface of the catalyst. Consequently, from the additional H_2 produced during hydrocarbon decomposition an increase in H_2/CO was expected; however, this was not observed. Hence, RWGS (Reaction 1.10) was suspected to be the dominant H_2-consuming reaction responsible for the observed constant H_2/CO value. Generally, it was noted that RWGS reaction was favored as reaction time progressed.

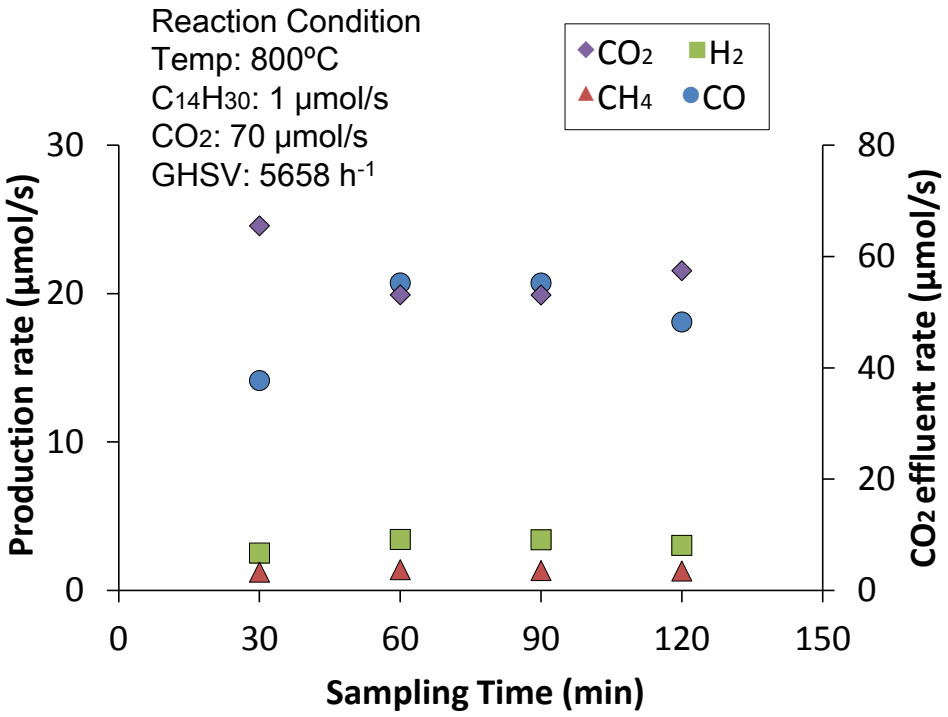

Figure 4.11a. Quantitative analysis of effluent gas during tetradecane reforming at 800ºC with 70µmol/s CO_2 performed over Kovar preoxidized at 700ºC for 120 min

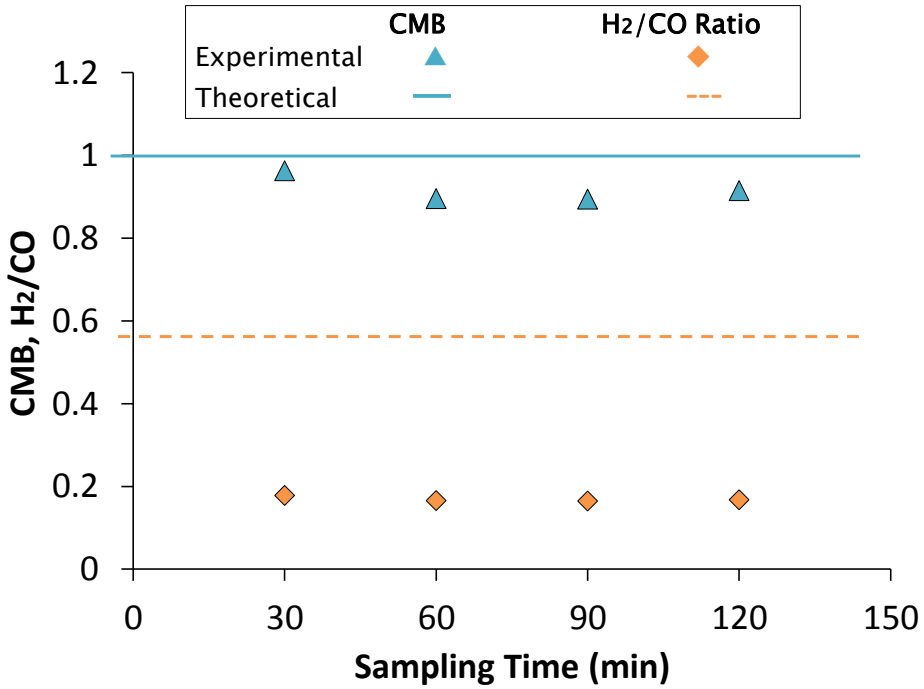

Figure 4.11b. Carbon mass balance and H_2/CO ratio of effluent gas during tetradecane reforming at 800ºC with 70µmol/s CO_2 performed over Kovar preoxidized at 700ºC for 120 min

4.4.3. Kovar Preoxidation Temperature: 800 to 1000°C

As prompted by the trend observed from the previous data, it was expected that a higher preoxidation temperature would further improve the catalyst. However, the opposite was obtained when the reaction was conducted over Kovar oxidized at 800°C (Fig. 4.12). Particularly, a constant decline in activity was indicated by the decreasing CO and H_2 production rates coupled with a decrease in CO_2 consumption rate in Figure 4.12a. Considering the observed drop in CO_2 consumption rate and H_2/CO (Fig. 4.12b), it may be ascertained that catalyst selectivity shifted to RWGS reaction. This was inferred to result from the flaky and poorly attached metal layer formed on the surface of the catalyst after oxidation at 800°C. Nonetheless, catalytic selectivity still seemed to favor RWGS reaction with time. On the other hand, carbon balance for this reaction remained high (Fig. 4.12b) which suggested that catalyst deactivation may not be primarily due to high carbon formation but rather from the disintegration of the flaky surface where the catalytically active component must be dispersed.

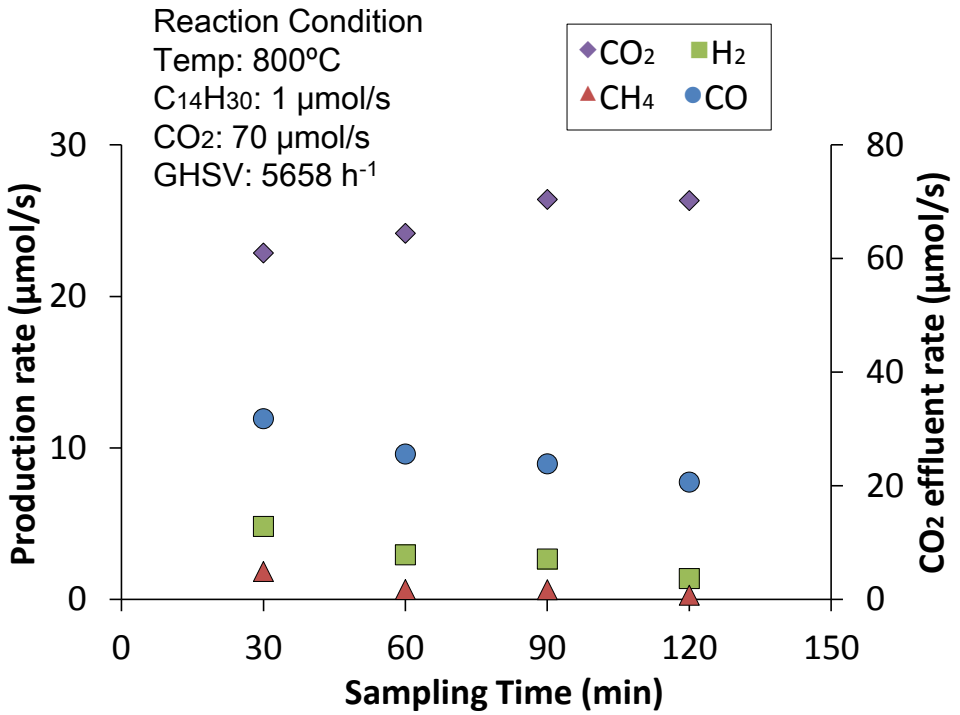

Figure 4.12a. Quantitative analysis of effluent gas during tetradecane reforming at 800ºC with 70µmol/s CO_2 performed over Kovar preoxidized at 800ºC for 120 min

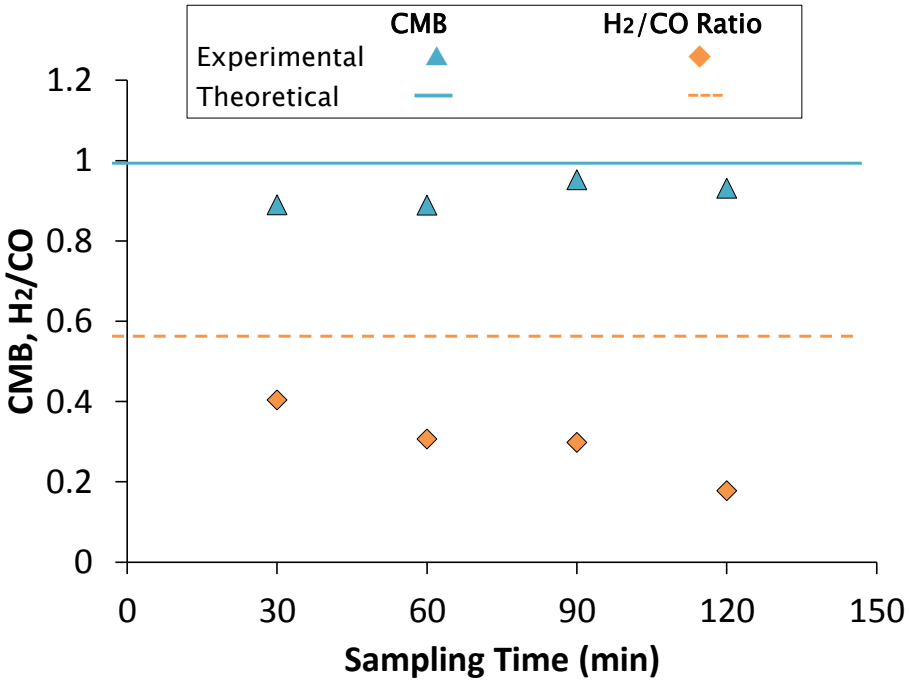

Figure 4.12b. Carbon mass balance and H_2/CO ratio of effluent gas during tetradecane reforming at 800ºC with 70µmol/s CO_2 performed over Kovar preoxidized at 800ºC for 120 min

The same trend in catalytic activity was noted when the reaction was conducted over Kovar preoxidized at 800°C (Fig. 4.12a) and 900ºC (Fig. 4.13a) even though higher CO and H_2 production rates were achieved when the preoxidation was conducted at 900ºC. In addition, CO production rate and H_2/CO ratio were constantly dropping throughout the experiment. This was assumed to be the effect of RWGS being favored over CO_2 reforming reaction as the experiment progressed. It is probable that as the reaction progressed, the catalyst's surface profile continuously changed which led to its eventual shift in selectivity. Furthermore, performing the reaction over Kovar preoxidized at 1000°C yielded the highest initial reaction rate (Fig. 4.14a) and lowest carbon balance (Fig. 4.14b). Based on the constant CO_2 consumption rate, it was inferred that the catalyst was able to maintain a stable hydrocarbon dry reforming reaction rate (Reactions 3.1 and 3.2). Conversely, CO production rate gradually declined while an opposite was seen with H_2 production rate (Fig. 4.14a). This production trend consequently gave the reaction a high H_2/CO (Fig. 4.14b) which implied that RWGS reaction has minimal effect on the over-all reaction. However, this does not totally eliminate the possibility of RWGS taking place with the desired reaction. The continued increase in H_2 production was most likely due to

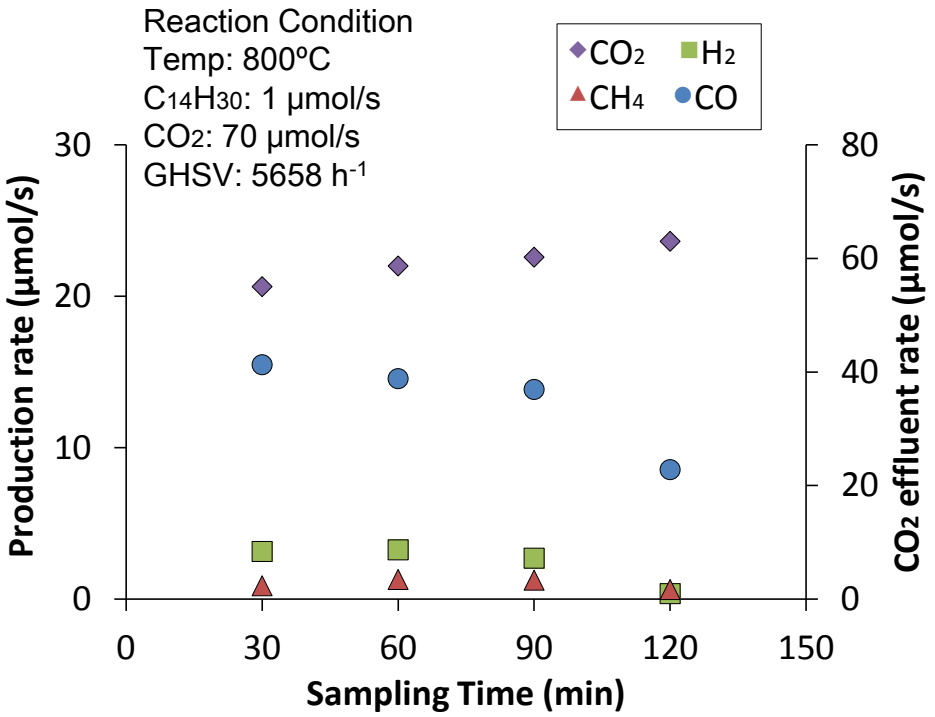

Figure 4.13a. Quantitative analysis of effluent gas during tetradecane reforming at 800ºC with 70µmol/s CO_2 performed over Kovar preoxidized at 900ºC for 120 min

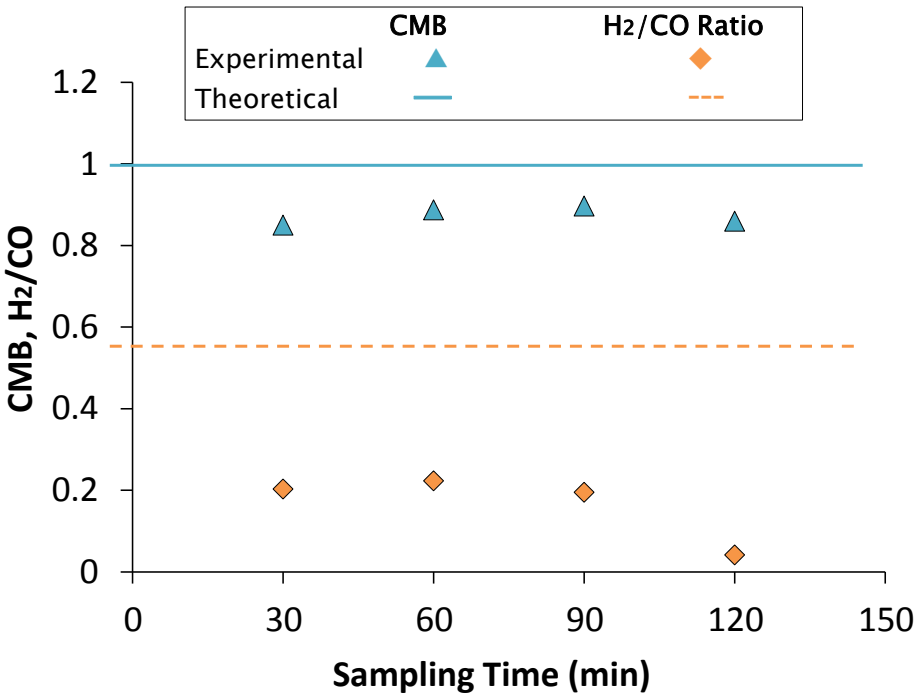

Figure 4.13b. Carbon mass balance and H_2/CO ratio of effluent gas during tetradecane reforming at 800ºC with 70µmol/s CO_2 performed over Kovar preoxidized at 900ºC for 120 min

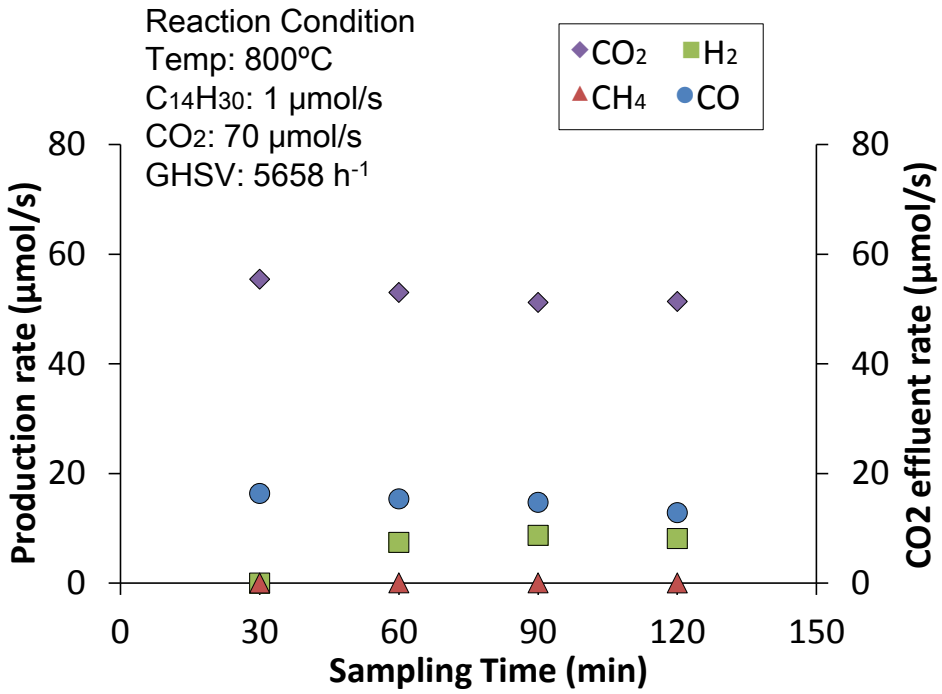

Figure 4.14a. Quantitative analysis of effluent gas during tetradecane reforming at 800ºC with 70µmol/s CO_2 performed over Kovar preoxidized at 1000ºC for 120 min

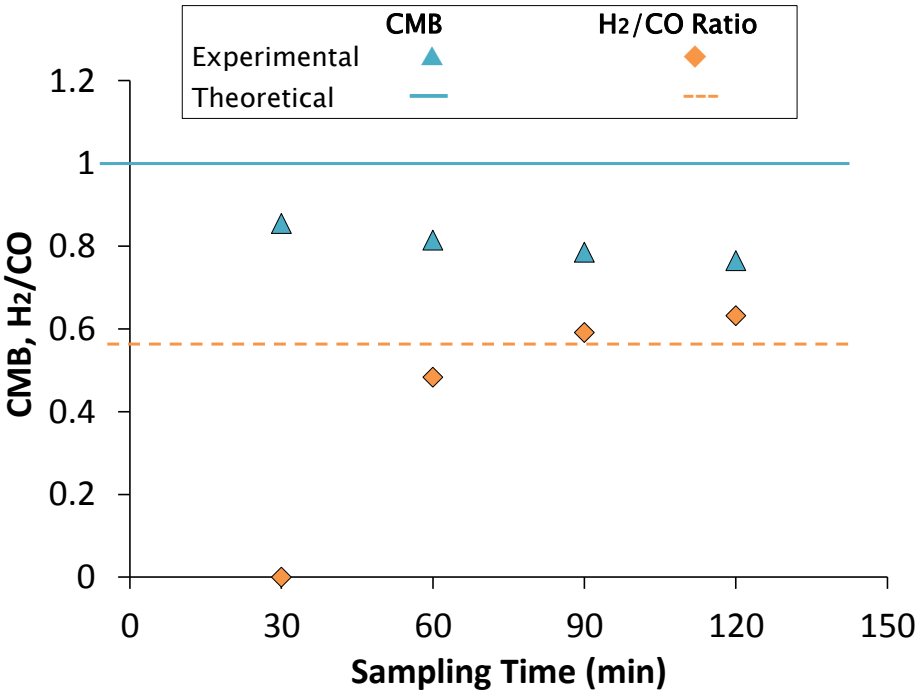

Figure 4.14b. Carbon mass balance and H_2/CO ratio of effluent gas during tetradecane reforming at 800ºC with 70µmol/s CO_2 performed over Kovar preoxidized at 1000ºC for 120 min

methane decomposition (Reaction 1.11) resulting into carbon formation as suggested by the low CMB of the reaction (Fig. 4.14b).

4.4.4 Section Summary

Comparing the catalytic activity of preoxidized Kovar in terms of CO and H_2 production rates (Fig. 4.15), highest CO_2 reforming reaction activity was exhibited when oxidation pretreatment was conducted at 700°C while the lowest was at 800ºC. Another noticeable trend observed from Figure 4.15 is that its CO production rate increased as the preoxidation temperature increased within the range of 500 to 700ºC. This was assumed to be an effect of the type and/or amount of metal oxide formed at different preoxidation temperature. The sudden drop in CO production rate which was observed when Kovar preoxidation was conducted at 800ºC was most probably a consequence of the spalled, flaky and poorly attached metal oxide scale formed on its surface. As the spalled, metal oxide scale thickened with preoxidation temperature (900 and 1000ºC), CO production rate again started to increase. However, it remained relatively lower when compared to those achieved with Kovar preoxidized at lower temperatures (500-700º). In terms of carbon mass balance (Fig. 4.16), it is interesting to note that the highest amount of carbon formation was observed with Kovar preoxidized at 1000ºC while the lowest amount of carbon was formed with Kovar preoxidized at 500ºC. Depending on the intended application and H_2/CO requirement, the effect of RWGS reaction should also be considered. The data gathered clearly showed that preoxidation temperature significantly affects the catalytic activity of Kovar towards dry reforming reaction.

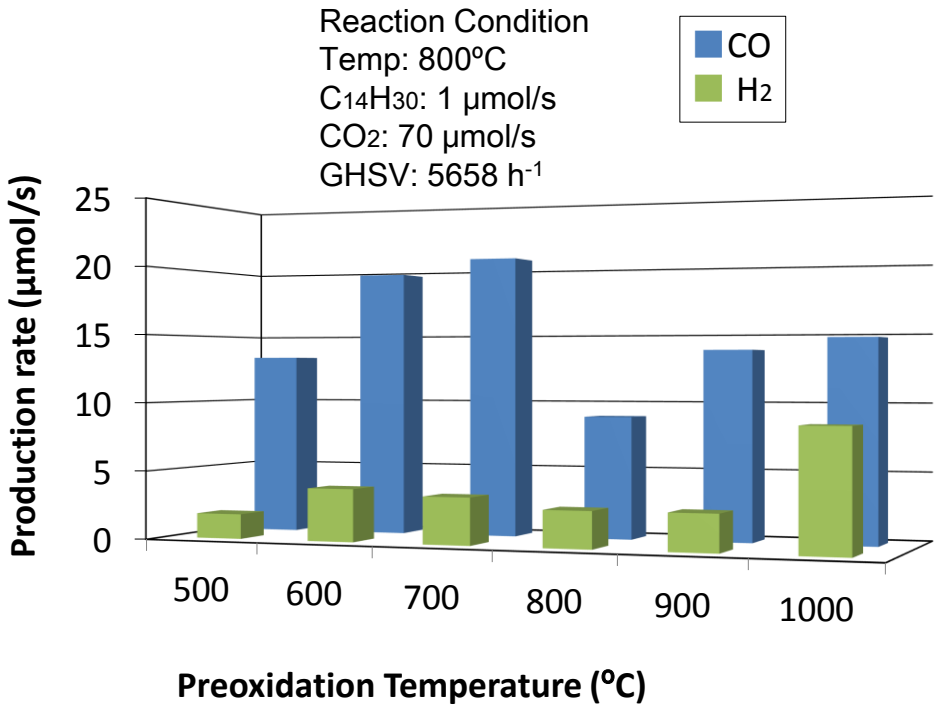

Figure 4.15. CO and H_2 production rates during tetradecane CO_2 reforming over Kovar alloy tube preoxidized at different temperatures for 120 min

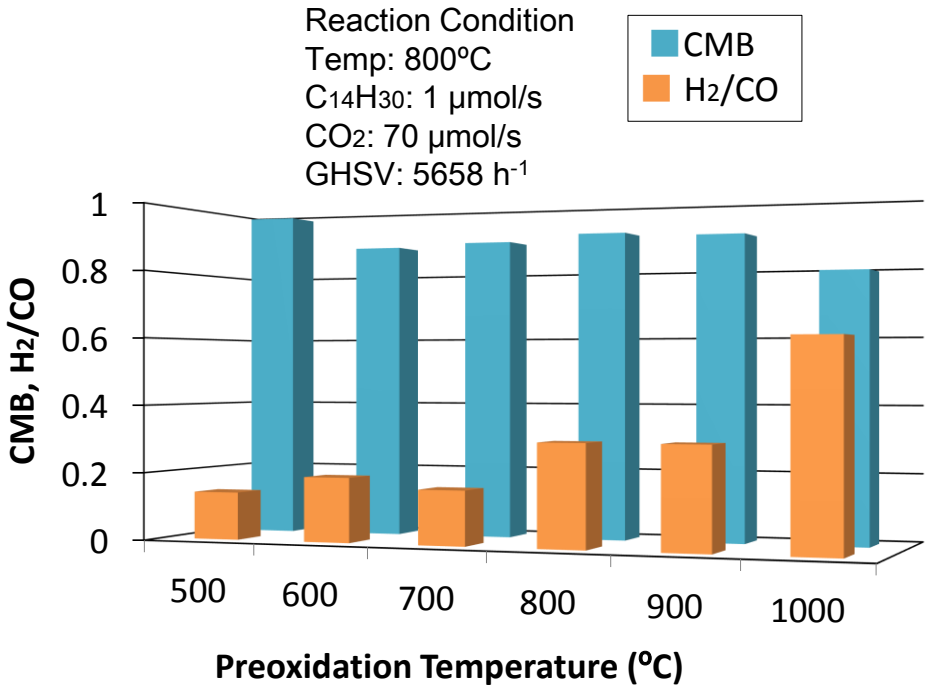

Figure 4.16. Carbon mass balance and H_2/CO ratio during tetradecane CO_2 reforming over Kovar alloy tube preoxidized at different temperatures for 120 min

4.5 Preoxidized Kovar as a Tetradecane Dry Reforming Catalyst

As a catalyst, iron alone is not catalytically active towards CO_2 reforming although it was assumed to improve the stability of nickel catalysts in the structure [55,56]. The catalytic activity displayed by Kovar towards tetradecane CO_2 reforming was possibly rendered by the nickel and cobalt components of the alloy [58]. At temperatures higher than 600ºC, homogeneous or very small crystalline sized nickel, cobalt or their respective oxides might be dispersed on the surface of the catalyst which made them undetectable by XRD analysis at oxidation temperatures higher than 600°C. This assumption was confirmed by the collected EDS data. As shown in Table 4.2 showing both cobalt and nickel were finely dispersed in the metal oxide layer. In addition, the amount of nickel on the surface of the catalyst decreased as oxidation temperature increased which was probably a combined effect of cobalt and iron migration towards the surface during the oxidation process. Also, the formation of more Fe_3O_4 was assumed to prevent O_2 from penetrating the Kovar tube beneath the separate metal oxide layer formed. This resulted into Fe_2O_3 being converted to more Fe_3O_4 at oxidation temperature ≥800°C. Aside from the formation of a more rigid oxide layer, other alloy components (Ni and Co) could have been covered by the thick layer of Fe_3O_4.

The data obtained from this study provided 2 trends with respect to oxidation temperature applied. The first includes Kovar preoxidized from 500 to 700°C. Particularly, increasing CO and H_2 production rates were observed with increasing preoxidation temperature. This was probably due to the dispersion and/or oxidation of nickel and cobalt on the metal oxide matrix which resulted into higher surface area. For heterogeneous catalysts, high surface area is essential in facilitating reactions. When the oxidation temperature was increased to 800°C, a drop in catalytic activity was noted (Fig. 4.12a and 4.16). This was insinuated to be an effect of the poorly attached metal oxide layer formed on the surface of Kovar.

Table 4.2. Surface composition (atomic weight) of oxidized Kovar

Element	**Oxidation Temperature (°C)**		
	600	**700**	**1000**
Fe	30.47	24.15	29.12
Ni	5.62	4.39	1.42
Co	6.29	15.42	12.18
O	57.62	56.04	57.28

Surface characterization suggested that the formation of Fe_2O_3 compromised both the mechanical stability and catalytic activity of Kovar. As oxidation temperature was further raised to 900 (Fig. 4.13a) and 1000°C (Fig. 4.14a), the catalytic activity of Kovar improved with oxidation temperature as summarized in Figure 4.16. The dominance of Fe_3O_4 that resulted from further oxidation of Fe_2O_3 rendered thicker and mechanically stable metal oxide layer. Although Fe_3O_4 functioned as a stabilizer for the catalytically active components dispersed on the metal oxide matrix, optimum thickness should be maintained to prevent it from covering the catalytically active components. The obtained data implied that a strong bond between the formed metal oxide matrix and the Kovar tube is required for better catalytic activity. Moreover, the presence of cobalt also prevented the formation of carbon except for reaction conducted over Kovar preoxidized at 1000°C. It was suspected that the rough texture of its surface have facilitated the formation of carbon by providing grooves where the hydrocarbon feedstock could accumulate and later on develop into carbonaceous deposits. Also, preoxidation at 1000ºC may have caused the formation of sintered particles which acted as nucleating sites for carbon accumulation [59].

4.6 Conclusion

The collected data showed that oxidation pretreatment rendered Kovar alloy tube active towards tetradecane CO_2 reforming with 700 and 1000°C being the respective optimum preoxidation temperature in producing CO and H_2. Oxidation pretreatment $\geq$ 700°C resulted into the formation of a separate oxide layer that was composed of Fe_2O_3, Fe_3O_4 and possibly oxides of nickel and/or cobalt which were inferred to be responsible for the observed catalytic activity. The strongly bonded metal oxide layer formed at 700 and 1000°C could have contributed to the relatively high CO_2 reforming reaction rate exhibited by the catalyst. Finally, the thickness of formed Fe_3O_4 should be controlled as to provide the needed mechanical stability to the metal oxide matrix while maintaining the optimum surface area for the active sites.

CHAPTER V

Summary and Conclusions

In this thesis, the feasibility of commercially available nickel-containing alloys was evaluated as reforming catalysts by oxidation pretreatment. The aim was to reform tar by-products obtained from biomass gasification process. Using tetradecane as a model compound, steam reforming, dry reforming and partial oxidation were conducted. The experiment was conducted over several commercially available alloys using steam, carbon dioxide and oxygen as reforming gases. Based on the results obtained from the screening studies, 2 alloys were further evaluated as dry reforming catalysts. SUS304 and Kovar were respectively chosen due to its relatively lower cost and high catalytic activity. The main goal of this research is to provide a robust, low-cost and readily available dry reforming catalyst for small, on-site reforming operations. Oxidation pretreated nickel-containing alloys (Fig. 5.1) have several advantages for this application, which include the formation of basic metal oxide layer that acts as a substrate for dispersed nickel, reaction promoter, and carbon formation retardant. All of these are important when developing a good dry reforming catalyst.

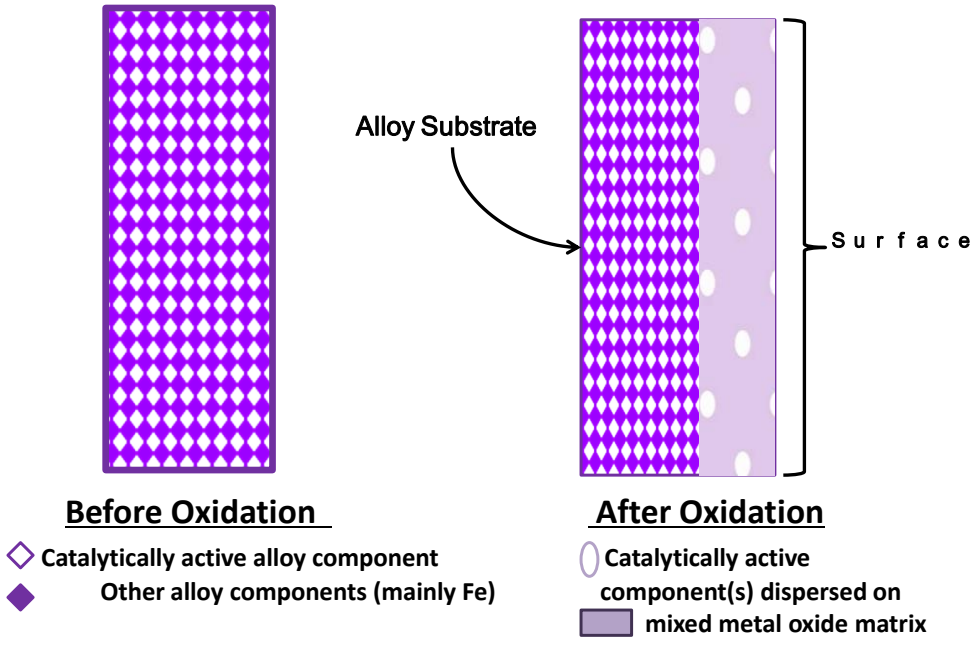

Figure 5.1. Simplified illustration of the surface of a preoxidized Ni-containing alloy

In general, Figure 5.1 illustrated that the formed oxide matrix was assumed to be a mixture oxides of basic components such as Fe and Cr which acted as a support for the active components. Ni should be one of the active components and several elements such as Co and Mo were expected to function as promoters or co-catalysts. Since Ni particles were finely dispersed and able to maintain a strong interaction with the support matrix, Ni were hardly sintered to form large particle that could act as nucleating sites for carbonaceous deposits.

In Chapter 1, the aim and the objective of this thesis were summarized along with the present issues involved in global energy supply and technology. Further, the developments and potential of biomass derived energy were also discussed. Hydrocarbon reforming was highlighted as a means of improving the efficiency and marketability of biomass gasification.

Chapter 2 discussed the screening tests done using 6 commercially available alloys tubes. This chapter is composed of 3 paper published by the authors which respectively presented the data on partial oxidation, steam reforming, and dry reforming using several model compounds. The mixed oxides formed after oxidation pretreatment and catalytic activity displayed by the alloys were correlated. SUS304 and Kovar were selected for further evaluation in terms of tetradecane dry reforming.

Chapter 3 presented the dry reforming activity of preoxidized SUS304 (1000ºC, 120 min) at different reaction temperatures and CO_2 flow rates using tetradecane as the model compound. The results showed that preoxidized SUS304 displayed high reaction rate and good resistant against carbon formation even at low reaction temperature (≤700ºC) by using high CO_2 flow rates (42 and 70 μmol/s). Nickel, probably as NiO, might be the active component while the trivalent- metal oxide Cr_2O_3 prevented the formation of carbon by improving the mobility of active oxygen species thus promoting its reaction with the hydrocarbon fragments to form CO and H_2. Another notable feature of preoxidized SUS304 is the formation of Fe_2O_3, a basic metal oxide that promotes the adsorption and dissociation of CO_2. Further work is needed to develop and characterize the catalyst before it can be commercially applied. The maximum performance of pretreated SUS304 was roughly 3 times as much as that of the untreated SUS304.

In Chapter 4, the feasibility of preoxidized Kovar as a dry reforming catalyst was discussed. In addition to nickel, Kovar also contains cobalt which was also identified to be catalytically active towards dry reforming reaction. Conducting the oxidation pretreatment at different temperatures revealed that at temperatures

>700ºC, a separate layer is formed on the surface of the alloy tube. Characterization done by XRD and SEM-EDS showed that the performance of Kovar as a dry reforming catalyst is significantly influenced by 3 factors: the oxidation state of iron, thickness of iron oxide (Fe_3O_4) layer, and mechanical stability of the formed metal oxide matrix. Among the tested preoxidation temperatures, optimum activity was observed with Kovar preoxidized at 700 ºC. In the future, catalyst pretreatment and reaction parameter optimization should be conducted to maximize the potential of Kovar as a dry reforming catalyst.

The data gathered confirmed the author's hypothesis on the application of oxidation on rendering commercially available Ni-containing alloys catalytically active towards dry reforming reaction. It was also deduced that oxidation temperature significantly affects the activity, stability, and mechanical robustness of the catalyst.

Some of the developed catalysts are now under further evaluation in the biomass gasification plant located in the "National Institute for Environment Studies" in Tsukuba, Japan for steam reforming reactions of tar produced by wood waste steam gasification. The next generation of this biomass gasification pilot plant is to operate with pure oxygen equipped with electrochemical oxygen purification system where the primary gasification process produces high temperature carbon dioxide. The developed catalysts are expected to play an important role in converting tar derived from biomass gasification into CO and H_2 via dry reforming reaction.

This study presented promising preliminary data on the potential of preoxidized SUS304 and Kovar as dry reforming catalysts. Further research on alloy based catalysts may also provide other researchers an alternative catalyst preparation that would circumvent the common problems encountered with supported metal catalysts.

References

[1] U.S. Energy Information Administration. (9 August 2011). Short-term Energy Outlook. Retrieved November 20, 2012, from http://www.eia.gov
[2] Planet for Life. (August 2008). Current World Oil Situation. Retrieved August 23, 2011, from http://www.planetforlife.com
[3] Dorian J, Franssen H, Simbeck D. Global challenges in energy. Energy Policy 34. 2006; 34:1984-1991.
[4] Singh B, Guldhe A, Rawat I, Bux F, Towards a sustainable approach for development of biodiesel from plant and microalgae. Renewable and Sustainable Energy Reviews. 2014; 29:216-214.
[5] Demirbas MF, Balat M, Balat H. Biowastes-to-biofuels. Energy Conversion and Management. 2011; 52:1815-1828.
[6] Kothari R, Tyagi VV, Pathak A. Waste-to-energy: A way from renewable energy sources to sustainable development. 2010; 14:3164-3170.
[7] Balat H and Kirtay E. Hydrogen from biomass- present scenario and future prospects. International Journal of Hydrogen Energy. 2010; 35:7416-7426.
[8] Edwards PP, Kuznetsov VL, David WIF. Hydrogen energy. Philosophical Transactions of the Royal Society A. 2007; 365:1043-1056.
[9] Nath K and Das D. Hydrogen from biomass. Current Science. 2003; 85(3):265-271.
[10] Armor JN. Catalysis and the hydrogen economy. Catalysis Letters. 2005; 1018(3-4):131-135.
[11] Knoef HAM (Ed). Review of applications of gases from biomass gasification. Syngas production and utilization. (Chapter 10) Handbook Biomass Gasification. 2005. The Netherlands: Biomass Technology Group.
[12] Ni M, Leung DYC, Leung MKH, Sumathy K. An overview of hydrogen production from biomass. Fuel Processing Technology. 2006; 87:461-472.
[13] Laurence LC and Ashenafi D. Syngas treatment unit for small scale gasification-application to IC engine gas quality requirement. Journal of Applied Fluid Mechanics. 2012; 58(1):95-103.
[14] Wang L, Weller C, Jones D, Hanna M. Contemporary issues in thermal gasification of biomass and its application to electricity and fuel production. Biomass and Bioenergy. 2008; 32:573-581.
[15] Ming Q, Healey T, Allen L, Irving P. Steam reforming of hydrocarbon fuels. Catalysis Today. 2002; 77:51-64.
[16] Nieva LS and Gama L. A study on the characteristics of the reforming of methane: a review. Brazilian Journal of Petroleum and Gas. 2010; 4(3):119-127.
[17] Zhu J, Zhang D, King KD. Reforming of CH_4 by partial oxidation: thermodynamic and kinetic analyses. Fuel. 2001; 80:899-905.

[18] Kobayashi Y, Horiguchi J, Kobayashi S, Yamazaki Y, Omata K, Nagao D, Konno M, Yamada M. Effect of NiO content in mesoporous NiO-Al_2O_3 catalysts for high pressure partial oxidation of methane to syngas. Applied Catalysis A: General. 2011; 395:129-137.
[19] Tsipouriari VA, Zhang Z, Verykios XE. Catalytic partial oxidation of methane to synthesis gas over Ni-based catalysts. Journal of Catalysis. 1998; 179:283-291.
[20] Wang S and Lu GQ. Carbon dioxide reforming of methane to produce synthesis gas over metal-supported catalysts: state of the art. Energy & Fuels. 1996; 10:896-904.
[21] Rostrup-Nielsen JR. Production of synthesis gas. Catalysis Today. 1993; 18:305-324.
[22] Mark MF, Mark F, Maier W. Reaction kinetics of the CO_2 reforming of methane. Chemical Engineering & Technology. 1997; 20:361-370.
[23] Solymosi F, Tolmacsov P, Zakar TS. Dry reforming of propane over supported Re catalyst. Journal of Catalysis. 2005; 233:51-59.
[24] Castro Luna AE and Iriarte ME. Carbon dioxide reforming of methane over a metal modified Ni-Al_2O_3 catalyst. Applied Catalysis A: General. 2008; 343:10-15.
[25] Gadalla AM and Bower B. The role of catalyst support on the activity of nickel for reforming methane with CO_2. Chemical Engineering Science. 1988; 43(11):3049-3062.
[26] Nakamura J and Uchijima T. Methane reforming with carbon dioxide. Shokubai. 1993; 35:478-484.
[27] Takano A, Tagawa T, Goto S. Carbon dioxide reforming of methane on supported nickel catalysts. Journal of Chemical Engineering of Japan. 1994; 27(6):727-731.
[28] Juan-Juan J, Roman-Martinez MC, Illan-Gomez MJ. Effect of potassium content I the activity of K-promoted Ni/Al_2O_3 catalysts for the dry reforming of methane. Applied Catalysis A: General. 2006; 301:9-15.
[29] Bradford MCJ and Vannice MA. Catalytic reforming of methane with carbon dioxide over nickel catalysts (I. Catalyst characterization and activity). Applied Catalysis A: General. 1996; 142:73-96.
[30] Ferreira-Aparicio P, Guerrero-Ruiz A, Rodriguez-Ramoz I. Comparative study at low and medium reaction temperatures of syngas production by methane reforming with carbon dioxide over silica and alumina supported catalysts. Applied Catalysis A: General. 1998; 170:177-187.
[31] Budiman AW, Song S. Dry reforming of methane over cobalt catalysts: a literature review of catalyst development. Catalysis Surveys from Asia. 2012; 16:183-197.
[32] Gronchi P, Fumagalli D, Del Rosso R, Centola P. Carbon deposition in methane and reforming with carbon dioxide. Journal of Thermal Analysis. 1996; 47:227-234.

[33] Courson C, Makaga E, Petit C, Kiennemann A. Development of Ni catalysts for gas production from biomass gasification. Reactivity in steam- and dry- reforming. Catalysis Today. 2000; 63:427-437.
[34] Takanabe K, Nagaoka K, Aika A. Titania supported cobalt and nickel bimetal catalysts for carbon dioxide reforming of methane. Journal of Catalysis. 2005; 232:268-275.
[35] Al-Fatesh ASA and Fakeeha AH. Effects of calcination and activation temperature on dry reforming catalysts. Journal of Saudi Chemical Society. 2012; 16:55-61.
[36] Choudhary VR, Rane VH, Rajput AM. Selective oxidation of methane to CO and H_2 over unreduced NiO-rare earth oxide catalysts. Catalysis Letters. 1993; 22:289-297.
[37] Chen P, Zhang H, Lin G, Tsai K. Development of coking-resistant Ni-based catalyst for partial oxidation and CO_2-reforming of methane to syngas. Applied Catalysis A: General. 1998; 166:343-350.
[38] Choudhary VR and Mamman AS. Simultaneous oxidative conversion and CO_2 or steam reforming of methane to syngas over CoO-NiO-MgO catalyst. Journal of Chemical Technology and Biotechnology. 1998; 73:345-350.
[39] Takano A, Tagawa T, Goto S. Carbon deposition on supported nickel catalysts for carbon dioxide reforming of methane. Journal of Japan Petroleum Institute. 1996; 39(2):144-150.
[40] Kutz M (Ed). High temperature oxidation. (Chapter 6) Handbook of Environmental Degradation of Materials. 2005. New York: William Andrew Publishing.
[41] Wallwork GW. The oxidation of alloys. Reports on Progress in Physics. 1976; 39:401-485.
[42] Avner SH. Alloy steels. (Chapter 9) Introduction to Physical Metallurgy. 1964. United States of America: McGraw-Hill Inc.
[43] Huntz AM, Reckmann A, Haut C, Severac C, Herbst M, Resende FCT, Sabioni ACS. Oxidation of AISI 304 and AISI 439 stainless steels. Materials Science and Engineering A. 2007; 447:266-276.
[44] Sridharan K, Worzala FJ, Dodd RA. Martensitic transformation and invar effect in Fe-Ni-Co alloys. Materials Chemistry and Physics. 1991; 30:115-119.
[45] Askeland DR, Fulay PP, Wright WJ. Dispersion strengthening by phase transformations and heat treatment. (Chapter 12) The Science and Engineering of Materials. 6th Edition. 2011. United States of America: Cengage Learning.
[46] Lou DW and Shen ZS. Oxidation behavior of Kovar alloy in controlled atmosphere. Acta Metallurgica Sinica (English Letters). 2008; 21(6):409-418.
[47] Tagawa T and Okada M. Recent advances in protium storage material and its application to chemical devices. Shokubai. 1999; 41, 504-509.

[48] Chikamatsu N, Tagawa T, Goto S. Reaction pathway and selective hydrogenation on catalysts derived from oxidation treatment of Mg_2Cu alloy. Bulletin of Chemical Society Japan. 1994; 67(6):1548-1552.
[49] Chikamatsu N, Tagawa T, Goto S. Characterization of new mixed oxide catalysts derived from hydrogen storage alloy. Journal of Materials Science. 1995; 30(5):1367-1372.
[50] Kawamoto K, Wu W, Kuramochi H. Development of gasification and reforming technology using catalyst at lower temperature for effective energy recovery: hydrogen recovery using waste wood. Journal of Environment and Engineering 2009; 4(2):409-421.
[51] Kawamoto K, Kobayashi J, Tagawa T, Yamada H. Development of waste gasification and catalytic reforming technologies with molecular separation phaseusing nanoporous membrane. Annual Report (2010), National Institute of Environment. Project No. K2106. 2011. Japan
[52] de la Rama SR, Yamada H, Tagawa T. Evaluation of surface oxidized SUS304 as tetradecane CO_2 reforming catalyst. Poster presented at the annual meeting of American Institute of Chemical Engineers at California, USA. 2013. 583dz.
[53] Environmental Protection Agency (EPA), 2009. Federal Register, Vol. 74, No. 68, Proposed Rules, p 16639.
[54] Ido Y, Yamada H, Tagawa T. Study on catalyst adsorped species during methane partial oxidation using pulse method. Poster presented at the 79th annual meeting of Society of Chemical Engineers- Japan at Gifu, Japan. 2014. SA1P90.
[55] Osojnik Crnivec IG, Djinovic P, Erjavec B, Pintar A. Effect of synthesis parameters on morphology and activity of bimetallic catalysts in CO_2-CH_4 reforming. Chemical Engineering Journal. 2012;207-208: 299-307.
[56] De Lima SM and Assaf JM. Ni-Fe catalysts based on perovskite-type oxides for dry reforming of methane to syngas. Catalysis Letters. 2006;108(1-2): 63-70.
[57] Provendier H, Petit C, Estournes C, Libs S, Kiennemann A. Stabilisation of active nickel catalysts in partial oxidation of methane to synthesis gas by iron addition. Applied Catalysis A: General, 1999; 180:163-173.
[58] Djinovic P, Crnivec g o, Erjavec B, Pintar A. Exceptional performance of novel Ni and Co bimetallic catalysts in methane dry reforming process. Proceedings of the 9th World Congress of Chemical Engineering, South Korea, 2013, 184.
[59] Rostrup-Nielsen J and Trimm D. Mechanisms of carbon formation on nickel-containing catalysts. Journal of Catalysis. 1977; 48: 155-165.

Appendix

List of Published/Accepted Papers

Peer-Reviewed Papers

1. Partial oxidation catalysts derived from Ni-containing alloys for biomass gasification process
   Chemical Engineering Transactions, Vol. 32, pp. 583-588 (2013)

2. Evaluation of pre-oxidized SUS304 as a catalyst for hydrocarbon reforming
   ISRN Environmental Chemistry, vol. 2013, Article ID 289071, 5 pages, 2013. doi:10.1155/2013/289071

3. Preliminary assessment of oxidation pretreated Hastelloy as hydrocarbon steam reforming catalyst
   Journal of Catalysts, vol. 2014, Article ID 210371, 7 pages, 2014. doi: 10.1155/2014/210371

4. Effects of Oxidation Pretreatment Temperature on Kovar Used as CO_2 Reforming Catalyst
   Journal of Fuel Chemistry and Technology, in press

Conference Proceedings

1. Tetradecane reforming using surface oxidized SUS304 as catalyst
   International Symposium on Ecotopia Science'11, Nagoya University, Nagoya, Japan, p. 83 (2011)

2. Hastelloy as hydrocarbon reforming catalyst for hydrogen production
   American Institute of Chemical Engineers Annual Meeting, Pittsburgh, Pennsylvania, USA (2012)

3. Screening test: Ni-containing alloy as steam reforming catalyst
   9th World Congress of Chemical Engineering, Seoul, Korea, p. 184 (2013)

4. Evaluation of surface oxidized SUS304 as tetradecane CO_2 reforming catalyst
   American Institute of Chemical Engineers Annual Meeting, San Francisco, California, USA (2013)

Appendix

List of Published/Accepted Papers

Peer-Reviewed Papers

5. Partial oxidation catalysts derived from Ni-containing alloys for biomass gasification process
   Chemical Engineering Transactions, Vol. 32, pp. 583-588 (2013)

6. Evaluation of pre-oxidized SUS304 as a catalyst for hydrocarbon reforming
   ISRN Environmental Chemistry, vol. 2013, Article ID 289071, 5 pages, 2013. doi:10.1155/2013/289071

7. Preliminary assessment of oxidation pretreated Hastelloy as hydrocarbon steam reforming catalyst
   Journal of Catalysts, vol. 2014, Article ID 210371, 7 pages, 2014. doi: 10.1155/2014/210371

8. Effects of Oxidation Pretreatment Temperature on Kovar Used as CO_2 Reforming Catalyst
   Journal of Fuel Chemistry and Technology, in press

Conference Proceedings

5. Tetradecane reforming using surface oxidized SUS304 as catalyst
   International Symposium on Ecotopia Science'11, Nagoya University, Nagoya, Japan, p. 83 (2011)

6. Hastelloy as hydrocarbon reforming catalyst for hydrogen production
   American Institute of Chemical Engineers Annual Meeting, Pittsburgh, Pennsylvania, USA (2012)

7. Screening test: Ni-containing alloy as steam reforming catalyst
   9th World Congress of Chemical Engineering, Seoul, Korea, p. 184 (2013)

8. Evaluation of surface oxidized SUS304 as tetradecane CO_2 reforming catalyst
   American Institute of Chemical Engineers Annual Meeting, San Francisco, California, USA (2013)